INFORMATION TO USERS

This manuscript has been reproduced from the microfilm master. UMI films the text directly from the original or copy submitted. Thus, some thesis and dissertation copies are in typewriter face, while others may be from any type of computer printer.

The quality of this reproduction is dependent upon the quality of the copy submitted. Broken or indistinct print, colored or poor quality illustrations and photographs, print bleedthrough, substandard margins, and improper alignment can adversely affect reproduction.

In the unlikely event that the author did not send UMI a complete manuscript and there are missing pages, these will be noted. Also, if unauthorized copyright material had to be removed, a note will indicate the deletion.

Oversize materials (e.g., maps, drawings, charts) are reproduced by sectioning the original, beginning at the upper left-hand corner and continuing from left to right in equal sections with small overlaps. Each original is also photographed in one exposure and is included in reduced form at the back of the book.

Photographs included in the original manuscript have been reproduced xerographically in this copy. Higher quality 6" x 9" black and white photographic prints are available for any photographs or illustrations appearing in this copy for an additional charge. Contact UMI directly to order.

UMI

A Bell & Howell Information Company
300 North Zeeb Road, Ann Arbor MI 48106-1346 USA
313/761-4700 800/521-0600

SOLUTION, SEMISOLID, AND SOLID NMR STUDIES OF LIPID MODEL MEMBRANES

by

Zhenjia Chen

A dissertation submitted to the Graduate Faculty in Chemistry in partial fulfillment of the requirements for the degree of Doctor of Philosophy, The City University of New York.

1996

This manuscript has been read and accepted for the Graduate Faculty in Chemistry in satisfaction of the dissertation requirement for the degree of Doctor of Philosophy.

8/16/96
Date

Ruth E. Stark
Chair of Examining Committee

9/3/96
Date

Executive Officer

Robert Bittman

Fred Naider

Supervisory Committee

The City University of New York

Abstract

Solution, Semisolid, and Solid NMR Studies of Lipid Model Membranes

by

Zhenjia Chen

Advisor: Professor Ruth E. Stark

Using a combination of 1D and 2D solution NMR, it is possible to assign all of the ^{1}H resonances for two complex C_8-based model digestive mixtures. Our new structural model based on two dimensional nuclear Overhauser effect spectroscopy (NOESY) and rotating-frame NOE spectroscopy (ROESY) describes the molecular organization of monoglyceride (MG), fatty acid (FA), and bile salt (BS) constituents. This proposal accounts for a large body of new NMR data, including Mn^{2+} titrations and NOE connectivities.

Magic angle spinning (MAS) assisted semisolid NMR was used to observe two distinct water resonances for *N*-monomethyldioleoylphosphatidylethanolamine (MeDOPE) bilayers in the liquid-crystalline phase. The downfield shifted peak with the shorter T_1 relaxation time was ascribed to hydrogen-bonded interlamellar water in slow exchange with other water molecules. The upfield peak with a long T_1

relaxation time arises from an exchange averaging between the bulk water and lipid solvation water. The hydrogen-bonded water also showed intense cross-peaks in the 2D magic angle spinning assisted NOESY spectrum with the lipid headgroup. In a second initiative, we used several deuterated DMPCs to systematically investigate the origin of the NOESY crosspeak between methyl groups of the lipid headgroup and the acyl chains. We have proposed a new mechanism for formation of these types of crosspeaks, which is through-space interactions between the headgroup and backbone protons and spin diffusion along the acyl chains. Thirdly, a series of MAS ^{1}H and ^{13}C NMR experiments were carried out for multilamellar dispersions formed by phosphatidylcholine (PC) /cholesterol (CH) and sphingomyelin (SPM)/cholesterol (CH), which lay the groundwork for systematic studies of packing and organization in model membranes with varying constituents and compositions.

Finally, solid-state ^{13}C and ^{2}H NMR spectroscopy was used to study the molecular structure and dynamic properties of lime and tomato cuticles. Controlled hydrolysis of the lime cutin polyester was carried out in order to elucidate its molecular architecture; the insoluble residues were analyzed with CPMAS ^{13}C NMR. To examine how hydration alters the dynamic properties of both tomato cuticle and absorbed D_2O, ^{2}H NMR investigations were conducted in parallel.

This thesis is dedicated to my mother and my daughter;
without their love this never could have happened.

Acknowledgments

I would like to thank my wonderful advisor, Dr. Ruth E. Stark, for introducing me to the field of solution and solid NMR, teaching me so many things about research of the mixed-lipid and plant polyester systems, and giving me the opportunity to work in her lab for graduate studies. Also, I really appreciate all her help during the preparation of this thesis. It is impossible for me to try and imagine the completion of this thesis without her help and advice.

I would also like to thank Dr. Naider and Dr. Bittman for being on my committee and giving me a lot of valuable advice.

I would also like to thank Dr. Van Gorkom for all of his help and training.

I would also like to thank Dr. Balogh-Nair for giving me opportunity to come this wonderful country, U. S. A.

Lastly, I would also like to thank all my fellow labmates: Cherryl, Anup, Mingming, Guo-hua, Feng, Wei-xing, Liang, and Cun xing in both The College of Staten Island and City College.

Again, thank you very much to everyone.

Table of Contents

List of Abbreviations & Symbols

Å	Angstrom
AQ	acquisition time
B_O	magnetic field strength (Tesla)
BS	bile salt
C_8	digestive samples with acyl chains having 8 carbons
C_{18}	digestive samples with acyl chains having 18 carbons
CH	cholesterol
COSY	two-dimensional correlated spectroscopy
CP	cross polarization
CRAMPS	combined rotation and multiple-pulse spectroscopy
CSA	chemical shift anisotropy
^{13}C	spin (1/2) isotope of carbon
D_2O	deuterium oxide
DD	dipolar decoupling
DMPC	dimyristoylphosphatidylcholine
DMPC-d_{27}(1)	1-myristoyl(d_{27})-2-myristoyl-*sn*-3-glycerophosphocholine
DMPC-d_{27}(1)	1-myristoyl-2-myristoyl(d_{27})-*sn*-3-glycerophosphocholine
DMPC-d_4	dimyristoylphosphatidylcholine(α,β-d_4)
DMPC-d_9	dimyristoylphosphatidylcholine(γ-d_9)
DMPC-d_{54}	1-myristoyl(d_{27})-2-myristoyl(d_{27})-sn-3-glycerophosphocholine

$DMSO-d_4$	dimethyl sulfoxide-d_4
DOPC	dioleoylphosphatidylcholine
DP	direct polarization
DQF	double-quantum filter
E	energy
EDTA	ethylenediaminotetraacetic acid
FA	fatty acid
FID	free induction decay
FT	Fourier transform
H_{CS}	magnetic shielding by surrounding electrons giving chemical shifts
H_D	direct dipole-dipole interaction with other nuclei
HMQC	heteronuclear multiple quantum coherence
H_Q	quadrupolar interaction which will be present for nuclei with spin > 1/2 only
H_{SC}	spin-spin couplings to other nuclei
H_Z	zeeman interaction with the magnetic field B_O
J	spin-spin coupling constant (Hz)
MAS	magic-angle spinning
MBS	mixed bile salts
MeDOPE	n-methyldioleoylphosphoethanolamine
MG	monoglyceride
MHz	megahertz
MIL	mixed intestinal lipids
NMR	nuclear magnetic resonance
NOE	nuclear Overhauser effect

NOESY	two-dimensional nuclear Overhauser effect spectroscopy
1D	one-dimensional
PC	phosphatidylcholine
ppm	parts per million, unit of the chemical shift
QLS	quasielastic light scattering
ROE	rotating-frame NOE
ROESY	two-dimensional rotating-frame NOE spectroscopy
SD	scalar decoupling
S/N	signal to noise ratio
SPM	sphingomyelin
ssb	spinning sideband
t_1, t_2	time dimensions (evolution, acquisition) in 2D NMR
T	temperature (K or °C)
T_1	spin-lattice relaxation time
T_2	spin-spin relaxation time
TC	taurocholate
TG	triglyceride
TO	triolein
TOCSY	two-dimensional total correlated spectroscopy
Tris	tris(hydroxymethyl)aminomethane hydrochloride
2D	two-dimensional
X_{PC}	mole fraction of phosphatidylcholine
γ_n	gyromagnetic ratio of nucleus n (s^{-1} T^{-1})
τ_c	correlation time (ns)
τ_m	mixing time in 2D NMR experiment

ν_{rot}	spinning speed (kHz)
ω	resonance frequency

List of Tables

List of Figures

I. Introduction to Solution, Semisolid, and Solid NMR

The first successful NMR spectrum was detected in late 1945 by E. M. Purcell at Harvard University and independently by Felix Bloch at Stanford University (Purcell et al., 1946; Bloch et al., 1946), and they shared the 1953 Nobel Prize in Physics for that work. Since then, our understanding of the properties of nuclear spin systems has come to maturity and NMR has developed into such a powerful tool that revolutionary new developments in instrumentation, data processing, and pulse sequences are continuously being added. Many of these developments have been derived from the application of high-resolution NMR in solids (Schaefer and Stejskal, 1976), two dimensional NMR (Jeener, 1971; Aue et al., 1976; Ernst et al., 1987), and the application of high-resolution NMR to biological problems. Nowadays, the combination of high field spectrometers, multidimensional techniques, and solid NMR techniques is used to obtain structural information for biological systems (Grand and Harris, 1995), that, as recently as the late 1960's were unthinkable even for small organic molecules.

The main interactions for nuclei with a magnetic moment (nuclear spins) may be written as in equation 1:

$$H = H_Z + H_D + H_{CS} + H_{SC} + H_Q \quad (1)$$

H_Z: Zeeman interaction with the magnetic field B_0

H_D: Direct dipole-dipole interaction with other nuclei

H_{CS}: Magnetic shielding by surrounding electrons giving chemical shifts

H_{SC}: Spin-spin couplings to other nuclei

H_Q: Quadrupolar interaction which will be present for nuclei with spin > 1/2 only

Zeeman Interaction H_Z

The Zeeman interaction H_Z occurs for all nuclei with odd atomic mass or odd atomic number between the magnetic moment of the nucleus and the applied magnetic field B_0, whether in solution state, solid, or semi-solid state. When a nucleus with spin I = 1/2 is placed in a magnetic field of strength B_O, two energy levels are generated: a lower state, which is generally labeled α, and contains the nuclear magnetic moment parallel to the applied magnetic field B_0; the upper state (β) in which the magnetic moments are anti-parallel to B_0. The two energy states are unequally populated, with the ratio of the populations governed by the Boltzmann distribution law. The difference of population yields a macroscopic longitudinal magnetization which is manipulated by radiofrequency pulses and delays and finally detected in the NMR spectrum. **Figure I-1** represents a 90° rf pulse, free induction decay (FID), and Fourier

transformation (FT) of time domain FID into the frequency domain signal for a typical one-pulse NMR experiment.

The Zeeman interaction scales linearly with the applied magnetic field B_0, larger separations of the energy levels occurring at higher fields with a corresponding increase in the population difference between them **(Figure I-2)** and an increase in the inherent signal to noise ratio (S/N) of the spectrum. The development of commercially available superconducting magnets cooled by liquid helium, the so-called cryomagnets, has made it possible to attain a proton resonance frequency of 800 MHz. Under the influence of the higher external magnetic field (B_0), the population difference between possible spin states of NMR-active nuclei is increased greatly, leading in principle to an improvement in sensitivity that goes as $B_0^{3/2}$. This is associated with a considerable shortening of the time required to achieve a certain S/N ratio. Moreover, a better resolution between the signals of nuclei with similar chemical shifts is obtained, whereas coupling constants remain unchanged since they are natural constants.

Chemical Shift Interaction H_{CS}

The chemical shift interaction H_{CS} scales linearly with the applied field, thus it will be proportionately larger and more important at higher magnetic field strengths.

Since H_{CS} is due to the shielding effect on the nucleus of the fields produced by the surrounding electrons, this interaction is the most sensitive to the geometry and identity of the other atoms surrounding a particular nucleus. Chemical shift anisotropy (CSA) means that if one were to take a single crystal of some substance and measure its NMR spectrum, the shift values observed would vary as the crystal was rotated relative to the static field. Because rapid molecular tumbling occurs in solution, chemical shift anisotropy (CSA) is averaged to zero, allowing the observation of sharp lines at the isotropic chemical shift. The resonance frequency of this single line is related to the electronic screening about the nucleus and contains most of the chemical information we seek. For a given compound the appearance of the spectrum is governed by intramolecular chemical shift differences, i.e. differences in resonance frequencies for different nuclei of the same molecule. This feature is of paramount importance for structure determination.

Solid powders, however, generally do not have rapid molecular motions; every orientation is present simultaneously, and the spectrum we observe is a superposition of the various lines and a dispersion of peak positions due to the CSA from different crystallites. The CSA depends upon $(3\cos^2\theta - 1)$, where is the angle between

the internuclear vector and the static magnetic field. When θ is 54°44', the term $(3\cos^2\theta - 1)$ becomes zero and this angle is referred to as the magic angle (Andrew et al., 1959; Lowe, 1959). Magic angle spinning (MAS) is the method that is used to reduce the CSA to its isotropic average, which in combination with cross polarization and high-power decoupling has provided truly high-resolution NMR spectra from solids.

In semi-solids such as phospholipid multibilayers, high-field nuclear magnetic resonance (NMR) experiments with magic-angle spinning (MAS) can generally yield narrow, multiline spectra from which isotropic chemical shifts can be identified. In addition, when the molecules are constrained from rotating as in a semisolid, the CSA can be measured and the resonance will have different shapes. The ^{31}P NMR CSA is partially averaged by molecular motion within, for example, a phospholipid headgroup, and the extent of averaging can be used to aid conformational studies and to investigate the phase behavior of lipids (King and Marsh, 1989). The lineshape in ^{31}P NMR spectroscopy is sensitive to the lipid arrangement in different phase structures **(Figure I-3)**. Moreover, the ^{31}P data can be acquired more quickly and more easily than with other NMR techniques. Therefore, the use of ^{31}P NMR CSA has become popular to characterize phospholipid phase behavior.

In samples where it is impossible to remove the CSA completely by MAS, the spectra retain a considerable contribution from spinning sidebands. The sideband intensities may of course be of interest, but in more complex molecules it can be difficult to distinguish between center bands and sidebands. The sidebands complicate interpretation, and the intensity that should be in the center band is dispersed in them as well. As the sample is spun faster and faster under MAS conditions, the sidebands move out and become less intense, and the spectrum becomes less complicated. The appearance of sidebands is field dependent because H_{CS} is field dependent, and it is possible to obtain spectra without sidebands by spinning very rapidly or with another method, TOSS (total suppression of sidebands), which produces a spectrum in which the sidebands are eliminated (Dixon et al., 1982).

Spin-Spin Coupling Interaction H_{SC}

The spin-spin coupling interaction H_{SC} is field independent and is usually much smaller (1-200 Hz) than the other interactions. It arises from indirect spin-spin coupling between two spins via their electronic surroundings. In fact, this implies the existence of coupling between nuclei and electrons. The interactions between the magnetic moments are due to nuclear spin and electron orbital motion and the dipolar interaction between

the electron and nuclear spins. The scalar coupling occurs because a bonding electron's spin tends to correlate with the spin of its neighboring nucleus. The electron has been influenced, and will influence other neighboring nuclear spins. The scalar interaction is manifested in the NMR spectrum as the J coupling. The spin-spin couplings observed in solution proton spectra have been used extensively for conformational analysis, especially in assignments of structure.

In order to obtain structural information it is necessary to assign all spins in the structure to be studied. For some proton NMR spectra, even at high fields, overlapping signals often make accurate chemical shift values and coupling constants difficult to obtain, for example in simple bile salts between 1.2 ppm and 2.5 ppm (**Figure I-4**). It is necessary to find additional ways to assign all protons to their respective chemical groups.

This problem has been simplified greatly by application of homonuclear 2D-Correlated Spectroscopy (COSY, DQF-COSY, and TOCSY). Historically, the concept of two-dimensional NMR was introduced by Jeener in 1971 and COSY was the first two-dimensional NMR experiment (Jeener, 1971). The basic COSY pulse sequence is quite straightforward and simply shown in **Figure I-5**. The preparation period is a

relaxation delay to ensure that the spin system is at equilibrium. The first 90° pulse flips the net magnetization vector into the xy plane and causes each spin to precess at its characteristic frequency during the evolution period. This effectively labels each spin according to its initial precession frequency during t_1. Basically, the 2D experiment adds another dimension in which to distinguish the nuclei of interest. The availability of this second dimension allows the overlapping resonances to be spread out and identified definitively. Moreover, 2D-COSY traces out the through-bond spin-spin connectivities in the molecules and allows spins pairs which are scalar coupled to be identified.

However, in a COSY spectrum, the largest peaks are on the diagonal and contain no coupling information. The methyl singlets often have very high intensities as single-proton resonances, causing other interesting resonances to be buried under t_1 noise. On the other hand, since the diagonal peaks in a phase-sensitive COSY spectrum are in pure dispersion mode and the cross-peaks are in pure absorption mode, a technique known as a double-quantum filtering (DQF) results in absorption-mode peaks for both diagonal and off-diagonal peaks, eliminating the long tail normally associated with diagonal peaks. The DQF-COSY pulse sequence (Piantini et al., 1982) is shown in **Figure I-6.**

Although double-quantum transitions are forbidden in a 1D spectrum, they can be created with 2D pulse sequences. By monitoring transfer of this double-quantum coherence, single-quantum transfer can be suppressed by suitable phase cycling. A COSY spectrum with a double-quantum filter (DQF-COSY) has much better resolution than a normal COSY because (a) singlets that cause the worst t_1 noise are eliminated, (b) the phase-sensitive COSY experiment is improved by adjusting both diagonal and cross peaks into pure absorption phase, and (c) the diagonal peaks are suppressed.

Another correlated experiment which relies on spin-spin couplings is Total Correlated Spectroscopy (TOCSY), which is also known as HOHAHA (Braunschweiler and Ernst, 1983). This experiment uses a pulse sequence is shown in **Figure I-7**. The first 90° pulse brings the equilibrium magnetization into the xy plane along the y axis, a new B_1 field (spin lock) is applied and magnetization precesses around it at a frequency that depends on the strength of the B_1. All coupled spins will have the same precession frequency and be strongly coupled. This technique contrasts with DQFCOSY in which cross peaks are directly coupled to each other without loss of signal intensity because the cross-peak multiplets are all in phase rather than anti-phase. Furthermore, the extent of the relay among spins is dependent upon both spin-lock mixing time and the spin-spin relaxation time of the

molecule. Ideally cross signals are formed between all the nuclei within a spin system. Short mixing times produce cross signals only between directly coupled nuclei, whereas longer mixing times give relayed and multiply-relayed cross peaks. Thus, we can use different mixing times to extract more information from the coupling system.

For solids, the scalar coupling is not averaged to zero by rapid molecular tumbling, but it is several orders of magnitude smaller than the dipolar interactions and thus is rarely observed in solid-state NMR spectra. For ^{1}H-^{13}C coupling, the dipolar decoupling required to observe solid-state spectra also removes these scalar interactions. In semisolids such as liquid crystals, gels, etc. with partial order, it is possible to use MAS assisted methods to obtain well-resolved ^{1}H NMR spectra and to carry out MAS-assisted two-dimensional correlated NMR experiments (COSY and TOCSY) for many types of protons in the liquid-like semisolid systems in order to assign overlapped ^{1}H resonances (Li et al., 1993; Gross et al., 1995).

Dipolar Interaction H_D

The dipolar interaction H_D arises from direct magnetic dipole-dipole interactions between nuclei: homonuclear dipole-dipole interactions (^{1}H-^{1}H, ^{13}C-^{13}C) and heteronuclear dipole-dipole interactions (^{1}H-^{13}C). For an isolated pair of

spin-1/2 nuclei, the dipolar coupling splits the line into a doublet, and the size of the splitting depends on the length and orientation of the internuclear vector relative to the static field. In the solid state, molecules are much less mobile than in the liquid state and all possible orientations are present in a powdered sample. Even in the simple case that all (proton) pairs are isolated, the dipolar couplings lead to a characteristic broad line shape because of a superposition of many doublets with different splitting. This direct dipole-dipole interaction is much bigger than the scalar coupling, and indeed exceeds chemical shift differences. For ^{13}C there is no homonuclear dipolar interaction to consider because it is a dilute nucleus (low natural abundance). The homonuclear dipolar coupling, ^{1}H-^{1}H, could be averaged by magic-angle-spinning (MAS) but for rigid solids this would require spinning speeds greater than the magnitude of the couplings, which for ^{1}H-^{1}H interactions of about 50 kHz is not feasible experimentally. The ^{1}H-^{13}C dipolar couplings are also very large, especially for directly bonded atoms. In order to obtain high-resolution NMR spectra of solids this dipole-dipole coupling should be removed. Fortunately, they can be removed by higher power heteronuclear decoupling; in practice, field strengths from 70 to 100 kHz are used.

In the liquid state, the molecules are tumbling rapidly and this rapid molecular motion averages the dipole-dipole interaction over all possible orientations of the molecule; thus the dipole-dipole interaction of ^{1}H-^{13}C is averaged to zero for liquids. Although the dipole-dipole interaction does not usually have any observable effect on spectra recorded in solution, the indirect way to examine this interaction is the nuclear Overhauser effect (NOE). The NOE in turn can be related to the strength of dipole dipole interactions between the nuclei involved (interatomic distance), the effective correlation time τ_c (molecular motion), and the nature of the nuclei themselves (γ). The strength of the dipole-dipole interaction will depend strongly on the internuclear distance.

For two protons in close proximity (<5Å), the observed NOE can be positive, negative, or zero, depending on the value of the molecular tumbling (correlation) time. The observed NOE between two close spins is positive for molecules such as small peptides and many synthetic low-molecular weight compounds that reorient rapidly (have a short correlation time). The observed NOE is negative for molecules such as proteins, oligonucleotides and aggregates that reorient slowly (have long correlation times). In addition, there exists an intermediate correlation time, for which the NOE is zero regardless of the spatial proximity of

interacting protons. The NOE intensity is a function of the correlation time τ_c according to the condition in Equation 2:

NOE	NOESY Crosspeak vs. Diagonal	When	
>0	<0	$\omega\tau < 1.12$	
=0	=0	$\omega\tau = 1.12$	(2)
<0	>0	$\omega\tau > 1.12$	

Two-dimensional NOESY (Jeener et al., 1979) and ROESY (Bax and Davis, 1985) provide a map of incoherent interactions among all proton pairs that undergo magnetization exchange arising from the nuclear Overhauser effect (NOE). The pulse sequence for NOESY is shown in **Figure I-8**. An additional fixed time, which is called the mixing time τ_m, is introduced to NOESY experiments to allow exchange of the magnetization through space. The resultant spectrum depends critically on the magnitude of the mixing time, and the cross-peak intensities reflect the amount of exchange that takes place during τ_m. Typically, NOESY experiments are carried out at several mixing times, permitting the buildup of the NOE to be monitored. The NOE will increase as a function of mixing time until a maximum is obtained.

In a NOESY spectrum phased with the diagonal peaks positive, positive NOEs appear as negative cross peaks and negative NOEs as positive cross peaks (see above). For molecules which belong to the intermediate region where NOEs are crossing over from positive to negative, the expected laboratory-frame NOE intensity will be zero. However, the evolution can take place under the influence of a spin locking field so that the rotating-frame NOE (ROE) is observed. Unlike the laboratory-frame NOE, which is observed in NOESY, the ROE is always positive. This feature makes ROESY a very useful tool for small biomolecules (peptides, natural products, etc.) which often have NOE intensities near zero. The pulse sequence for ROESY is shown in **Figure I-9**.

In semisolids such as liquid crystals, gels, etc. with partial order, although molecular motion reduces the magnitude of dipole-dipole interactions, it is not completely averaged to zero as in isotropic solutions. If segmental reorientation is liquidlike for all chemical moieties, the motion can be rapid enough to fully average ^{13}C-^{1}H dipolar interactions. At slow MAS speeds the ^{1}H resonances for these groups probably reflect the residual ^{1}H-^{1}H dipolar interactions. It is then possible to use MAS-assisted methods to obtain well-resolved ^{1}H NMR spectra and

to carry out two-dimensional NOESY and ROESY to identify proximal interactions between two constituents.

In contrast to liquidlike reorientation, greater motional restrictions exist in some semisolid systems, in which case their behavior becomes solidlike and suggests that either ^{13}C-^{1}H or ^{1}H-^{1}H dipolar interactions contribute significantly to the proton line widths. Given this fact, high resolution ^{1}H NMR spectra are not obtained. Despite a slowing of molecular motion, high resolution ^{13}C NMR spectra can be obtained when high-power ^{1}H-^{13}C decoupling is employed. MAS ^{13}C NMR conducted with various decoupling conditions can identify the mobility of chemical groups in semisolid systems (Li et al., 1993).

Also, dipole-dipole interactions can occur between one spin and a distant neighbor spin via intermediate spins. Usually in such a very slowly tumbling multi-spin system the excitation of one spin can pass to the next spin, and the next. The propagation of population disturbance from one spin to another in this way is known as spin diffusion, although it is the population information that is diffusing, rather than the spins themselves. In the extreme slow tumbling limit, spin diffusion is both rapid and far reaching. This spin diffusion removes all the useful distance specificity from the NOE experiment in large

molecules. In order to avoid such spin diffusion in large molecules, the mixing time τ_m should be kept short (50-200 ms). If the time is sufficiently short, only the NOE between spatially close protons is observed before spin diffusion becomes more effective.

Quadrupolar Interaction H_Q

In addition to these magnetic interactions, nuclei with spin I>1/2 can have electric quadrupole moments. The quadrupolar interaction H_Q arises from the interaction of the nuclear electric quadrupole moment with the non spherically symmetrical field gradient around the nucleus. This interaction is usually larger than both the chemical shift and the dipolar coupling, so that the magnitude of the interaction (~180 kHz for ^2H and several MHz for ^{14}N) completely dominates the spectrum, even in the case of ^2H which has the smallest quadrupole moment. The direct consequence for the observation of quadrupolar nuclei (I = 1) is a doublet for an oriented single crystal and a characteristic wide static pattern for a powder. For the commonly studied ^2H nucleus, the quadrupolar coupling is vastly greater than the chemical shift range and the line shapes obtained reflect only the quadrupolar interaction. The relaxation times and the line shape for quadrupolar nuclei are very sensitive to the motions, and this type of NMR is a powerful tool in the study of molecular dynamics.

Nevertheless, the basic problem is that the spectral range is so large that it is hard to obtain uniform excitation and detection of the signal with pulse methods. So far as excitation is concerned, the highest possible rf field strengths and the shortest possible 90° pulse widths are used. Pulse widths down to 1-2 μs can be achieved reasonably routinely in probes employing a horizontal sample, corresponding to field strengths from 125 to 250 kHz. A spin echo, known in this case as the quadrupolar echo (Davis et al., 1976; Sternin et al., 1983), is used in order to regenerate the early part of the FID after a sufficient time for probe ringdown and receiver recovery. This technique substantially improves the detection of wide line shapes, but it is necessary to interpret the results with care in the presence of molecular motion because this may cause the line shape to become dependent on the choice of echo interval. In these studies, the well-defined shape of the signals is a function of the mobility of the deuterium environment.

Cross Polarization

The line-narrowing techniques of dipolar decoupling (DD) and magic angle spinning (MAS) provide the resolution necessary to obtain chemical and structural information on individual dilute spins in solids. Sensitivity still remains a problem with ^{13}C NMR and conventional pulsed FT NMR

detection (Bloch decay) suffers the disadvantage of requiring lengthy recycle delays because of the long T_1 of ^{13}C. The technique of cross polarization (CP) provides both signal enhancement and much shorter recycle delays after which spin polarization is transferred from abundant spins to dilute spins via the static dipolar interaction (Pines et al., 1972).

The key concept is that magnetization of the I- and S-spin systems can be brought to internal equilibrium along separate, applied magnetic fields in a rotating-frame experiment. If the I-spin magnetization is aligned along a RF field B_{1I}, stationary in a frame rotating at $\omega_{1I} = \gamma_I B_{1I}$, and the S spins are aligned along a field B_{1S}, stationary in a second rotating frame with $\omega_{1s} = \gamma_s B_{1s}$, the two spin systems can be brought into resonance and the I-S spin-flip process becomes allowed, provided:

$$\omega_{1I} = \gamma_I B_{1I} = \gamma_s B_{1s} = \omega_{1s} \quad (3)$$

Equation 3 is called the Hartmann-Hahn condition (Hartmann and Hahn, 1962). When this condition is satisfied, polarization transfer can take place to enhance the NMR signals of the dilute ^{13}C spins.

When reference is made to "magic angle spinning" ^{13}C NMR spectroscopy, what is almost always meant is the combination of cross polarization (CP), the actual rotation of the sample at the magic angle of $54^{\circ}44'$ (MAS) and dipolar decoupling (DD) of the ^{1}H nuclei from the observed ^{13}C nucleus (Stejskal and Schaefer, 1976). This is called a CPMASDD experiment. The CPMAS experiment has found wide application because it allows the regeneration of high-resolution ^{13}C spectra of solid materials.

In semi-solids, CP procedures are expected and found to be inefficient because of motional averaging, especially in liquid-like systems. Direct polarization (DP) or ramped-amplitude (Peersen and Smith, 1993) are the methods of choice for spectral acquisition in these samples. Direct polarization magic-angle spinning (DPMAS) ^{13}C NMR, either with 50-kHz high power decoupling (dipolar decouplig, DD) or 8-kHz low power decoupling (scalar decoupling, SD), will provide additional information about segmental motion (Li et al., 1993).

Figure I-1. Representation of a 90° radiofrequency pulse, Free Induction Decay (FID), and Fourier transformation of time domain FID into the frequency domain signal (Bovey, 1988).

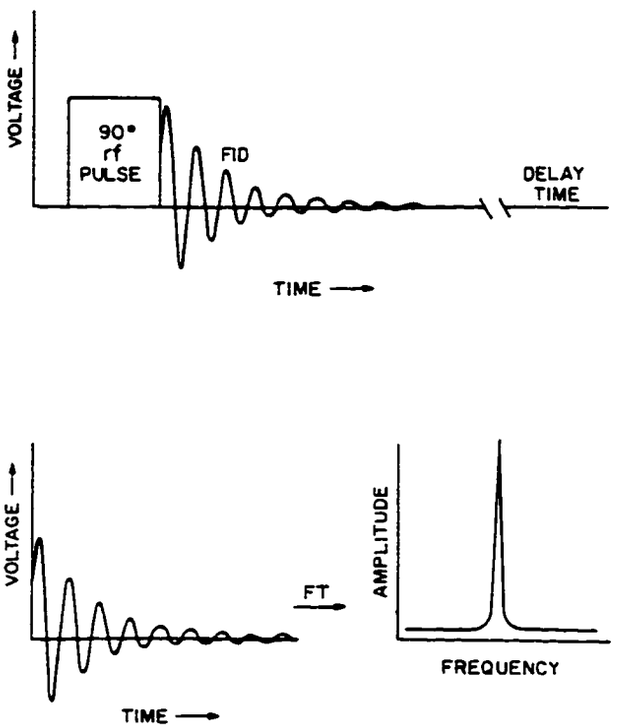

Figure I-2. The splitting of magnetic energy levels for two protons, expressed as resonance frequency V_0 as a function of magnetic field strength, expressed in tesla (T).

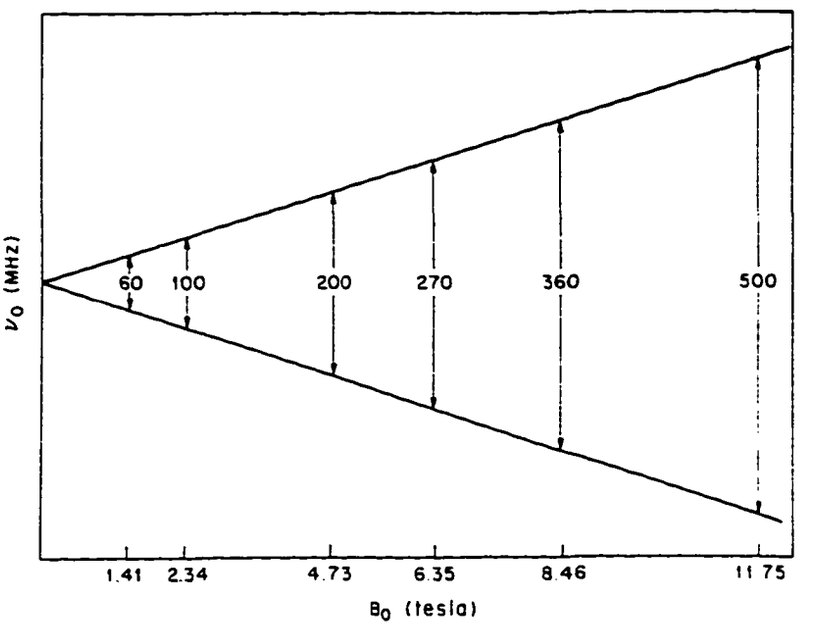

Figure I-3. ^{31}P NMR spectra of 1-palmitoyl-2-lysophosphatidylcholine in 23 wt% aqueous polyethylene glycol at different temperatures (Knowles and Marsh, 1991).

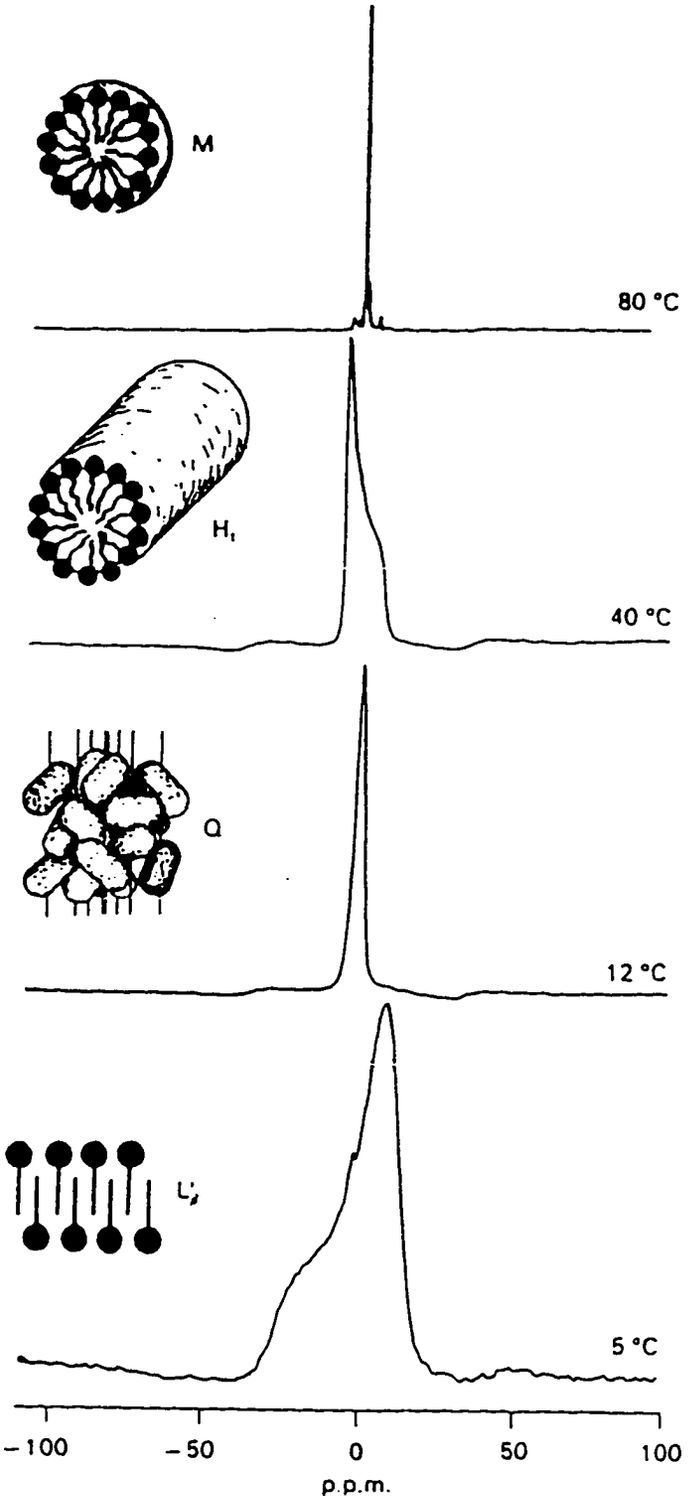

Figure I-4. Typical 500-MHz ^{1}H spectrum of a simple bile salt (sodium taurocholate) with presaturation to suppress the solvent (HDO) resonance.

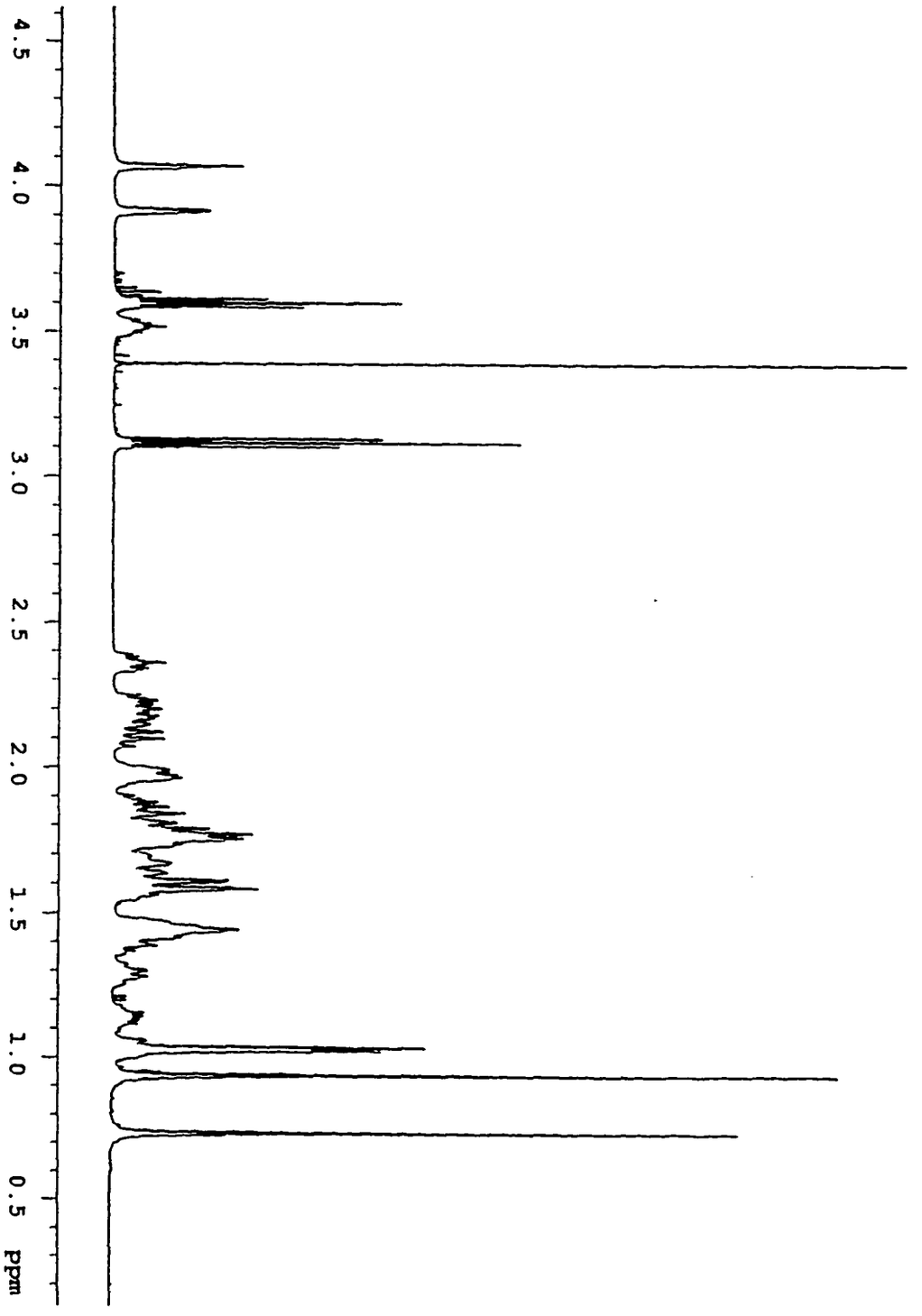

Figure I-5. The pulse sequence for two dimensional COSY NMR (Jeener, 1971).

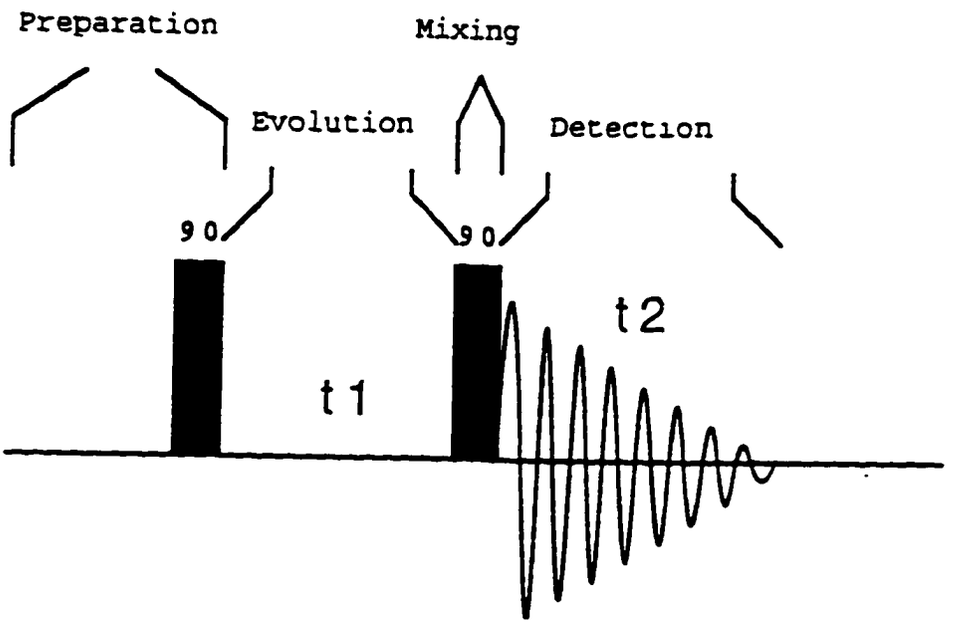

Figure I-6. The pulse sequence for two dimensional DQF-COSY NMR (Piantini et al., 1982).

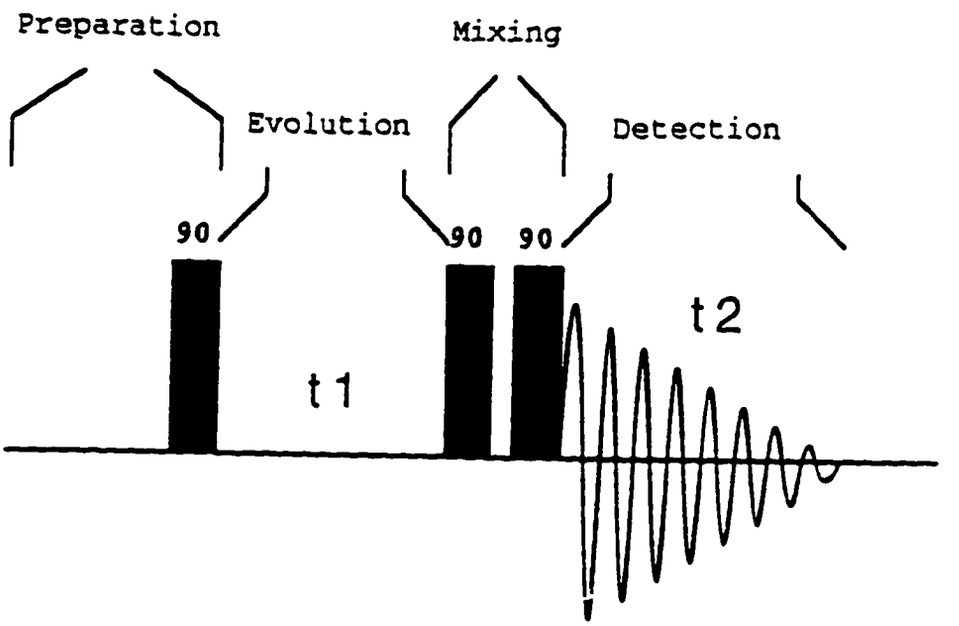

Figure I-7. The pulse sequence for two dimensional TOCSY NMR.

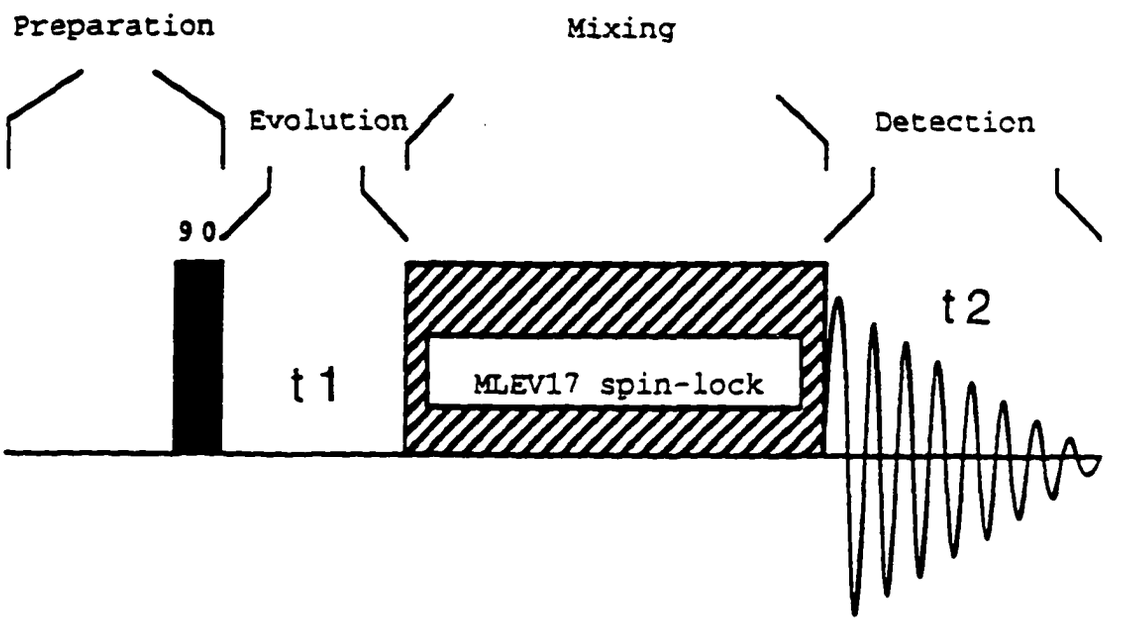

Figure I-8. The pulse sequence for two dimensional NOESY NMR (Jeener et al., 1979).

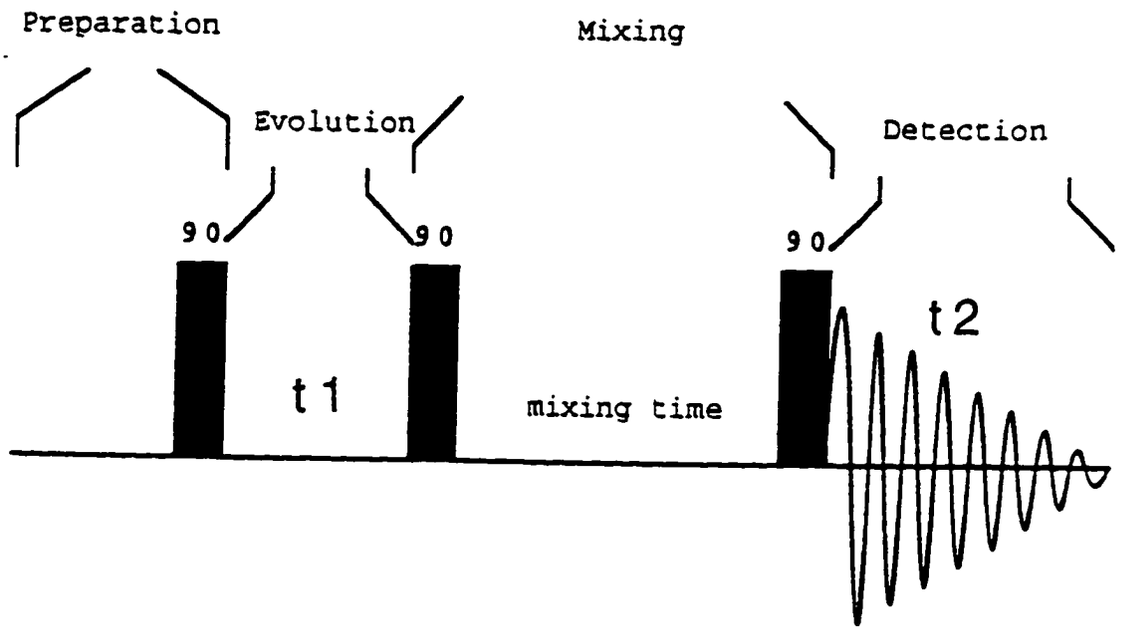

Figure I-9. The pulse sequence for two dimensional ROESY* NMR (Bax and Davis, 1985).

* The ROESY (ratio) macro sets up parameters for a ROESY pulse sequence, where the optional argument ratio is used to adjust the effective spin-lock field strength provided by the transmitter during the spin-lock period. If ratio is set too short, TOCSY peaks begin to appear.

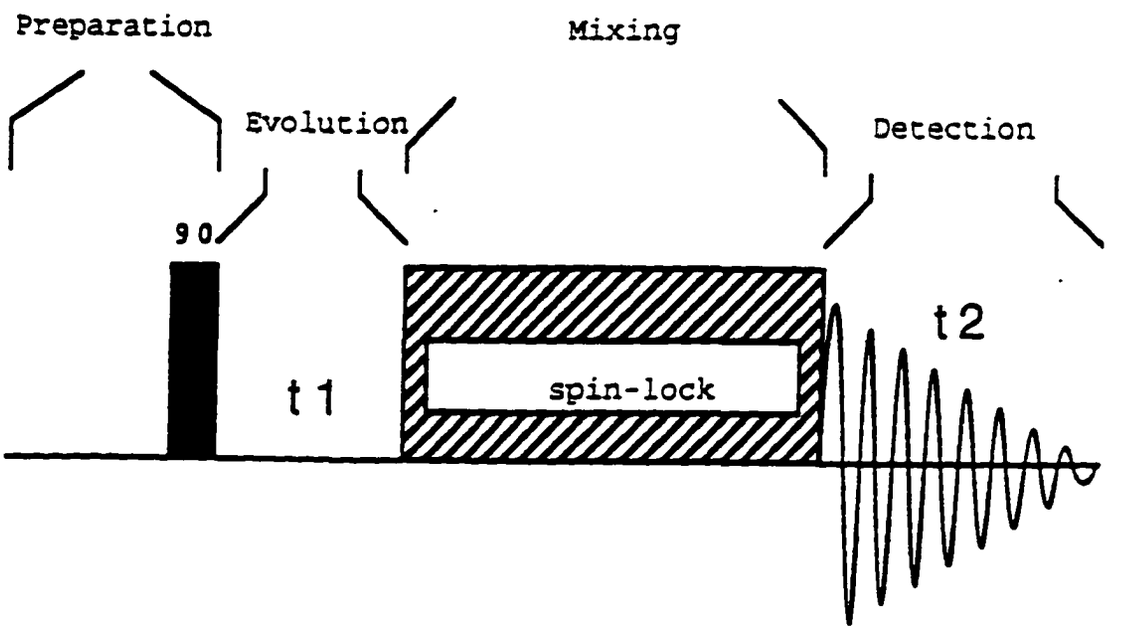

II. Materials & Methods

A. Sample Preparation

1. Chemicals

Caprylic (octanoic) acid (FA C_8), 1-monocapryloyl-*rac*-glycerol (MG C_8), and cholesterol (CH) were purchased from Sigma Chemical Company (St. Louis, MO); sodium taurocholate (BS) was obtained from Calbiochem (San Diego, CA). Deuterium oxide (99.96%) was purchased from Cambridge Isotope Laboratories (Woburn, MA), deuterium oxide (99.9%) was purchased from Isotec, Inc. (Miamisburg, OH), and manganese chloride was purchased from Aldrich Chemical Company (Milwaukee, WI). All lipids were commercially available and used without further purification: MeDOPE, brain sphingomyelin (SPM), egg PC, DOPC, DMPC-d_4, DMPC-d_9, DMPC-d_{54}, and DMPC-d_{27} were purchased from Avanti Polar Lipids Inc. (Alabaster, AL). All solvents were obtained Burdick and Jackson (Muskegon, MI).

2. Model Digestive Mixtures

Aqueous C_8 lipid samples were prepared from methanolic stock solutions of FA, MG, and BS constituents mixed volumetrically in the appropriate molar ratios, then dried under a stream of N_2 and under vacuum overnight to remove any remaining solvent. The mixtures were rehydrated in D_2O

buffer (100 mM phosphate, 150 mM NaCl, pH 6.5), incubated for 5 h and stored at 5 °C. All C_8 samples were optically clear and monophasic. The samples had a total lipid concentration of 2.00 g/dL and molar ratios of 20:80/20:1 and 20:80/1:1.25, respectively. The ratios denote MBS:MIL/FA:MG, where MBS = total bile salt concentration, MIL = FA + MG = total mixed lipid concentration, FA = fatty acid concentration, and MG = monoglyceride concentration. The final concentrations of each component are listed in **Table II-1**.

3. Model Membrane Mixtures

The lipids were first solubilized in 2:1 (v/v) chloroform-methanol, and dried under a stream of N_2 and at reduced pressure overnight to remove any remaining solvent. Aqueous dispersions were made by hydrating the lipid films (a) with D_2O buffer (20 mM Trizma, 1 mM EDTA, 150 mM NaCl, pH 7.6) for MeDOPE; and (b) with D_2O that was 150 mM in NaCl for other lipids at room temperature. The lipid-to-buffer weight ratio was 1:1, except as noted. The lipid dispersions were vortexed vigorously for 10 min and freeze-thawed at least five times using dry ice/acetone. The samples remained dispersed as a single phase for the duration of the MAS NMR experiments.

4. Lime Cutin

Cutin was isolated from the skin of limes as described previously (Walton and Kolattukudy, 1972; Deas et al., 1974; Pacchiano et al., 1993). Briefly, the procedure involved three steps: (1) removing peels from the fruit and disrupting the pectinaceous layer, (2) degrading residual pectin and other carbohydrates enzymatically, and (3) extracting waxes repeatedly from the cutin matrix.

To 500 mg of cutin were added 0.4 mL of deionized water and 20.0 mL of 1.5 N methanolic KOH; the mixtures were fitted with a reflux condenser and stirred at 70-75 °C for 8 or 22 h. Cutin monomers were extracted with chloroform:methanol (2:1) using standard procedures (Bligh and Dyer, 1959). The dried extract was weighed; typical yields were 60-65% and 80% for 8-h and 22-h alkaline hydrolysis, respectively. These materials were separated and analyzed for purity by reversed-phase HPLC (Ray et al., 1994).

5. Deuterium-Exchanged Tomato Cuticle

The tomato cuticle was prepared using published procedures (Walton and Kolattukudy, 1972; Deas et al., 1974; Pacchiano et al., 1993). Tomato cuticle (500 mg) was placed in a 25-mL round-bottom flask and dried in a vacuum oven at 80 °C for 24 h in the presence of phosphorus pentoxide. After the flask was sealed under dry nitrogen, 10 mL of D_2O

was added and the mixtures was refluxed 4 h under N_2, then the mixture was filtered to remove the solvent and dried again. This procedure was repeated five times, each time with fresh D_2O, to ensure complete exchange with deuterium. After the final treatment the sample was dried in a Speed-Vac for 48 h at 45 °C. A reference sample which had not been treated with D_2O was dried in a Speed-Vac 48 h at 45 °C under the same conditions.

B. NMR Spectroscopy

1. Solution-State ^1H NMR Experiments

1D- and 2D-^1H experiments were performed using any of three NMR instruments: Varian Unity*plus* -600 (^1H resonance frequency = 600 MHz) at the College of Staten Island; Varian Unity*plus* -500 (^1H resonance frequency = 500 MHz) and JEOL GX-400 (^1H resonance frequency = 400 MHz) at Hunter College. Data were processed using either Varian software or NMR1 software from Tripos/New Methods Research (St. Louis, MO) running on SUN Sparc I or IPX workstations (SUN Microsystems, Mountain View, CA). 1D ^1H NMR data were obtained using a one-pulse experiment with 8-μs or 18-μs 90° pulses and solvent irradiation during the relaxation delay of 1.5 s. High-resolution spectra were acquired with 32-64 signal-averaged free induction decays, each containing 16K-32K data points. A line broadening of 0.3-0.5 Hz was

usually applied prior to Fourier transformation. The spectral width was 5.25 ppm (Hz as governed by the field strength), and chemical shifts were referenced to external DMSO and also quoted with respect to CH_3-18 of taurocholate (0.73 ppm)

2. Solution-State ^{13}C NMR Experiments

1D ^{13}C experiments were performed with a Bruker/IBM Instruments WP-200 spectrometer (^{13}C resonance frequency = 50 MHz) at the College of Staten Island and were acquired with broadband decoupling of protons. Typically a spectral width of 12,500 Hz (250 ppm) was used. 6,000 transients were acquired due to the lower natural abundance of this nucleus compared with ^{1}H. A 2-s delay was used between successive transients of 16K data points; a line broadening of 10 Hz was applied to the data before Fourier transformation. Data were processed using NMR1 software from Tripos/New Methods Research (St. Louis, MO) running on a SUN Sparc I workstation (SUN Microsystems).

3. Solid-State Cross Polarization ^{13}C NMR Experiments

The solid state MAS-assisted NMR measurements were made using either of two NMR instruments: a Bruker/IBM Instruments WP 200 spectrometer, equipped with high-power amplifiers and a 7-mm Doty Scientific probe for magic-angle spinning; or Varian Unity*plus*-300 widebore spectrometer

equipped for both liquid-state and solid state NMR. Samples weighing 110-150 mg were packed into 7-mm cylindrical, double-bearing Zirconia rotors (Doty Scientific, Columbia, SC). For our wet samples, the Doty rotors were equipped with Macor end caps and O-ring seals. The resonance frequencies were 200.13 MHz (^{1}H) and 50.33 MHz (^{13}C) for the Bruker instrument or 300.00 MHz (^{1}H) and 75.440 MHz (^{13}C) for the Varian instrument. The sample temperature was regulated to ±1 °C with variable-temperature accessories. The NMR spectra were obtained with 4.0-5.0 kHz MAS, 47 kHz matched ^{1}H-^{13}C polarization transfer (CP) lasting 1.0 ms, 47 kHz ^{1}H decoupling during signal acquisition, and a 2-s delay between acquisitions. ^{13}C Chemical shifts are quoted with respect to tetramethylsilane, using *p*-di-*tert*-butylbenzene (DTBB) as a secondary substitution reference for 200-MHz NMR and using hexamethylbenzene (HMB) as a substitution reference for 300-MHz experiments.

4. Semi Solid-State ^{1}H, ^{13}C, and ^{31}P NMR Experiments

The NMR measurements were made using a Varian Unity*plus* -300 widebore spectrometer equipped for both liquid-state and solid-state NMR. The resonance frequencies were 300.00-MHz (^{1}H), 50.33 MHz (^{13}C), and 121.44 MHz (^{31}P), respectively. Spinning speeds (V_{rot}) were adjusted to 2000 (±5) Hz.

^{31}P NMR measurements conducted under static conditions were performed with direct polarization (Bloch decays), using 4-5 μs 90° pulses for phosphorus nuclei and a 42-kHz ^{1}H decoupling field during signal acquisition. Recycle delays of 4 s and auxiliary air flow through the center of the probe were used to control the temperature during these experiments. Typically, 1000 acquisitions of 4K time domain points spanning a spectral width of 24 kHz were zero-filled to 8K points, multiplied by a decaying exponential (line broadening of 50 or 100 Hz), and processed by Fourier transformation.

MAS ^{1}H NMR spectra were acquired with 14-ms 90° pulses, 10-kHz spectral widths, and 1.5-s recycle delays. Spinning speeds (ν_{rot}) were adjusted to 2000 (±5) Hz. In a typical experiment, 32 transients composed of 8K time-domain points were collected, zero-filled to 16K points, apodized with a decaying exponential corresponding to 0.3 Hz of line broadening, and subjected to Fourier transformation.

MAS-assisted nuclear Overhauser spectroscopy (^{1}H-^{1}H NOESY) was performed at ^{1}H frequency of 300.00 MHz. The pulse sequence $(90°\text{-}t_1\text{-}90°\text{-}\ t_m\text{-}90°\text{-acquire}\ [t_2])_n$ was employed with n = 16 and 256 t_1 values. The States method was employed for phase-sensitive acquisition (States et al., 1982). The mixing times were varied between 50 and 1000 ms

in separate 3-h NOESY experiments. All data were analyzed with VNMRX software (Varian Associates, Palo Alto, CA).

DP ^{13}C NMR was carried out with 5-μs 90° pulses, MAS as described above, and 50-kHz decoupling (dipolar decoupling) gated on during signal acquisition. Typical spectra used 1000-3000 acquisitions and 3-s recycle delays. CP ^{13}C NMR spectra were acquired with 4.8-kHz MAS, 47-kHz matched ^{1}H-^{13}C polarization transfer lasting 1.0 ms, 47-kHz ^{1}H decoupling during signal acquisition, and a 1-s delay between acquisitions. ^{13}C Chemical shifts were referenced as described above.

Table. II-1 Compositions of C_8 Model Digestive Systems*

Code#	MBS:MIL FA:MG	[BS]	[FA]	[MG]
20:1	20:80/ 20:1	18 mM	68 mM	3.4 mM
1:1.25	20:80/ 1:1.25	9.8 mM	17 mM	22 mM

* The mixtures had total lipid concentrations of 2,00 and 1.25 g/dL, respectively, and were prepared as described in Sample Preparation.

III. Studies of Model Mixtures for the Late-Stage Products of Triglyceride Digestion by Solution State NMR

A. Introduction

Lipids constitute an important part of the human and animal diet. The average Western adult consumes about 150 g of triglyceride and only 4-8 g of phospholipids each day. Triglycerides (TG) provide fatty acids for brain development and mediate cellular function in higher plants and animals (Brindley, 1991). Whereas the molecular details of glyceride digestion and absorption are not completely understood, the general mechanistic scheme is well documented.

Digestion and absorption of lipids involve several complex steps. These include: emulsification, lipase hydrolysis, aqueous dispersion and absorption **(Figure III-1)**. The coarse droplets of oil become coated with bile salts that help to disperse the oil droplets and impart a negative charge to their surfaces. They are located at the oil-water interface with their hydrophobic faces pointing into the oil and the hydrophilic surfaces interacting with the aqueous phase of the luminal contents. As would be expected, the hydrophobicity of TG's makes them insoluble in

aqueous solution and requires phospholipid and bile-salt (BS) detergents to promote the formation of stable emulsion particles. The water-soluble lipase and colipase enzymes, which are responsible for triglyceride digestion, are activated by these substrate aggregates, with hydrolysis presumably occurring at the oil-water interface. As digestion proceeds, the monoacylglycerols, fatty acids, lysophospholipids, cholesterol, and bile salts dissociate from the surface of the oil droplets to form a micellar solution (Brindley, 1991). In this work, we refer to the emulsions as the Early-Stage Substrates and the micellar solutions as Late-Stage Products.

Although most prior studies of molecular structure have focused on the digestive enzymes (Winkler et al., 1990; van Tilbeurgh et al., 1993), the studies presented herein focus on the late-stage digestive products because this step is the rate-limiting step for fat absorption. Given the functional importance of the late stage aggregates in fat absorption, determination of their molecular structure represents a vital step towards understanding their role. The mixtures examined in this work each contain a bile salt (taurocholate), a monoglyceride (C_8 acyl chain), and a fatty acid (C_8 acyl chain), combined in physiologically appropriate ratios (Carey et al., 1983). These medium-chain-length FAs and MGs typify the main products of milk

and butter fat digestion. In addition, C_8 analogs are administered therapeutically to patients suffering from digestive dysfunction (Mascioli et al., 1989).

Significant work has been done on the equilibria, size and polydispersity for related C_{18} samples using light microscopy and quasielastic light scattering (QLS) (Staggers et al., 1990). The mixtures consisted of mixed intestinal lipid (oleic acid, monoolein, diolein, and PC), mixed bile salts (mixture of 10 glycine- and taurine-conjugated bile salts), and cholesterol at various molar ratios, total lipid concentrations, and pH. The investigators showed that the mixed-lipid systems form multiphase mixtures with physical chemical and equilibration properties that depend on what proportion of each component is present and whether micelles, vesicles, or liquid crystals are formed. For related C_{14}-based model digestive mixtures, both ^2H NMR spectra and X-ray diffraction patterns have been used to distinguish micellar, multilamellar, and crystalline states (Westerman, 1995).

Although the individual lipid components in digestive mixtures have well-known molecular structures, little direct information has been obtained regarding their organization within aggregate assemblies. To obtain complementary information at the molecular level, nuclear magnetic

resonance of these mixed-lipid assemblies has addressed such issues as particle surface composition, bilayer formation and asymmetry, and dynamic behavior of different lipid constituents.

Previous investigations of the C_8 analogs have confirmed the presence of mixed aggregates of bile salts, fatty acid, and monoglyceride in aqueous solution by examining several NMR parameters (^{13}C spin-lattice T_1 relaxation time and $^{13}C\{^1H\}$ NOEs) in both aqueous and methanolic solutions and suggested that the fatty mixtures are forming mixed micellar monomers of the three components. Additionally, the results of the NMR study allowed the carbons to be grouped into the following types: interfacial, hydrophobic and hydrophilic (Wang et al., 1992). The segmental tumbling times and local order parameters derived from these experiments are consistent with micellar structures in which the alkyl chains are packed in an organized fashion and a belt of polar groups covers the aggregate-water interface.

Whether the samples are in a solution state or a semisolid state, NMR provides details of molecular structure for both stages involved in lipid digestion. With the wide availability of high-field NMR spectrometers and multidimensional techniques have come enhanced spectral

resolution and improved information regarding both though bond and through-space proton interactions. Though the well developed protocols for peak assignment in peptides and proteins are inappropriate for the interconnected spin systems of steroids and glycerides, it is possible to extend the two-dimensional NMR methods used for steroids (Croasmun and Carlson, 1994) in order to assign all ^{1}H and ^{13}C resonances in a complex digestive mixture. This assignment information paves the way for other NMR experiments with proven applicability to micellar aggregates: paramagnetic broadening of aqueous-accessible functional groups (Burns and Roberts, 1981; Stark et al., 1985); and two-dimensional nuclear Overhauser enhancements (NOESY) between proton pairs that are close in space (Stark et al., 1986; Gabriel and Roberts, 1987). A detailed model for molecular organization in BS/MG/FA aggregates is proposed and evaluated in the context of digestive function.

B. Results

1. ^{1}H NMR Assignments of a C_8 FA-Rich Mixture 20:1 (MBS:MIL/FA:MG = 20:80/20:1)

The results described here are derived from 1D and 2D high resolution solution NMR spectral studies on late-stage model mixtures for triglyceride digestion. The 500-MHz 1D

^1H NMR spectrum of C_8 mixture 20:1 (MBS:MIL/FA:MG = 20:80/20:1) is shown in **Figure III-2**. The methyl protons (BS-18, BS-19, BS-21, and FA-8), some methylene protons (BS-25, BS-26, FA-2, and FA-3), and the protons at carbon atoms with hydroxyl groups (BS-3β, BS-7β, and BS-12β) were easily identified from conventional 1D NMR spectra, by analogy with published data (Barnes and Geckle, 1982; Campredon et al., 1986; Halvorsen et al., 1989; Davis and Thompson, 1993; Croasmun and Carlson, 1994). Many of the individual protons cannot be assigned because of signal overlap, even with a high field NMR spectrometer. In particular, the steroid protons of BS in the upfield portion of the spectrum (1.0-2.5 ppm) complicate the assignment. In order to obtain structural information it is first necessary to identify these protons in our system using a combination of DQF-COSY and TOCSY techniques (Zakrzewka et al., 1994).

The analysis of the DQF-COSY spectrum always begins at good entry points in the spectrum. In our steroid system it is necessary to find more than one entry point and repeat the process for different parts of the molecule.

The protons at C atoms with hydroxyl groups (BS-3β, BS-7β, and BS-12β) are readily recognized. BS-2, BS-1, BS-6, BS-8, and BS-11 are also connected in some way with other signals in the spectrum **(Figure III-3)**. Use of their

further scalar connections allowed us to locate the next set of neighbors, and so on, until all that set of connections has been used. Another entry point is BS-23 from the side chain, whose chemical shift can be identified at 2.37 and 2.21 due to its proximity to the carbonyl group. Then, BS-23 permits assignment of the BS-22 and their coupled partners BS-20, and so on until the assignments confirm the position of BS-17 using the first entry point. **Figure III-4** shows the upfield region of the TOCSY spectrum at short mixing time (10 ms), which can be used to confirm the spin systems and make these assignments unambiguous. In addition, we can easily assign the FA-2, FA-3, FA-4-7, and FA-8 based on the DQF-COSY data. The complete ^1H assignments for bile salt and C_8 mixture 20:1 are presented in **Table III-1**.

2. Surface Accessibility of Protons in Model Digestive Aggregates

The paramagnetic property of Mn^{2+} makes it a good structural probe to study accessibility of functional groups within the BS/MG/FA micelle to the aqueous environment (Burns and Roberts, 1981; Stark et al., 1985). Generally, resonances from protons (or carbons) that are accessible to the paramagnetic reagent such as Mn^{2+} are preferentially broadened in the NMR spectrum. We used Mn^{2+} titrations to

determine which groups in sample C_8 20:1 (MBS:MIL/FA:MG = 20:80/20:1) are exposed to the aqueous environment. Significant differences occur between hydrophobic groups at the micellar interior and boundary groups at the lipid-water interface (Wang et al., 1992). The FA(2) near the surface active hydroxyl groups is more strongly affected by Mn^{2+} than any other group. The effects of Mn^{2+} on the FA acyl chain (FA (4)-(8)) and on the methyl groups on the steroid ring (18,19) are negligible **(Figure III-5)**. A similar situation is observed for sample 1:1.25 (MBS:MIL/FA:MG = 20:80/1:1.25). The 2' and 3' positions of MG are the most sensitive to Mn^{2+}, because MG 1' is a boundary group and MG 2', 3' are hydrophilic groups exposed to the aqueous solution **(Figure III-6)**. When the relative concentration of the three components is changed, Mn^{2+} additions produce similar broadening trends **(Figure III-7)**. Thus, the organization and surface accessibility are probably similar in the two sample.

3. Mn^{2+}-induced ^{13}C NMR Spectra of a C_8 Sample

It is logical to ask why the FA boundary group is so different from other boundary groups if they are located in the same position within the aggregate. It seems that being at the boundary is not a sufficient explanation. In addition, the relative Mn^{2+}-induced effect for boundary

groups should depend on the distance and the relative affinity of Mn^{2+} for the group of interest. Different electron charges on each chemical group could also affect the Mn^{2+}-induced changes. Since all carboxyl groups are deprotonated at pH 6.5, Mn^{2+} binding to the carboxyl groups should neutralize the negative charge and allow a closer approach.

We tried to use the Mn^{2+}-induced ^{13}C NMR line broadening to discriminate between carboxyl groups on FA, MG, and BS components of the micellar aggregate. Addition of high concentrations (0.251 mM and 0.331 mM) of Mn^{2+} caused the carboxyl group of FA to be selectively broadened and reduced the peak height compared with the other carboxyl groups from MG and BS **(Figure III-8)**. The carboxyl groups of MG are not affected even with very high concentrations of Mn^{2+}. These results are not surprising since the carboxyl groups of MG are thought to be located in boundary groups, and the carboxyl groups of FA or BS are located in hydrophilic groups that are exposed to Mn^{2+}. Of course, more detailed explanations probably require further experiments.

4. NOESY and ROESY of a C_8 20:1 Model Digestive Mixture

2D NOESY and ROESY provide a powerful and easily exploited method for solution-state structure determination. NOE interactions for steroids in organic solution have been reported previously (Laurance and Sanders, 1980 & 1981). The NOESY spectra can be crowded with strong geminal and axial-equatorial crosspeaks, and they generally lack crosspeaks for longer range NOE interactions. These latter interactions, the 1,3-diaxial arrangements of hydrogens and methyls in the rigid steroid framework and cross-ring proximities, may be observed using 1D difference NOEs. The NOEs observed for simple BS micelles in water are all very weak. They are found between protons geminal to the hydroxyl groups, methyl protons and nearby steroid protons. So far no published reports of NOESY exist on mixed-lipid systems.

Figure III-9 shows the NOESY spectra of BS **(III-9a)** and C_8 20:1 mixture **(III-9b)**, which were acquired at short mixing time (200 ms) in order to avoid spin diffusion. Both BS and C_8 20:1 have strong cross peaks between protons geminal to the hydroxyl groups, methyl protons and nearby steroid protons. But only in C_8 20:1 mixture are there many longer range crosspeaks between the BS methyl protons (18,19), the 1,3-diaxial protons (11β, 6β, 8β, and 15β), the protons at carbon with hydroxyl groups(3β, 7β, and 12β) and protons at side chain (20,21,22). These interactions arise

from the restraint of motion due to the formation of large aggregates and the presence of dimers (or tetramers) within such aggregates, compared to the monomers in organic solution or dimers in dilute aqueous solution.

Peak overlap becomes extensive with increasing molecular weight and complexity, making ambiguous the assignment of either COSY- or NOESY-type spectra. In our case many NOESY cross peaks crowd the upfield region between 0.73 ppm and 2.5 ppm. Intramolecular interactions between the geminal and vicinal protons will appear in both NOESY and TOCSY spectra, whereas intermolecular through-space interactions (e.g. BS18/BS7β,12β,11, and BS/FA) will appear only in the NOESY experiments. It is then possible to simply superimpose 2D TOCSY on 2D NOESY to isolate the long-range through space cross peaks for the C_8 20:1 mixture **(Figure III-10)**.

Usually, large molecules or molecular aggregates move sluggishly and exhibit crosspeaks with the same sign as the diagonal peaks in the spectrum (negative NOE effects). Small molecules with more motion have crosspeaks with opposite sign to the diagonal (positive NOE effects). In our simple BS system most crosspeaks have the same sign as the diagonal peaks, but the protons of the side chain (25,26,22,23) have the opposite sign. This suggests that

these protons may be located at the aggregate surface where they can undergo more motion.

It is interesting that the FA in C_8 20:1 mixture has both positive and negative cross peaks. An example is shown in **Figure III-11-a**. The proton (23) at side chain no longer has negative cross peaks. Two molecular species may be present: a large aggregate with less motion and a small dimer (Oakenfull and Fisher, 1977) or micelle with fast motion.

As mentioned earlier, unfavorable correlation times may lead to the 'crossover' region for NOEs (ω_c near 1.12), and hence to a situation in which there are weak crosspeaks or no crosspeaks. In addition, NOESY crosspeak intensities are very sensitive to different individual correlation times within the same molecule. This can easily lead to misinterpretation of NOESY data in terms of spatial proximity. These pitfalls may be important for our BS/MG/FA system, since both large and small aggregates may be present and both positive and negative crosspeaks are observed experimentally.

Our solution for these problems is provided by a ROESY experiment. In contrast to the NOESY, the ROESY effect is always positive (negative crosspeaks with respect to the

diagonal). Conversely, COSY, TOCSY, and spin-diffusion interactions appear as crosspeaks which have signal intensity in phase with the diagonal (Bax and Davis, 1985). ROESY is therefore a powerful experiment for discriminating between true NOEs and spin-diffusion effects.

ROESY spectra collected for C_8 20:1 mixture were found to contain both types of crosspeaks, indicating the presence of scalar and dipolar interactions. However, careful analysis of the ROESY spectrum shows modest but clearcut intercomponent NOE interactions. This is shown in **Figure III-11-b**, in which diagonal has one contour and cross peaks are shown with 20 contours. There are some crosspeaks between FA(2) and BS(22) that did not show up in NOESY. This intermolecular dipole-dipole interaction may be located in the intermediate motional regime for which $\omega_c = 1.12$. **Tables III-2** and **III-3** list the NOE interactions that are observed for BS and C_8 20:1 mixture, classified according to whether they are intra- or intermolecular in origin.

C. Discussion

The mixture we studied here contains a bile salt (taurocholate), a C_8 saturated monoglyceride, and a C_8 saturated fatty acid, combined in physiologically appropriate ratios (Carey, 1983). This is an excellent

model for the late-stage products of triglyceride digestion. The individual lipid components in digestive mixtures have well-known molecular structures, but little direct information has been obtained regarding their organization within aggregate assemblies. Previous researchers of the C_8 system have confirmed the presence of mixed aggregates of bile salt (BS), fatty acid (FA), and monoglyceride (MG) in aqueous solution by examining $T_1(^{13}C)$ relaxation times and $^{13}C\{^1H\}$ NOE (Wang et al., 1992). They concluded that there are different mobilities and order for different groups in the aggregate and that these motions depend on the location (hydrophilic groups, hydrophobic groups, and boundary groups). The segmental tumbling times and local order parameters derived from these experiments are consistent with micellar structures in which the alkyl chains are packed in an organized fashion and a belt of polar groups covers the aggregate-water interface.

In agreement with these previous results, our high-field and multidimensional NMR studies provide extensive NMR evidence to support the formation of mixed micellar aggregates in the C_8 mixture. In addition to the appearance of new NOESY crosspeaks when bile-salt dimers are incorporated into larger mixed aggregates, the particle organization exposes only selected molecular moieties to the surrounding aqueous environment. By looking at both ^1H and

^{13}C NMR spectra, we can obtain a more unified picture of which constituents and which regions are most sensitive to Mn^{2+} additions. Although backbone positions 2' and 3' of the MG are aqueous accessible, neither position 1' nor its associated carbonyl group appears to be situated close to the paramagnetic ion. The lack of broadening effects for BS steroid groups is entirely expected, but surprisingly modest effects are also observed for protons and carbonyl groups of its polar side chain. Finally, the most dramatic Mn^{2+}-related broadening is observed for polar positions of the FA constituent. This last result is consistent with the proposed location of these groups near the aqueous interface of the mixed micelle. In addition it suggests that especially close contacts between Mn^{2+} and COO^- groups are permitted by both steric and electrostatic effects.

The paramagnetic broadening experiments support the overall expectation that hydrophilic groups are most accessible to the aqueous solvent, whereas hydrophobic groups are protected form water by the aggregate organization. Nonetheless, the high Mn^{2+} to-amphiphile ratios required to induce broadening in the BS/MG/FA mixtures suggest that the multicomponent digestive aggregates are more tightly packed than previously studied phospholipid-triglyceride micelles (Burns and Roberts, 1981)

and can accommodate fewer water molecules within their micellar structure.

In the simple bile salt system, Small et al. (1969) proposed that bile salts form two types of globular aggregates: primary and secondary micelles. Primary micelles have 2 to 9 monomers held together based on the hydrophobic interaction between the hydrophobic "back" of the steroid framework. Then, larger aggregates are formed by hydrogen bonding between the hydroxyl groups of the primary micelles. The Oakenfull and Fisher rod-like model is different in that the first stage of aggregation is the formation of hydrogen bonded dimers; larger aggregates are formed by "back-to-back" hydrophobic interaction (Oakenfull and Fisher, 1977). The formation of a hydrogen bond is accompanied by a decrease in volume, whereas association due to the hydrophobic interaction is accompanied by an increase in volume (Nemethy and Scheraga, 1962; Oakenfull and Fisher, 1977).

In our more complex bile salt - fatty acid - monoglyceride systems, useful information regarding aggregate structure and organization comes from the observation of the dipolar interactions using NOESY and ROESY experiments. Both simple bile-salt solutions and the C_8 20:1 mixture show a large number of intracomponent NOEs,

with the most informative spectral features being long-range intramolecular NOEs (not geminal or vicinal) and intermolecular BS-BS NOEs found especially in the C_8 20:1 mixture **(Table III-2)**.

The NOESY/ROESY connectivities between BS and FA (or MG) protons confirm the involvement of FA (or MG) molecules in large molecular aggregates **(Table III-3)**. We looked for essential features such as (a) back-to-back bile-salt dimers with extensive intermolecular interactions between the steroid skeletons **(Figure III-12a)**; (b) hydrophobic interactions between bile salts and fatty acid acyl chains **(Figure III-12b)**. Several intercomponent crosspeaks observed in NOESY/ROESY spectra of the C_8 20:1 mixture are of particular structural interest: the FA(2)/BS-20 and FA(2)/BS-16β crosspeaks confirm that these proton may be located at the lipid-water interface, whereas the hydrophobic FA(8)/6β and FA(8)/5β crosspeaks suggest that these steroid protons are located at the hydrophobic micellar interior. Thus these crosspeaks constrain the relative alignment of BS and FA molecules as shown in **Figure III-12b**. The computer models shown in **Figure III-13** predict distances less than 5 Å corresponding to 14 of 15 the intermolecular NOESY crosspeaks shown in **Table III-3**.

These NMR observations are consistent with prior proposals of micellar structures in which the alkyl chains of the FA are packed with the hydrophobic steroid skeletons of BS in an organized fashion and a belt of polar groups such as FA(2) and BS(20,21 etc.) covers the aggregate-water interface (Wang, et al., 1992). This overall picture of the aggregate is built up from our observation of back-to-back structures in the bile salt tetramers and back-to-FA (or MG) interaction in the C_8 20:1 mixed micelles. In addition, the observation of more long-range BS-BS crosspeaks (as compared with simple BS micelles) fits well with our hypothesis of tightly packed mixed micelles that accommodate fewer water molecules within their structure.

We may propose two new structural models for the micellar aggregates involved in glyceride absorption, in which only hydrophilic groups are exposed to water and hydrophobic groups are extensively associated, either in a globular or a disklike arrangement **(Figure III-14)**. Although both of these models are consistent with our prior ^{13}C NMR relaxation studies of mixed-micelle aggregates, only "tennis-ball" proposal fits well with the pattern of aqueous accessibilities deduced from the Mn^{2+} titrations and the NOE-derived proximities discussed above.

In our globular model of C_8 20:1 mixtures, it is possible to imagine the first stage of aggregation consisting of the formation of hydrogen bonded bile-salt dimers. Then, the tetramers are formed by "back-to-back" hydrophobic interactions, allowing larger aggregates that involve the hydrophobic parts of FA and MG **(Figure III-13)**.

Finally, it is possible to test the tennis-ball model of late-stage model digestive mixtures against quasielastic light scattering (QLS) estimates of aggregate size for the C_8 20:1 mixture (Wu and Stark, unpublished results). As shown in **Figure III-15**, the predominant particles present in this mixture have a hydrodynamic diameter of ~25 nm; very few large aggregates contribute to the scattering intensity, and any small FA dimers would scatter the laser light too weakly to be observed. For a globular arrangement of BS and FA molecules such as that proposed in **Figure III-14**, standard molecular dimensions allow us to estimate a size of ~4 nm. A possible structural arrangement that accounts for this discrepancy in size would add water molecules at the hydrophilic interior of the tennis ball.

Table III-1. ^{1}H NMR Resonance Assignments for Sodium Taurocholate and a C_8 20:80/20:1 Late-stage Model Digestive Mixture

	Chemical Shift (ppm)			
Bile salt Proton No.	TC α-Protons	TC β-Protons	Mixture α-Protons	Mixture β-protons
1	1.82	1.01	1.84	1.01
2	1.40	1.68	1.43	1.70
3		3.51		3.52
4	2.10	1.74	2.15	1.74
5		1.44		1.44
6	1.60	1.97	1.63	1.95
7		3.91		3.92
8		1.59		1.55
9	2.18		2.18	
11	1.64	1.56	1.66	1.59
12		4.06		4.06
14	1.88		1.92	
15	1.76	1.14	1.80	1.12
16	1.98	1.29	2.01	1.29
17	1.78		1.82	
18		0.73		0.73
19		0.93		0.93

20		1.43		1.44
21		1.02		1.02
22	1.44	1.76	1.48	1.75
23	2.36	2.22	2.37	2.21
25	3.59		3.59	
26	3.11		3.11	

Glyceride Proton No.	Mixture Chemical Shift (ppm)
(2)	2.24
(3)	1.60
(4)-(7)	1.34
(8)	0.91
1'	4.19
2'	4.00
3'	3.64, 3.72
[2]	2.41
[3]	1.66
[4]-[7]	1.36
[8]	0.92

Table III-2. Intramolecular NOEs for a C_8 20:80/20:1 Late-Stage Model Digestive Mixture**

Connectivity, ppm	Proton Assignments	Description	ROESY phase
4.06, 1.82	12β, 17α/15α/1α	cross-ring	
4.06, 1.66	12β, 11α(3)	vicinal	
4.06, 1.59	12β, 11β	vicinal	
4.06, 1.02	12β, 21/1β	ring-methyl	
4.06, 0.73	12β, 18	ring-methyl	
3.92, 1.95	7β, 6β	vicinal	
3.92, 1.81	7β, 15α/17α	cross-ring	
3.92, 1.63	7β, 6α	vicinal	
3.92, 1.55	7β, 8β	vicinal	
3.59, 3.11	25, 26	vicinal	+/-
3.52, 2.15	3β, 4α	vicinal	absent
3.52, 1.74	3β, 4β/22β	vicinal	
3.52, 1.70	3β, 2β	vicinal	
3.52, 1.43	3β, 2a/5β/20β	vicinal	
3.52, 1.01	3β, 1β/21	1,3-diaxial	
2.37, 1.02	23α, 21/1β	other	
2.24, 1.60	(2), (3)	vicinal	+/-
2.21, 1.02	23β, 21/1β	other	
2.18, 1.92	9α, 14α	1,3-diaxial	absent

2.01, 1.82	16α, 17α	vicinal	+
2.01, 1.12	16α, 15β	vicinal	
1.95, 1.63	6β, 4α	geminal	
1.95, 0.93	6β, 19/(8)	1,3-diaxial	
1.92, 1.80	14α, 15α	vicinal	
1.92, 1.12	14α, 15β	vicinal	
1.84, 1.01	1α/17α, 1β/21	geminal	
1.84, 0.93	1α/17α, 19/(8)	ring-methyl	
1.80, 1.12	15β/17α, 15β	geminal	
1.70, 1.01	2β, 1/21	vicinal	
1.66, 0.93	11α/(3), 19/(8)	ring-methyl	
1.60, 1.34	(3), (4)-(7)	vicinal	+/-
1.59, 0.93	11β, 19/(8)	1,3-diaxial	
1.59, 0.73	11β, 18	1,3-diaxial	
1.55, 0.93	8β, 19/(8)	1,3-diaxial	
1.55, 0.73	8β, 18	1,3-diaxial	
1.44, 1.02	20β/2α/5β,21/ 1β	vicinal	
1.44, 0.93	5β/2α/20β, 19(8)	other	
1.44, 0.73	20β/2α/5β, 18	other	
1.43, 1.01	2a/5β/20β, 1β/21	vicinal	+
1.29, 1.12	16β, 15β	vicinal	
1.29, 0.73	16β, 18	other	

1.12, 0.73	15β, 18	other
1.02, 0.73	21/1β, 18	other

Table III-3. Intermolecular NOEs for a C_8 20:80/20:1 Late-Stage Model Digestive Mixture

Connectivity, (ppm)	Proton Assignments	Description	Distance(Å)
4.06, 0.93	12β, 19	back-to-back	2.1
3.92, 1.12	7β, 15β	back-to-back	4.9
3.92, 0.93	7β, 19	back-to-back	4.2
3.92, 0.73	7β, 18	back-to-back	4.2
2.24, 1.44	(2), 20	BS-FA	4.0
2.24, 1.29	(2), 16β	BS-FA	2.1
1.95, 0.91	6β, (8)	BS-FA	3.8
1.80, 0.73	15α/17α/1α,18	back-to-back	1.5
1.66, 0.73	11α/6α, 18	back-to-back	3.8
1.60, 0.93	(3), 19	BS-FA	4.0
1.60, 0.73	(3), 18	BS-FA	?
1.44, 0.91	5α, (8)	BS-FA	4.9
1.34, 0.93	(4)-(7), 19	BS-FA	4.0
1.34, 0.73	(4)-(7), 18	BS-FA	4.7
0.93, 0.73	19, 18	back-to-back	3.6

Figure III-1. Schematic representation of lipid digestion and absorption in the small intestine (Brindley, 1991).

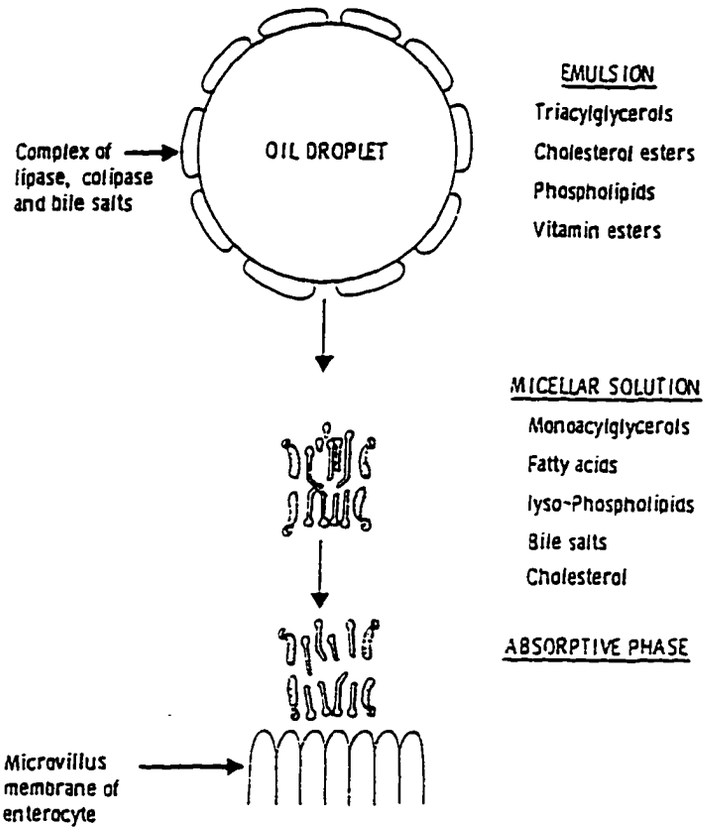

Figure III-2. Typical 500-MHz 1D ^{1}H NMR Spectrum of C_8 20:1 mixture with presaturation to suppress the solvent (HOD).

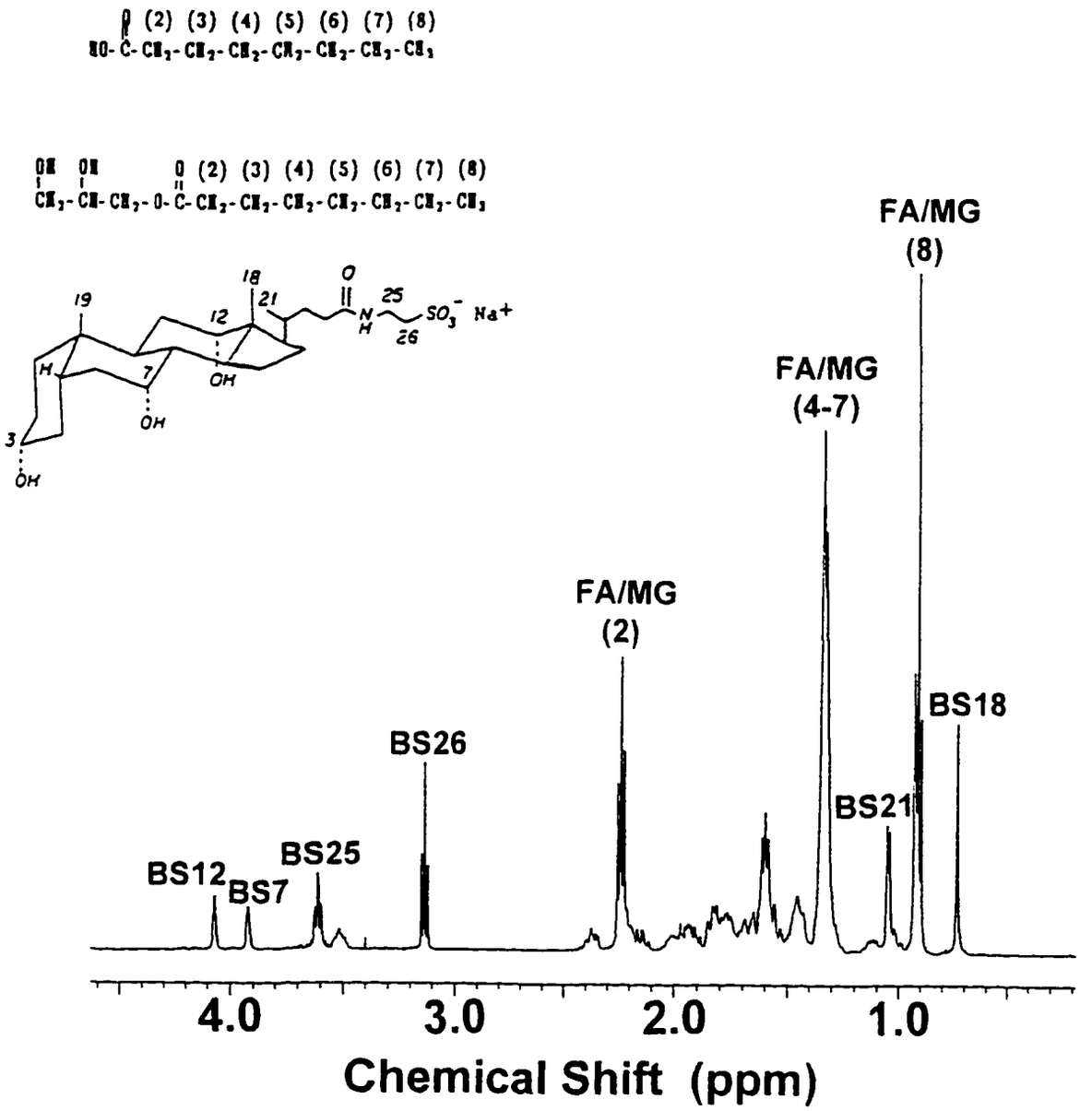

Figure III-3. 2D 500-MHz DQFCOSY spectrum of C_8 20:1 mixture in D_2O: Upfield portion of the spectrum.

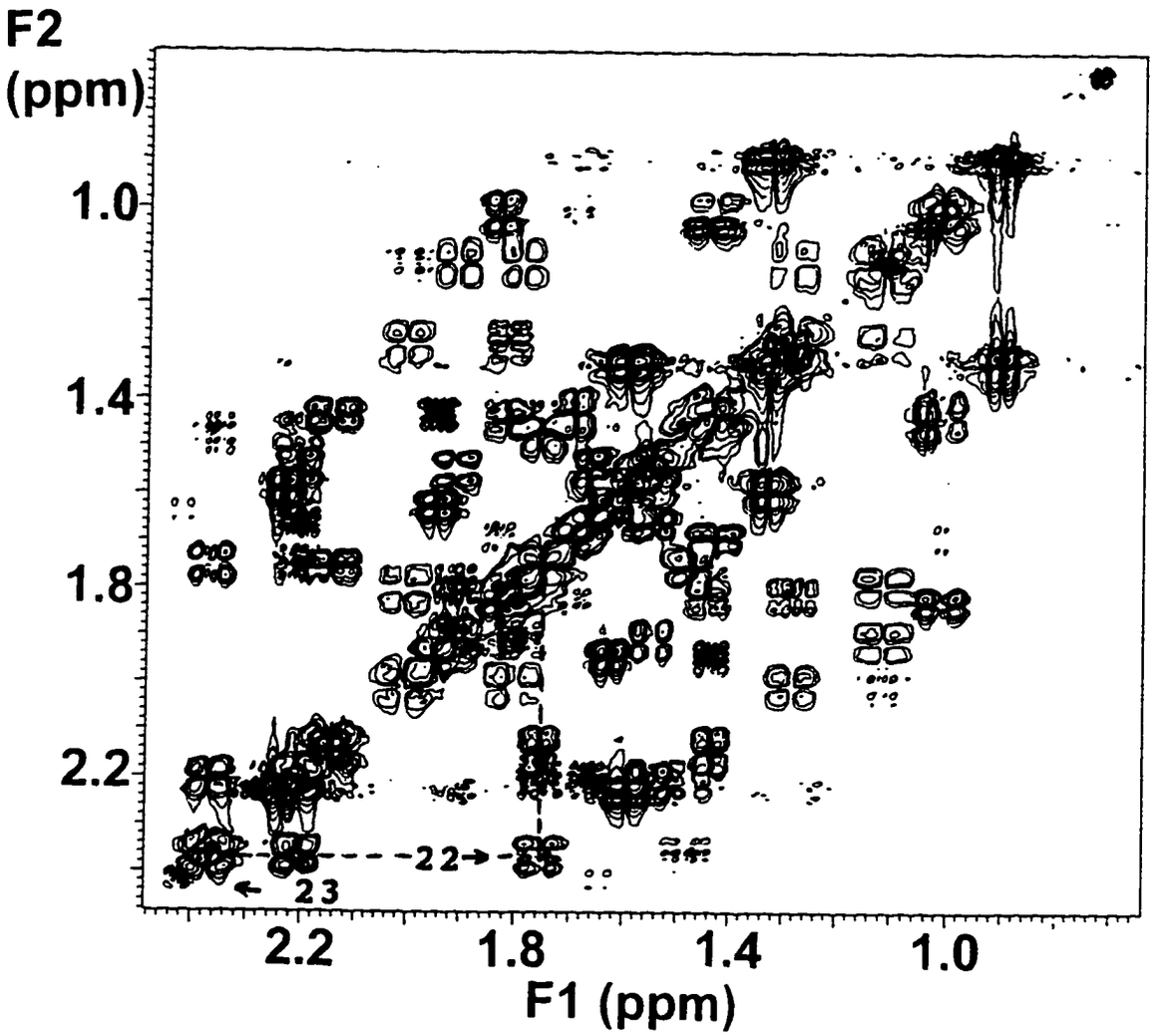

Figure III-4. 2D 500-MHz TOCSY spectrum of C_8 20:1 mixture in D_2O at mixing time τ_m = 10 ms: Upfield portion of the spectrum.

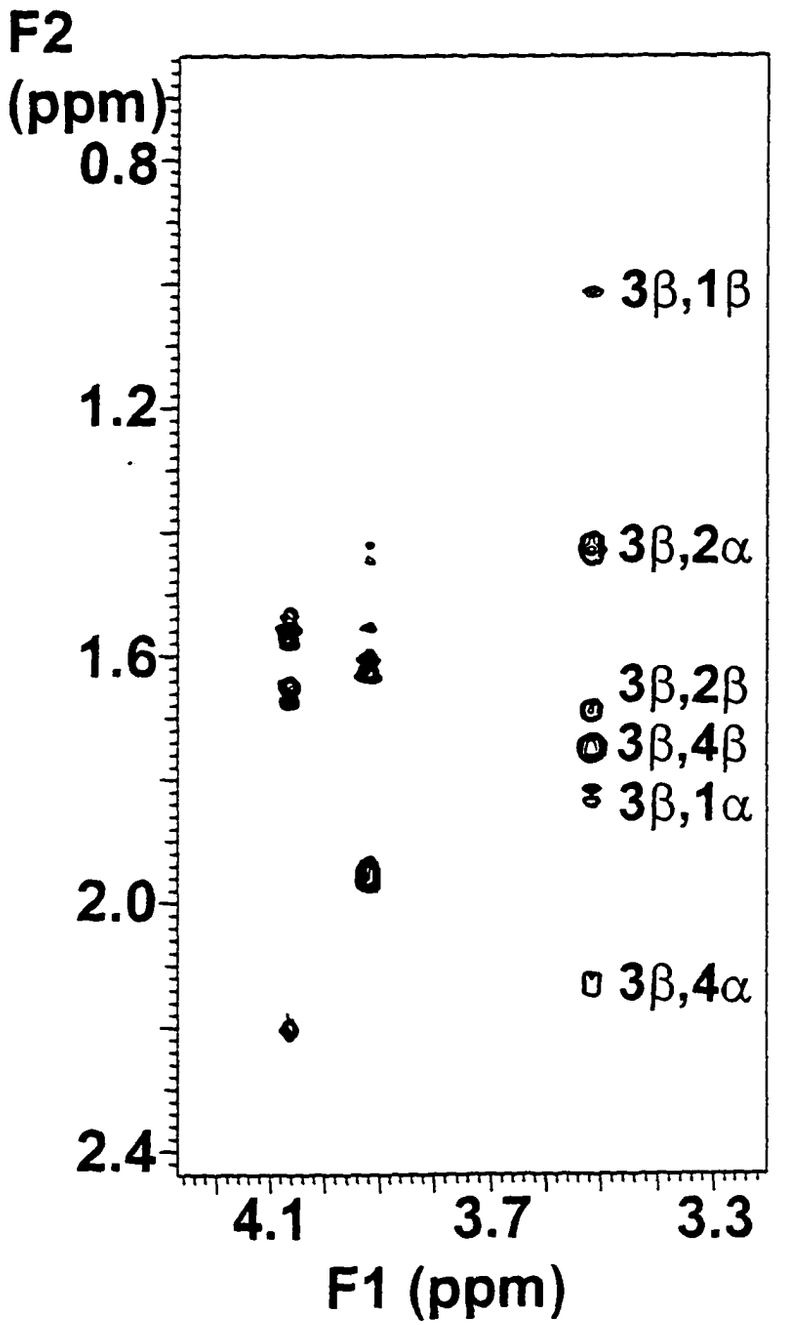

Figure III-5. 1D 400-MHz ^{1}H NMR spectrum C_8 20:1 mixture with added Mn^{2+}.

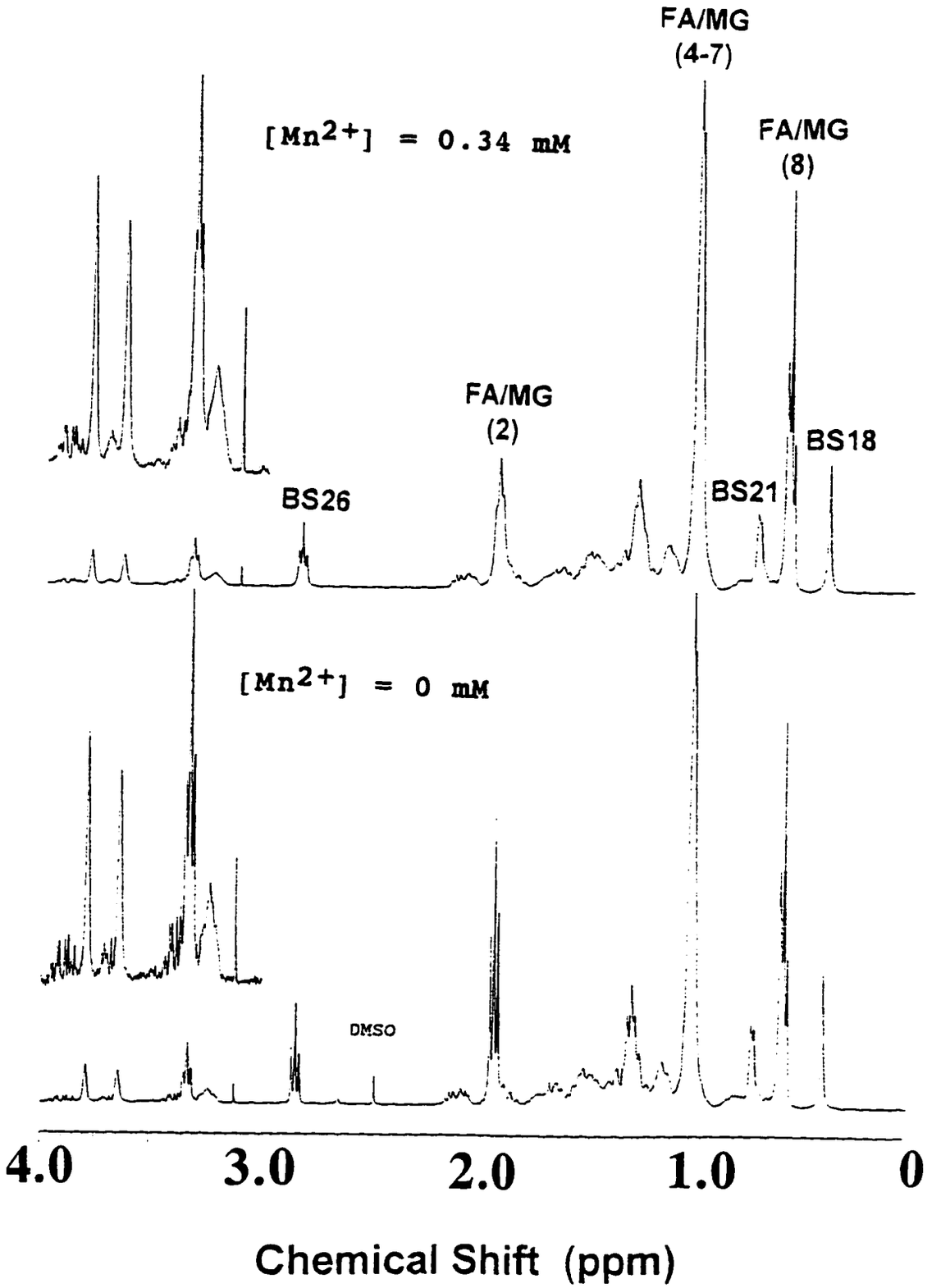

Figure III-6. 1D 400-MHz ^{1}H NMR spectrum C_8 1:1.25 mixture with added Mn^{2+}.

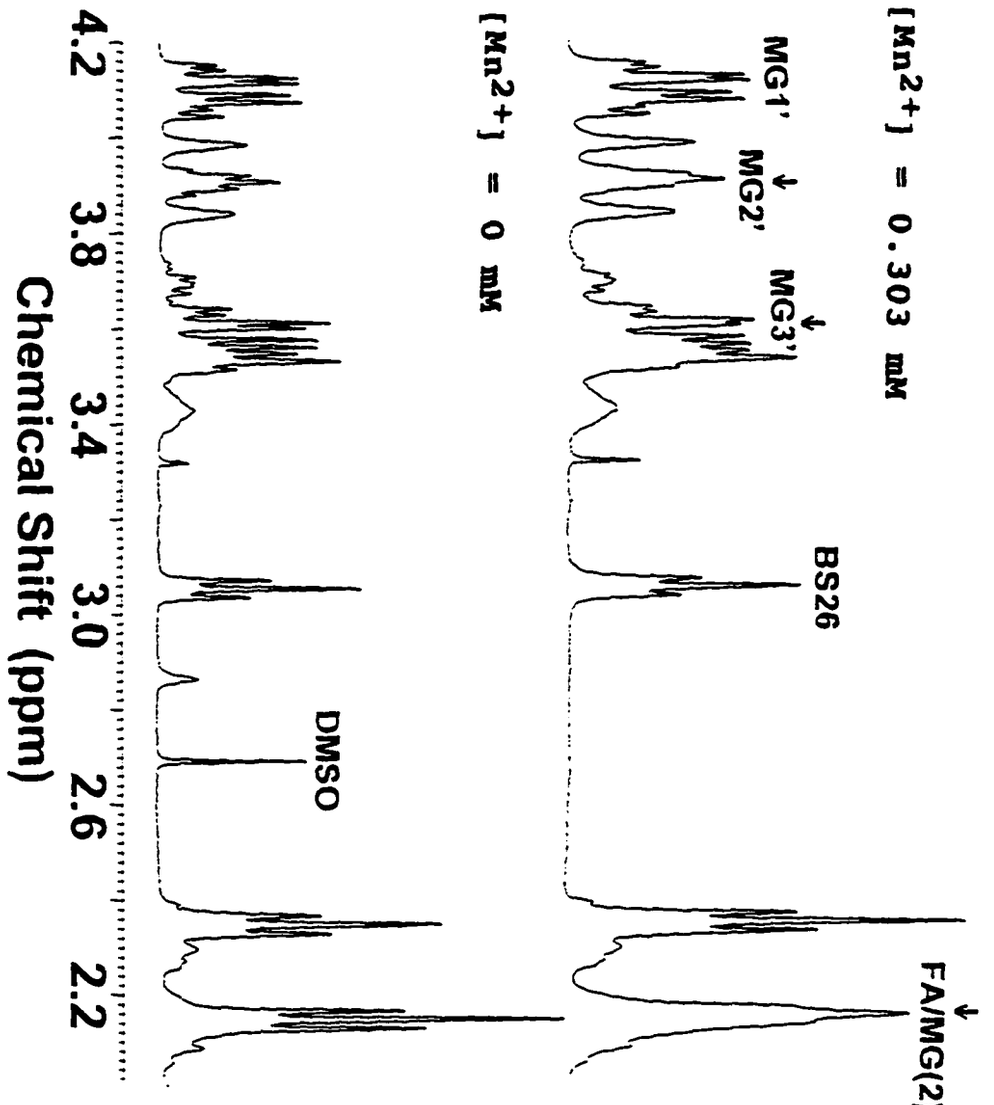

Figure III-7. $MnCl_2$ titrations of proton line width for C_8 20:1 mixture and C_8 1:1.25 mixtures.

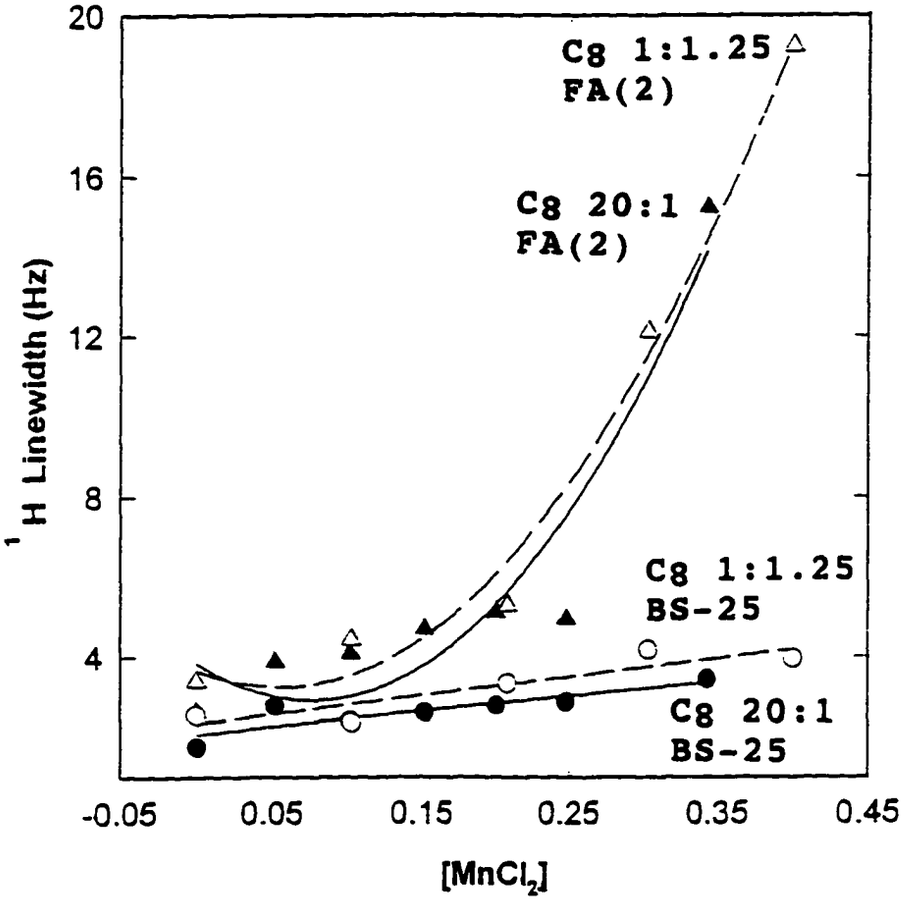

Figure III-8. 1D 50-MHz ^{13}C NMR spectrum C_8 20:1 mixture with added Mn^{2+}.

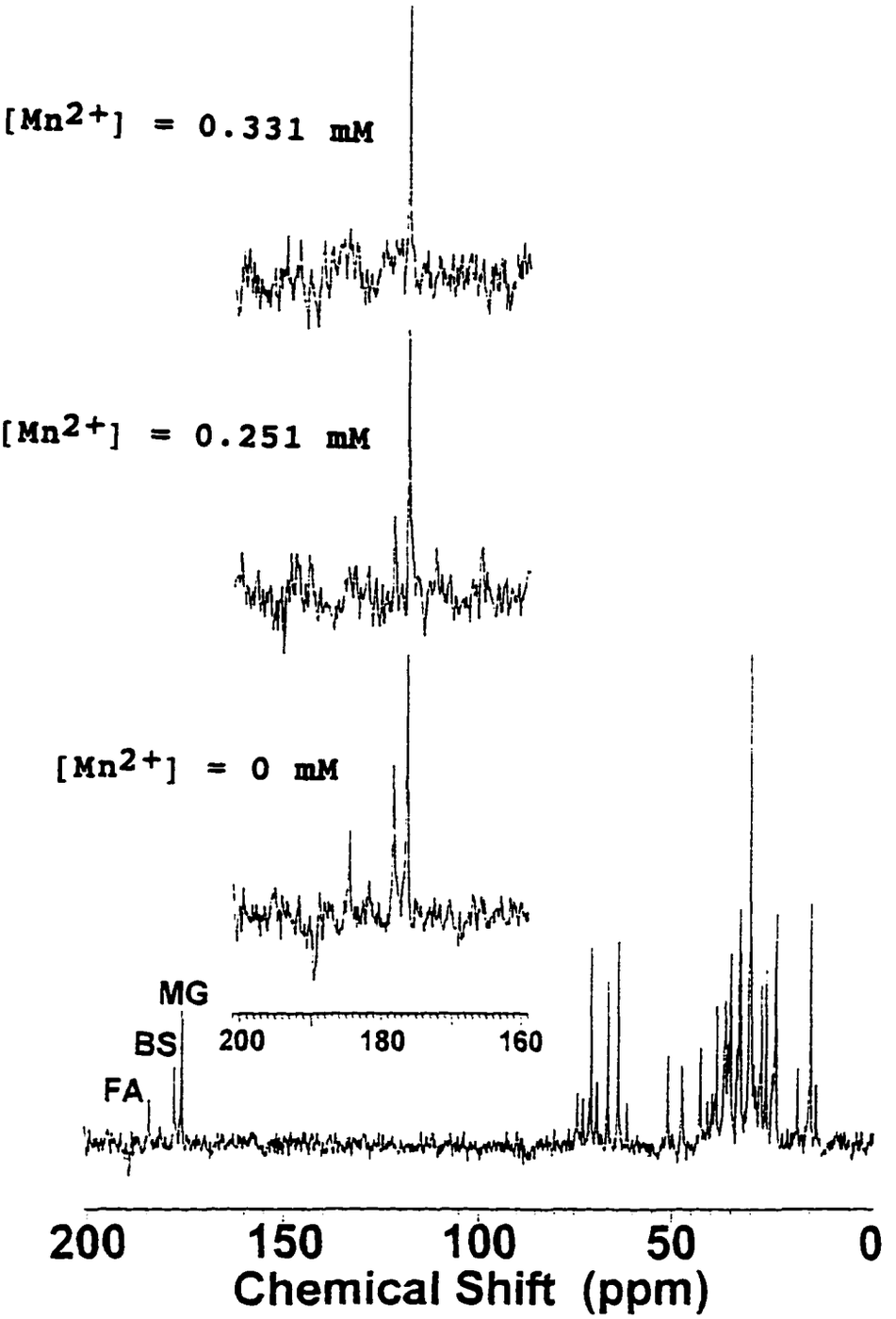

Figure III-9. 2D 500-MHz NOESY spectrum (τ_m = 200 ms) of simple BS (20 mM) and C_8 20:1 mixture in D_2O: a. Bile salt; b. C_8 20:1 mixture.

a

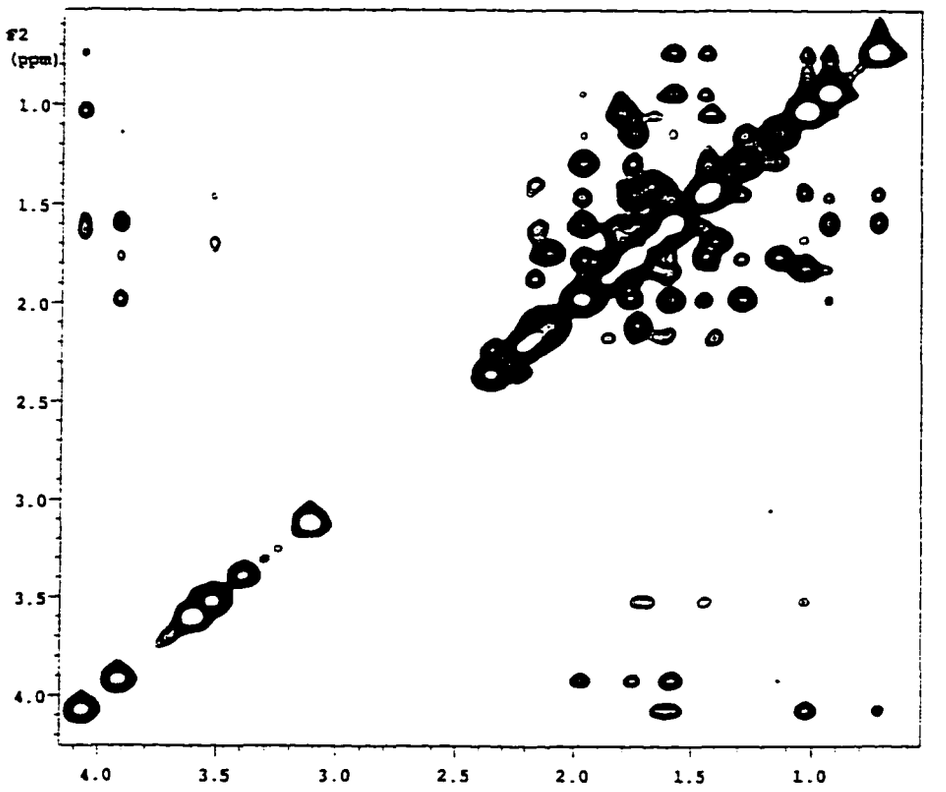

b

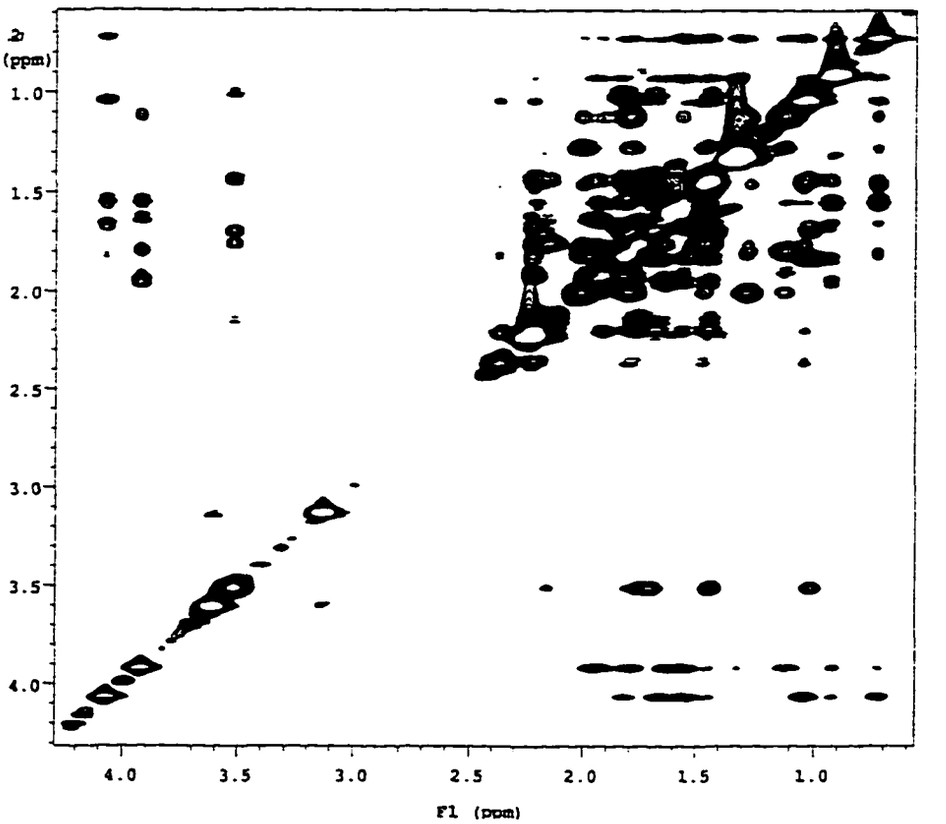

Figure III-10. 2D 500-MHz TOCSY superimposed on the 2D 500-MHz NOESY spectrum of C_8 20:1 mixture.

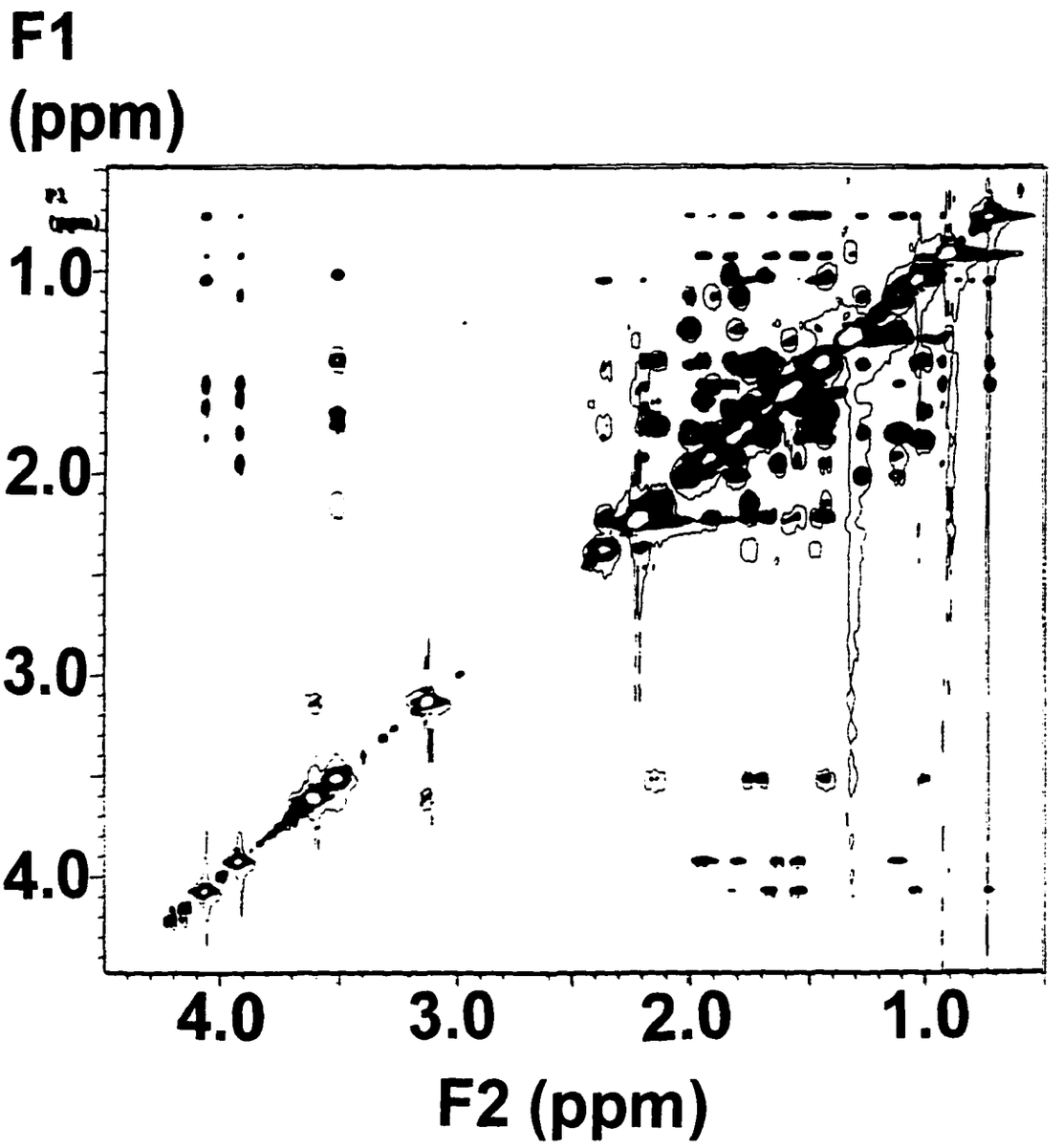

Figure III-11. a. 2D 500-MHz NOESY spectrum (τ_m = 200 ms) of C_8 20:1 mixture in D_2O; b. 2D 600-MHz ROESY spectrum (τ_m = 120 ms) of C_8 20:1 mixture in D_2O.

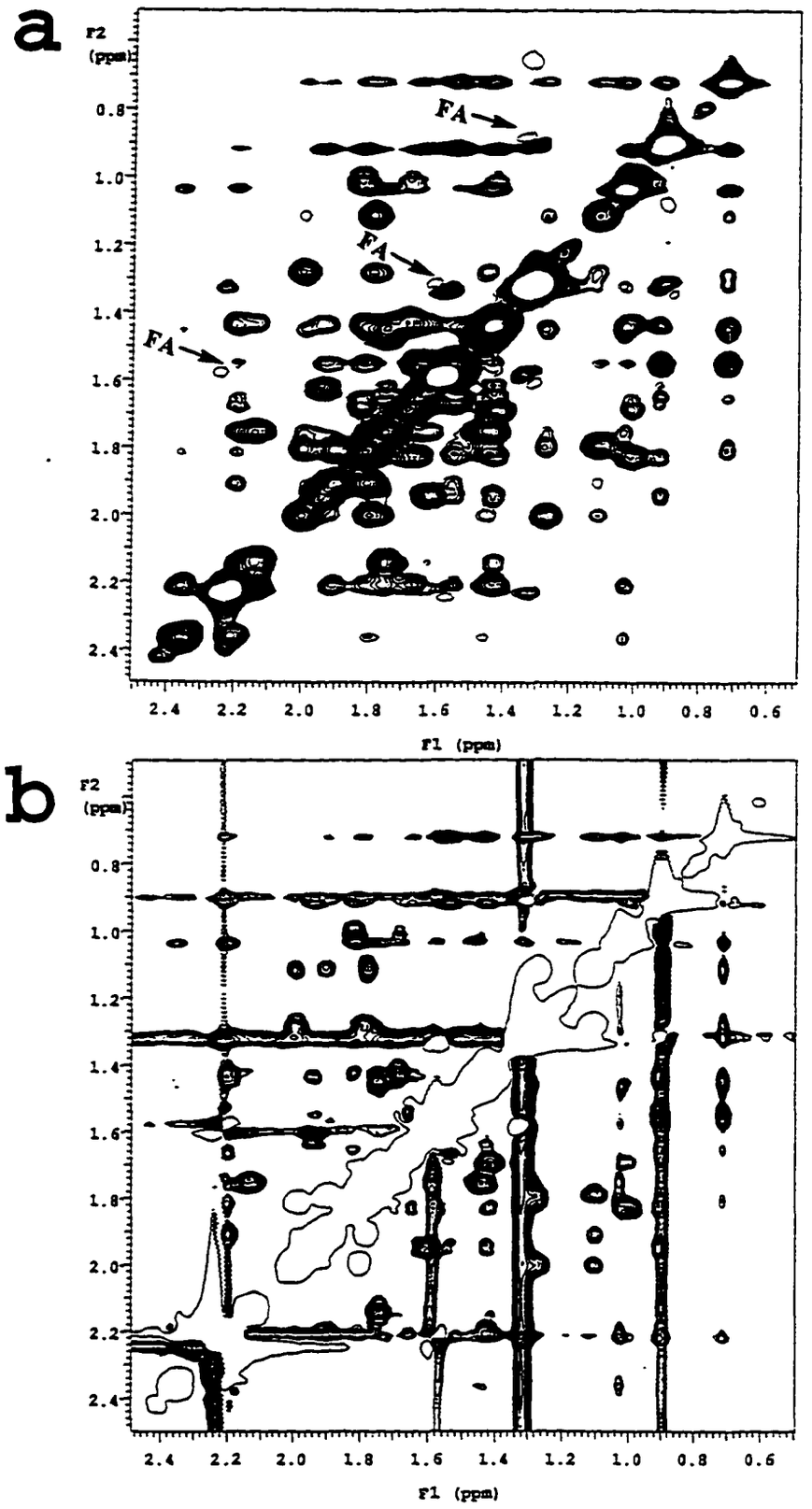

Figure III-12. Two computer models for spatial relationships of the C_8 20:1 mixture. a: back-to-back bile-salt dimers; b: bile salts and fatty acid.

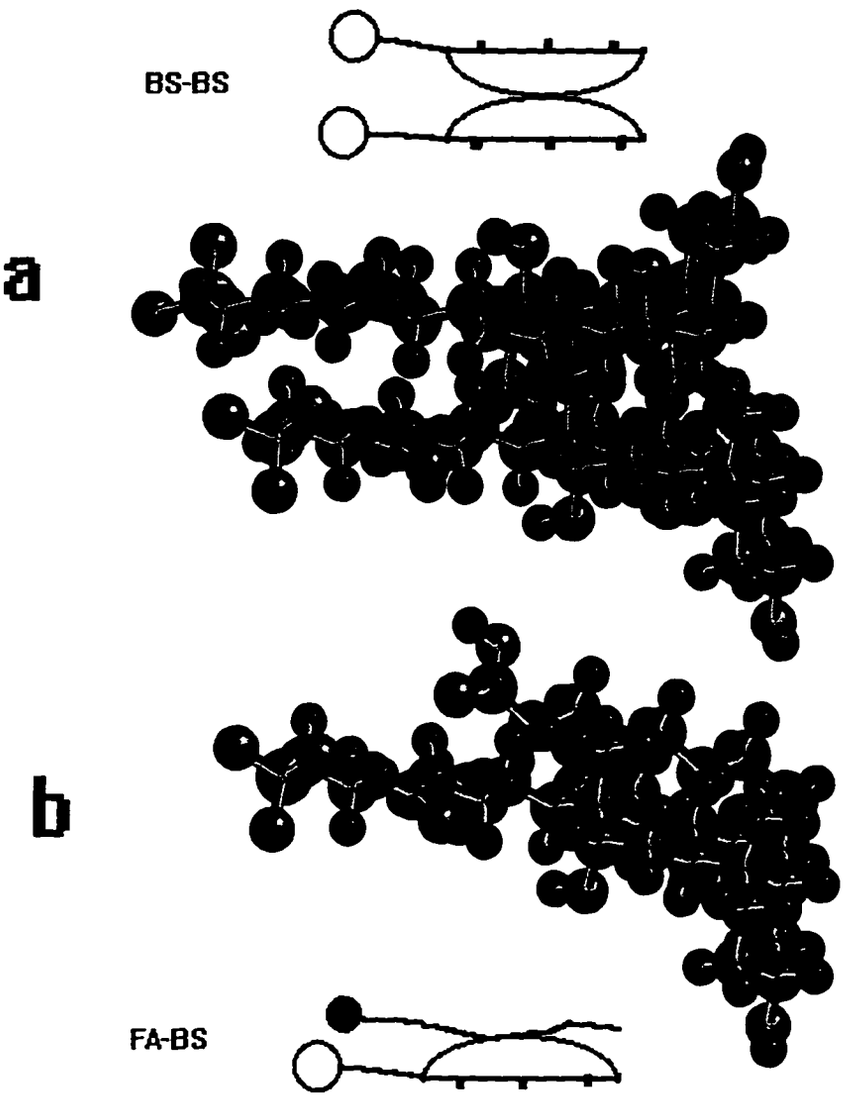

Figure III-13. Computer models for the formation of molecular aggregates in the C_8 20:1 mixture.

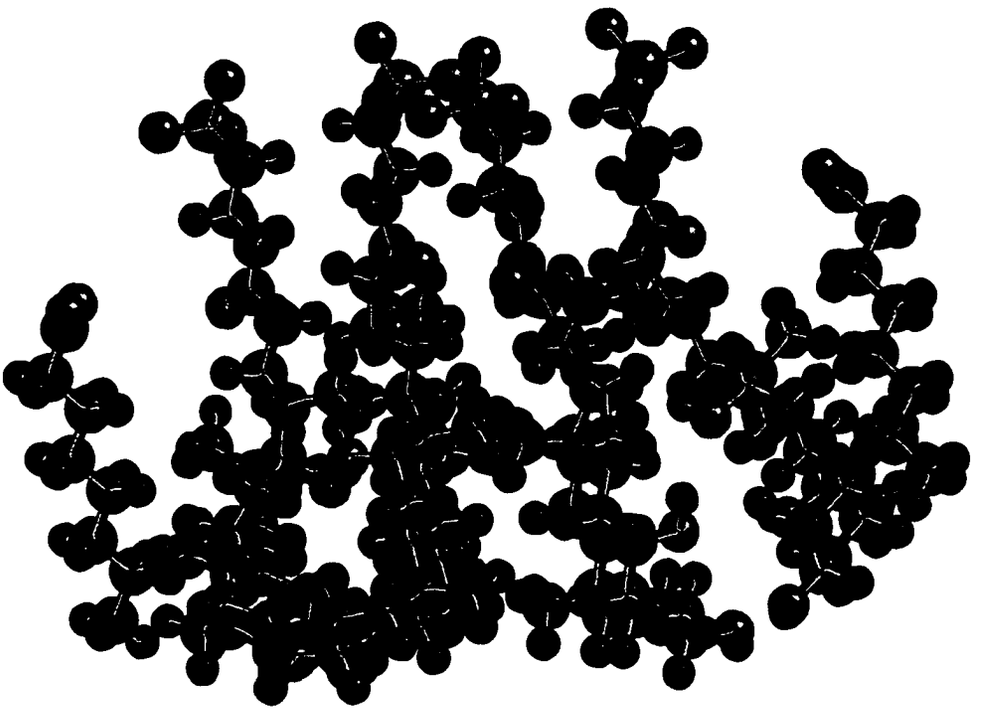

FA-BS-BS-BS-BS-FA

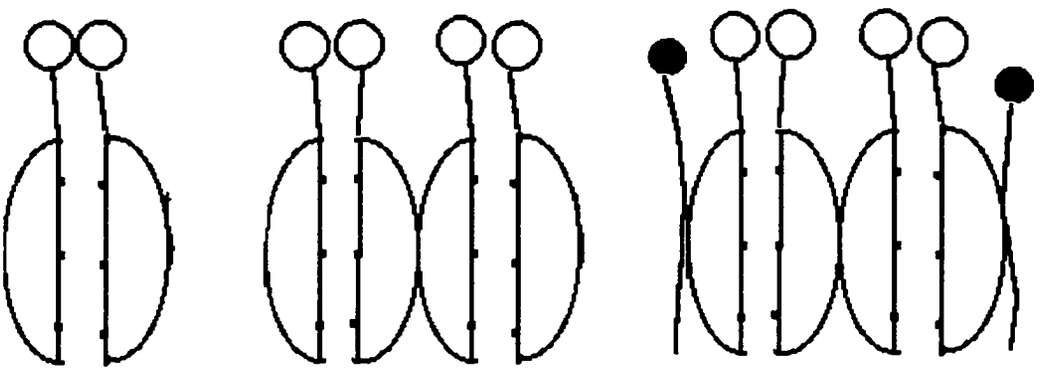

BS-BS BS-BS-BS-BS FA-BS-BS-BS-BS-FA

Figure III-14. Two new models for molecular aggregates in the C_8 20:1 mixture.

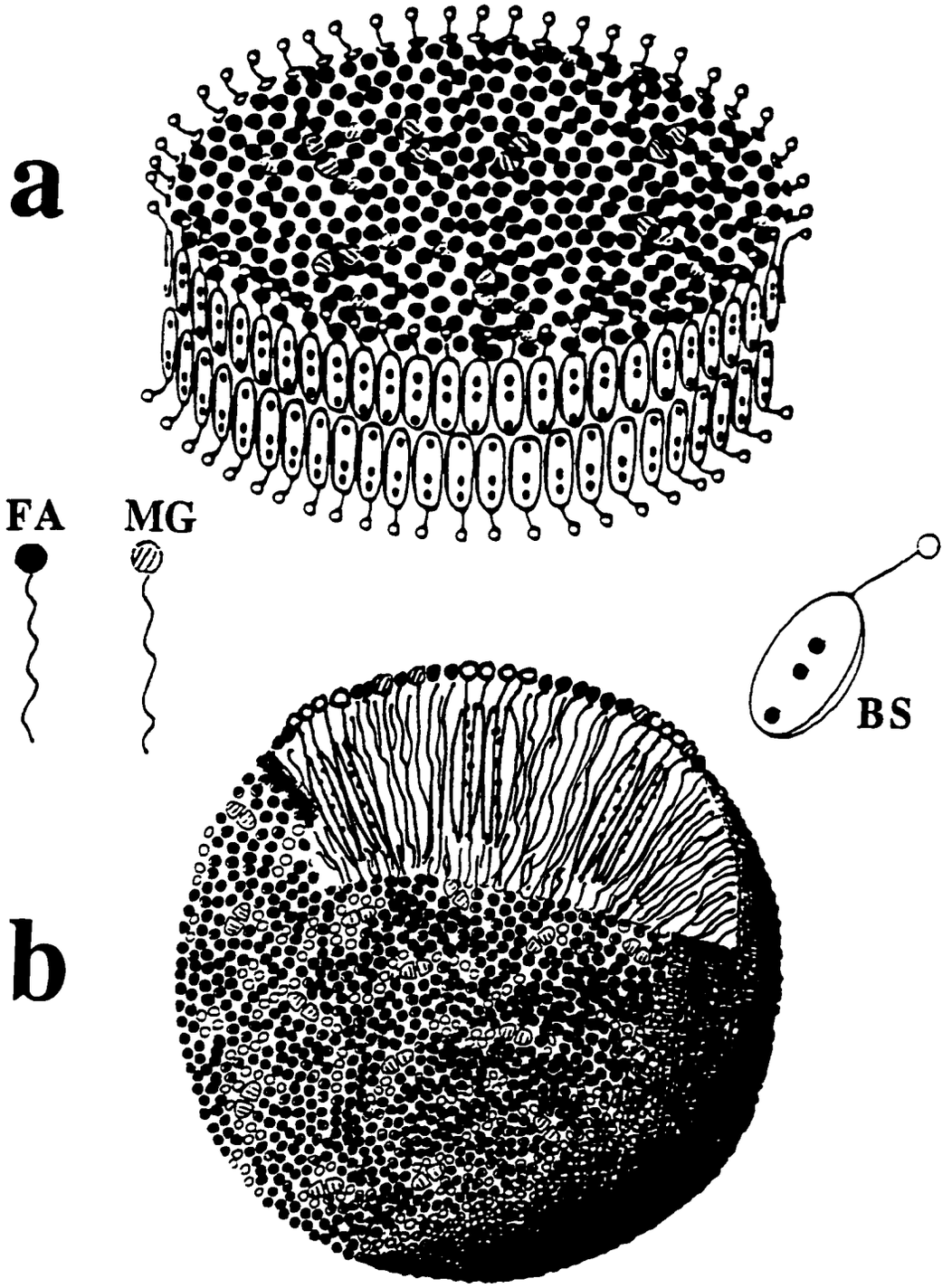

Figure III-15. Size distribution analysis by QLS for molecular aggregates in the C_8 20:1 mixture.

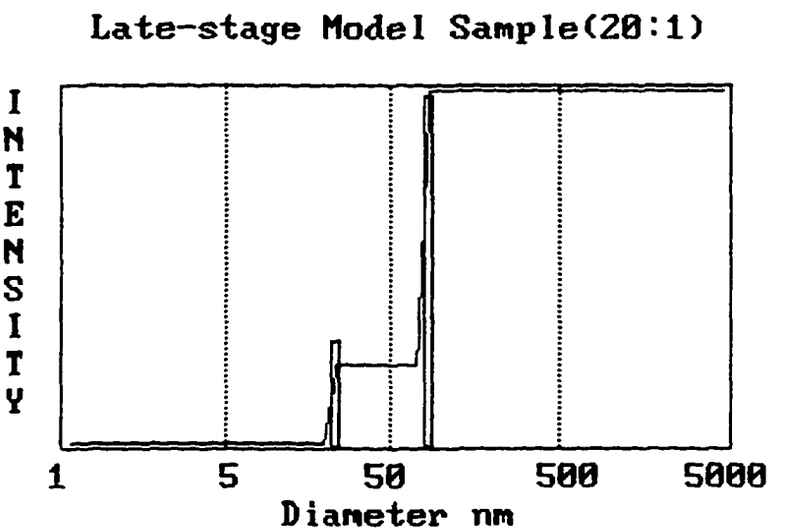

IV. Studies of Model Lipid Membrane by Semi-Solid NMR

A. Introduction

Biological membranes contain an astonishing variety of lipids. The ability of lipids to assume the basic bilayer organization is dictated by a unifying characteristic of membrane lipids, the presence of a polar or hydrophilic head group region, and a nonpolar or hydrophobic region **(Figure IV-1)**. This bilayer lipid organization provides a permeability barrier between exterior and interior compartments of cells and organelles. It has remained a dominant theme in the understanding of the organization and function of biological membranes (Cullis and Hope, 1991).

The fluidity of membranes depends on the nature of the acyl chain region comprising the hydrophobic domain of most membrane lipids. Most lipid species in isolation can undergo a transition from a very viscous gel state to the fluid liquid-crystalline state as the temperature is increased. However, most membrane lipids are fluid under physiological conditions (Vance and Vance, 1991); thus, the major emphasis of our work will concern the properties of liquid-crystalline lipid systems.

Because the structure and function of biological membranes is very important, phospholipids have been the subject of numerous NMR and other physical studies during the last 25 years (Grant and Harris, 1995). This research work is divided into two categories: (1) small unilamellar vesicles or micelles by solution-state NMR and (2) extended multibilyers in the liquid crystalline or gel states by static solid-state NMR. Since both lateral diffusion and axial rotation cause significant averaging of proton-proton dipolar interactions in liquid-crystalline model membranes, it is possible to obtain reliable high-resolution spectra with MAS alone at modest spinning speeds (2-4 kHz). Thus, high-field NMR experiments with MAS generally yield narrow, multiline spectra for most fluid liquid-crystalline-phase lipid bilayer systems, from which isotropic chemical shifts can be assigned and proximal chemical groups within the lipid assemblies can be deduced by analysis of MAS two dimensional NMR. Bilayer packing and local order have been deduced from MAS-^{13}C NMR. Also, aggregate morphology has been derived from ^{31}P lineshapes, and MAS sideband patterns and bilayer order have been deduced from ^{1}H sideband intensities.

B. Results and Discussion

1. MAS NMR Studies of Lipid Hydration in Monomethyl Dioleoylphosphatidylethanolamine (MeDOPE) Multilayers

(Portions of this section were published: Z-J Chen et al., 1996.)

One of the important aspects of the interfacial properties of membrane bilayers is the nature and extent of hydration of the membrane surface. There have appeared several elegant studies that measure the amount and affinity of membrane-bound water (Rand and Parsegian, 1989; McIntosh and Simon, 1994). Interrelated with hydration is the property of monolayer curvature strain (Gruner, 1992). The extent of hydration, interlipid hydrogen bonding, and steric repulsion are among the factors that affect intrinsic membrane curvature (Cullis et al., 1985). The phenomenon of curvature strain is attracting increased interest as a mechanism for the regulation of biological activity (Epand, 1996).

Water has a primary role in the formation and maintenance of cell membrane architecture, the basic lipid bilayer structure being an obligatory response of phospholipids exposed to an aqueous environment. A knowledge of the location of the water molecules and their lifetimes inside and at the surface of lipid membranes should increase our understanding of the lipid-water

interface, the ionic distribution, and stability of membrane conformations.

Of the spectroscopic techniques employed to study the molecular structure of lipid bilayers, NMR provides complementary information to X-ray diffraction, fluorescence, and infrared spectrometry. For multilamellar lipid dispersions and mixtures that mimic natural biological membranes, NMR techniques have been exploited usefully in studies of lipid morphology as well as of molecular dynamics and order (Griffin, 1981; Knowles and Marsh, 1991).

We have investigated the hydration behavior of the model membrane lipid, MeDOPE, a synthetic lipid that has the propensity of forming hexagonal phases and phases with inverted cubic symmetry (Van Gorkom et al., 1992), using solid-state ^{31}P, ^{1}H MAS NMR, and 2D-NOESY MAS NMR spectroscopy. Recently, ^{2}H NMR has been applied to studying the ordering and dynamics of water at membrane surfaces (Gawrich et al., 1992; Volke et al., 1994); MAS ^{1}H NMR has also been used in conjunction with nOe (Forbes et al., 1988) to assess membrane hydration (Volke and Pampel, 1995). The lipid we have chosen to study, MeDOPE, exhibits well-documented polymorphic behavior (Gruner et al., 1988; Siegel and Banschbach, 1990). It is also the model lipid that was used to demonstrate the presence of curvature strain in L_α

phase (Epand and Epand, 1994). In the current work we demonstrate the consequences of inverted phase formation or surface hydration of the lipid. The methodology used should be generally useful in the study of the solvation of the lipid structures.

^{31}P NMR of MeDOPE NMR Spectra: Lipid Morphology

In order to examine the phase behavior and morphology of model membranes, ^{31}P data were acquired in parallel for both MeDOPE and DOPC over the temperature range 25-75 °C. The use of ^{31}P NMR to confirm the lipid phase of MeDOPE is illustrated in **Figure IV-2** compared with that of DOPC.

^{31}P NMR spectroscopy differentiates phases on the basis of motional averaging of the residual CSA and the symmetry of lipid arrangement (King and Marsh, 1989). The hexagonal phase has increased motional averaging compared with the lamellar phase and inverted hexagonal symmetry. More complete motional averaging in the cubic phase can further average the CSA, and the isotropic resonances can result from cubic symmetry in the cubic phase.

The powder patterns of the ^{31}P NMR spectra reflect the symmetry of the corresponding lipid phases at different temperatures (Van Gorkom et al., 1992). Lipid dispersions of MeDOPE below 60 °C show a liquid-crystalline bilayer

arrangement with axially symmetric rotational motion. The formation of a hexagonal phase was not observed when the sample was heated to a temperature of 65 °C. The amount of hexagonal phase with inverted symmetry increases with time even if the temperature is kept constant at 65 °C. At higher temperature (75 °C) the H_{II} phase completely converts into an isotropic phase with a higher symmetry of the phase. The cubic/hexagonal phase cannot convert back to the bilayer phase upon cooling from 75 °C to room temperature, and an isotropic ^{31}P NMR signal still persists.

^{1}H NMR Spectra: Lipid Hydration

Figure IV-3 shows the ^{1}H MAS NMR spectra of DOPC and MeDOPE in the lamellar phase at room temperature. All proton resonances are assigned in Table **IV-1** made by analogy with prior work (Halladay et al., 1990). Surprisingly, in the bilayer phase at room temperature the ^{1}H spectrum of the MeDOPE lipid dispersion shows two well resolved water proton resonances in distinct environments, which have different chemical shifts (4.75 and 4.88 ppm). The two slowly exchanging population of water present in the room-temperature lamellar phase of an aqueous MeDOPE dispersion may be ascribed to (a) bulk water outside of the multilamellar vesicles (4.75 ppm) and (b) interlamellar water (4.88 ppm). The chemical shift of the latter population is altered because of strong interactions with

the lipid, likely by hydrogen bonding. The exchange rate between population (a) and (b) is less than about 400 s^{-1}, presumably because of the multiple membrane barriers. It should be noted, however, that multilamellar vesicles (MLVs) of DOPC do not exhibit two separate water peaks, nor does MeDOPE when it is present in an inverted phase. This phenomenon is therefore diagnostic of strong interactions between the solvent and membrane.

Our samples have a 40:1 water-to-phospholipid molar ratio. Approximately 20 water molecules are required to fully hydrate MeDOPE in the L_α phase (Gruner et al., 1988). This number would then correspond to the interlamellar water, in rapid exchange with (a) water molecules that are hydrogen-bonded to the lipid headgroup through its protonated amine and/or phosphate groups; and (b) amino groups of the MeDOPE headgroup. The remaining water comprises the extralamellar bulk water and thus would be present at a level comparable to that of the interlamellar water. Our spectra exhibit an intensity ratio of about 1:1 for the two water resonances, in agreement with these assignments.

When the sample is heated above the established lamellar-to-hexagonal phase transition temperature for MeDOPE, both water signals in the ^1H spectrum shift upfield

around 0.4 ppm, indicating a decrease in hydrogen bonding **(Figure IV-4)**. If the MeDOPE is cooled to room temperature again, only one water resonance is observed, suggesting the formation of a metastable phase. This phase allows rapid exchange between lipid-associated and bulk water. Only freezing of the samples restores the lamellar phase, and the ^1H NMR spectra of such samples show two resolved water resonances.

Spin-Relaxation Times: Lipid Hydration

Differences in hydrogen bonding between the two types of water are also reflected in the ^1H T_1 relaxation times. **Figure IV-5** summarizes the temperature dependence of T_1 for both water resonances. Water (HOD) molecules, whether bound to the head groups of MeDOPE or not, have the same proton-proton distances; differences in their dipole-dipole relaxation rates effectively reflect only τ_c. The motions are within the fast correlation time limit because we find T_1 relaxation times increase with temperature. Therefore, increasing motion will result in longer T_1 relaxation times and decreasing motion will result in shorter T_1 relaxation times. The downfield water signal exhibits a considerably shorter T_1 at all temperatures, suggesting reduced mobility of water molecules in that environment and supporting the notion of strong hydrogen bonding, which may bridge $^+NH_2CH_3$ with PO_4^-. The upfield water signal represents free water

which is exchangeable with solvation water; it has shorter τ_c and longer T_1 (4.66 s). The T_1 relaxation time of bulk HOD in DOPC at the same temperature is 2.24 s.

At temperatures above 55 °C, the proton T_1 increases more sharply for the downfield water and actually decreases for upfield water---trends that cause their respective spin-lattice relaxation times to approach a common intermediate value above 65 °C. It is also interesting to observe that above 65 °C, the T_1 relaxation time of the hydrogen-bonded water starts to increase rapidly until it reaches a similar values to relaxation times for bulk hydration water. Greater motional freedom is certainly expected at higher temperatures, due to simple reorientation of bulk water or weakening of the hydrogen bonds and lowering of the bilayer barriers. Both T_1's should then continue to rise, but at the same time they begin to be averaged by more efficient chemical exchange. This implies that above temperatures at which cubic inverted phases are formed, the hydrogen bonded water may no longer be involved in very strong hydrogen bonding or that increased motions at the lipid water interface result in an increase of the T_1 times.

2D NOESY NMR of MeDOPE: Lipid Hydration

In order to establish which areas of the lipid molecule are involved in specific through-space interactions with

water, we have performed a series of ^1H 2D NOESY experiments while rotating the samples at the magic angle for multibilayers of both MeDOPE and DOPC. The interesting interactions we focus on are the head group NCH_3 cross-relaxation with HOD molecule. For the DOPC standard in the bilayer phase, there are no observable NOESY crosspeaks between the water resonance and any lipid functional groups **(Figure IV-6)**. It has been suggested that the hydration waters are freely associated with the lipid-water interface. The transitional diffusion constant of water at the DOPC interface will then be on the order of 1 ns and thus no positive NOEs will be exhibited in the 2D spectrum (Volke and Pampel, 1995).

By contrast, the strong dipole-dipole interactions between the head group NCH_3 and downfield HOD group are observed in the bilayer system of MeDOPE **(Figure IV-7)**. The NOESY spectra of MeDOPE dispersions are quite different from these of DOPC and the two water resonances behave substantially different from each other. The downfield water peak shows a strong positive nOe crosspeak with the NCH_3 and CH_2N segments of the headgroup moiety of the lipid. This implies that the diffusion constant of water in this environment is longer than 10 ns. This reduced diffusion makes reasonable observations that (a) hydrogen-bonded water (downfield peak) has the shorter T_1 relaxation time,

indicative of restricted motion and (b) the observation of two distinct water resonances. The upfield resonance, however, does not show any crosspeaks with any lipid segments. Therefore, it is believed not to be involved in strong interactions with the lipid headgroup. This latter population of hydration water is believed to behave similarly to hydration water in DOPC lipid dispersions and have a diffusion constant on the order of 1 ns.

Upon heating of the MeDOPE dispersion, NOESY crosspeaks between the downfield water resonance and the lipid headgroup gradually diminish in intensity. **Figure IV-8** shows the intensity of the crosspeak of the head group NCH_3 in MeDOPE with the HOD as function of temperature. Obviously, these kinds of crosspeaks were not found in the DOPC system. The intensity of the MeDOPE crosspeaks is smoothly reduced when increasing the temperature because the hydrogen bond between the water and head group becomes weaker; in addition the dipole-dipole interaction may become weaker due to motional averaging. When a hexagonal or cubic isotropic phase is formed in which the head groups are close to each other, the hydrogen bond is broken; the water is expelled from head groups and may now exchange more freely with bulk water. The crosspeaks disappear entirely at temperatures above the lamellar-to-hexagonal phase transition. Finally, only one resonance of water is

observed. So, both motional averaging and weakening of the lipid water hydrogen bonds may account for this trend in crosspeak intensity. This last observation indicates that water in the cubic phase is no longer involved in very strong hydrogen bonding with the phospholipid headgroup.

Of particular interest here is that the MeDOPE cross peaks developed between the head group NCH_3 with HOD group are not observed in the isotropic cubic system at the same temperature RT(2) **(Figure IV-9)**. Upon cooling from the hexagonal phase to room temperature, a metastable isotropic phase with cubic symmetry is formed. Lipid dispersions in this phase show only one water resonance, with a T_1 relaxation time comparable to that of bulk water. This water does not show any nOe with the lipid, and it is concluded that water in the cubic phase is no longer involved in very strong hydrogen bonding with the lipid headgroup.

NMR helps to locate the water molecules proximal to and distant from headgroups for the MeDOPE and DOPC systems. We can visualize water molecules being strongly hydrogen bonded between neighboring MeDOPE lipid molecules in the lamellar phase. The possible water-lipid interactions in MeDOPE dispersions may be summarized as follows. In the lamellar liquid-crystalline phase, hydrogen bonding may

occur though (a) interaction between water hydrogens and PO_4^- ; (b) interaction between water oxygens and $NH_2CH_3^+$; or (c) formation of water bridges between $NH_2CH_3^+$ and PO_4^- groups of neighboring phospholipid molecules. Water bridges between oppositely charged lipid headgroups have been suggested previously (McIntosh and Simon, 1986). However, the formation of such water bridges may be precluded for DOPC because of steric hindrance and inability of $N(CH_3)_3^+$ groups to form hydrogen bonds. The MeDOPE molecules have one methyl group on the head group and have less steric hindrance so that they can form hydrogen bonds with water easily. Our data support the formation of a hydrogen bond between N^+CH_3 and PO_4^- for MeDOPE.

At higher temperatures, the exchange rate will increase, and also the fraction of H-bonded water in the MeDOPE will decrease as the amount of hexagonal phase increases. The acyl chains should occupy more space and the lipid headgroups will be squeezed closer together; thus water-lipid interactions may occur less readily and the molecules at the membrane surface will diffuse more rapidly. T_1 relaxation data and NOESY suggest that increased motional averaging and/or weakening of the hydrogen bond does occur. Finally, the cubic phase formed upon cooling of the sample should completely displace the water molecules that may be bridging adjacent phospholipid molecules and gain extra

stability from direct hydrogen bonding between oppositely charged $NH_2CH_3^+$ and PO_4^- groups of any neighboring lipid molecules. This will result in the fact that the H-bonded water will disappear, and one only has one average water signal representing free/solvation water. Under those conditions all behavior of water in MeDOPE system is similar to that of the DOPC system. The formation of direct hydrogen bonds between neighboring lipid molecules in the MeDOPE results in the metastable behavior of the cubic phase, which is not converted back into the bilayer structure upon lowering to room temperature. Only freezing, and destruction of cubic phase and consequent rearrangement will reform the $L\alpha$ phases.

2. Spin-diffusion in the Dimyristoylphosphatidylcholine (PC) Multilayer System (Portions of this section are in press: Z-J Chen and R. E. Stark, 1996)

The potential of using MAS-assisted data acquisition in concert with "liquid-state" experiments such as 2D COSY and NOESY was recognized early on for phospholipid dispersions (Forbes et al., 1988). The goals of such hybrid experiments include making spectral assignments of ^{1}H and ^{13}C spectra and elucidating the bilayer organization of phospholipid membranes. A number of useful applications of MAS-assisted NMR have been demonstrated recently, including heteronuclear and homonuclear chemical-shift correlation spectroscopy (Lee and Griffin, 1989; Li et al., 1993; Gross et al., 1995) and NOESY for structural studies of bilayer interaction (Halladay et al., 1990). Nevertheless, many investigators have exercised caution in the interpretation of NOESY results for both vesicle and multilayer phospholipid aggregates, since the crosspeaks may be due to spin diffusion rather than dipole-dipole interactions of ^{1}H nuclei that are close in space (Kalk and Berendsen, 1976; Keepers and James, 1984; Fejzo et al., 1991).

In phospholipid multilayer systems, magnetization exchange occurs in several regions, as exemplified above for the MeDOPE and DOPC systems shown in **Figure IV-6** and

Figure IV-7, respectively. Many of these connectivities are expected based on the molecular structure of the phospholipids: $POCH_2$, CH_2N, and NCH_3 interactions within the headgroup; ω-CH_3, $(CH_2)_n$, and HC=CH interactions along the acyl chains. Surprisingly, we observed crosspeaks between headgroup NCH_3's and both $(CH_2)_n$ and ω-CH3 portions of the acyl chains. In the PC system the two fatty acid chains are approximately parallel to one another and the phosphocholine moiety (polar head group) points in the opposite direction. It is evident that in an aqueous medium their polar head groups will have an affinity for water, whereas their hydrocarbon tails will avoid water. For long-chain phospholipids these preferences are satisfied by formation of a lipid bilayer, in which methyl groups of the headgroup and acyl chains are not expected to be in close proximity.

Several other possible rationales for the observed magnetization transfers were proposed previously. The crosspeaks between the acyl chain protons and polar head groups could involve any one of the three possible mechanisms of magnetization transfer **(Figure IV-10)**: (a) via spin diffusion; (b) through intermolecular proximities in a mixed interdigitated arrangement; and (c) and (d) through intra- and inter-molecular chain bends (Xu and Cafiso, 1986; Gabriel and Roberts, 1987; Forbes et al., 1988). Thus, it is very important to delineate the sources

of these crosspeaks which are involved in lipid dispersions. In order to address this issue systematically, several MAS-NOESY experiments were carried out on a series of selectively deuterated liquid-crystalline DMPC multilamellar systems **(Figure IV-11)**. A model is proposed for spin communication between headgroup and acyl-chain protons within the lipid assembly.

^1H MAS NMR in Unlabelled DMPC Multilamellar Systems

A 300-MHz MAS ^1H NMR spectrum is shown in **Figure IV-12** for an aqueous dispersion of DMPC above its gel-to-liquid crystalline transition temperature. As expected, with magic-angle spinning we obtained the narrow ^1H spectral lines and resolved all major functionalities of the phospholipid headgroup ($POCH_2$, CH_2N, $N(CH)_3$), backbone (CH_2O, CHO), and acyl chains ($(CH_2)_n$, ω-CH_3). **Figure IV-13** shows typical results of MAS-assisted NOESY experiments conducted on multilamellar DMPC systems. Strong dipolar connectivities are exhibited for selected pairs of protons even at the relatively short mixing time of 150 ms. Again, an unexpected feature that has been observed in DOPC and MeDOPE is the NOESY crosspeaks between $N(CH_3)_3$'s of the choline headgroup and ω-CH_3's of the acyl chains.

NOESY Crosspeaks in Labeled DMPC-d_4 Multilamellar Systems

It is well known that for very slowly tumbling systems the dipole dipole interaction via other spins may contribute to the NOE between two protons of interest if irradiation is continued indefinitely (Kalk and Berendsen, 1976). This indirect magnetization transfer could occur in a semi-solid system during the mixing time. The geometrical arrangement of protons in PC system provides many such pathways. This spin diffusion has several effects: (1) the appearance of multistep cross peaks from pairs of spins that are not near neighbors and (2) the removal of all the useful distance specificity from the NOE experiment in large molecules.

In order to prevent intramolecular magnetization exchange between $N(CH_3)_3$'s of the choline headgroup and ω-CH_3's of the acyl chains, the NOESY experiments were carried out using DMPC-d_4 **(Figure IV-14)**. When CH_2CH_2 protons near the headgroup $N(CH_3)_3$ are replaced with deuterium, possible spin diffusion pathways originating at the choline methyl groups should be terminated. Since molecular models show that the closest protons are now situated at least 7.4 Å from one another, intramolecular NOEs involving the $N(CH_3)_3$ should be absent. However, no significant reduction in the crosspeak intensity between ω–CH_3 and $N(CH_3)_3$ is observed even at a short mixing time (200 ms). Thus, the spectra of DMPC-d_4 should exhibit no intramolecular alkyl chain/headgroup interactions through spin diffusion.

NOESY Crosspeaks in Labeled DMPC (d_9/d_{54}=1/1) Multilamellar Systems

In earlier NMR studies both Oldfield et al. (1988) and Roberts et al. (1987) determined which mechanism is responsible for the observed NOESY crosspeaks between *N*-methyl and terminal methyl groups in their multilayer and asymmetric unilamellar vesicles, respectively. A number of 2D NOESY experiments were performed with deuterated lipids. The crosspeaks between *N*-methyl and terminal methyl groups disappeared upon deuteration, and they considered the NOESY cross peaks to reflect spin diffusion along the acyl chains and to headgroup protons within the molecule, not spatial or intermolecular transfer of magnetization. Oldfield suggested that such spin diffusion may be rather weak (Forbes et al., 1988).

We have followed their strategy by conducting MAS-NOESY experiments on a 1:1 mixture of DMPC-d_{54} and DMPC-d_9. Since half of the lipid molecules are chain-perdeuterated and half are headgroup-perdeuterated, intramolecular spin diffusion between ω-CH_3 and $N(CH_3)_3$ groups should be excluded and only intermolecular NOESY interactions are permitted between these portions of the phospholipid.

Contrary to the prior results, we did find ω-CH_3 /$N(CH_3)_3$ crosspeaks in the 2D NOESY spectrum, with a

diminished intensity but seen clearly **(Figure IV-15)**. These results indicate that intermolecular interactions rather than intramolecular spin diffusion are responsible for these spectral features.

NOESY Crosspeaks in DMPC (d_{27}-1 and d_{27}-2) Multilamellar Systems

As shown in **Figure IV-10**, either chain bendback or interdigitation could bring $N(CH_3)_3$ and ω-CH_3 protons from neighboring molecules close to one another in space. Cafiso's group used NOESY to examine cross-relaxation in a sonicated phospholipid vesicle system and found that small but significant magnetization exchange is developed between the head group *N*-methyl resonance and the terminal methyl resonance (Xu and Cafiso, 1986). They believed that the NOESY interaction could occur by events such as lipid interdigitation or alkyl chain bends that terminate lipid chain ends near the membrane surface.

With selectively deuterated DMPC's, it is possible to test whether either of these organizational models accounts intermolecular NOESY crosspeaks in our multilamellar system. We carried out the 2D NOESY experiments in the liquid-crystalline phase on both DMPC-d_{27} (chain 1) and DMPC-d_{27} (chain 2) and found the crosspeaks between ω-CH_3/$(CH_2)_2$ and $N(CH_3)_3$ **(Figure IV-16)**.

The strategy in these experiments is that when acyl chain 1 is completely replaced with deuterium, these crosspeaks between $N(CH_3)_3$ and ω-CH_3 due to either chain bending or interdigitation should disappear **(Figures IV-10b and IV-10c)**. If the 2-chain is perdeuterated, this NOESY crosspeak should disappear if the intermolecular interactions occur via bendback of this acyl chain **(Figure IV-10d)**. In fact a strong NOESY crosspeak is retained between $N(CH_3)_3$ and ω-CH_3, regardless of which DMPC-d_{27} species is examined. These crosspeaks between ω-CH_3/$(CH_2)_2$ and $N(CH_3)_3$ indicate that chain bends or interdigitation are unlikely to be responsible for these features.

Based on the crystal structure with two water molecules of hydration (5% w/w) (Pearson and Pascher, 1979), the headgroups of DMPC lie close to the backbone of adjacent DMPC molecules. The thickness of the DMPC bilayer in the liquid-crystalline phase is 55.4 Å. The magnitude of the crosspeaks produced by ω-CH_3 and $N(CH_3)_3$ in this PC multilayer system suggests that a large portion of the magnetization transfer occurs neither by an intramolecular along backbone spin diffusion mechanism, nor via intermolecular lipid interdigitation and alkyl chain bends.

The model we propose for spin communication between ω-CH_3 and $N(CH_3)_3$ consists of intermolecular headgroup-backbone

interaction combined with intramolecular spin diffusion within the acyl chain. If the choline methyl groups are close in space to the glycerol backbone of a neighboring DMPC molecule, then $N(CH_3)_3$-CH_2O and $N(CH_3)_3$-CHO NOESY crosspeaks are expected and observed in all of the multilamellar dispersions. **Figure IV-17** provides a framework for understanding the foregoing MAS-NOESY data. Supporting evidence for this mechanism of spin-spin interaction comes from several sources. For 1:1 mixtures of DMPC-d_{54} and DMPC-d_9, the intermolecular headgroup-backbone interaction should occur for half of the DMPC molecules (cases b and c). Subsequent spin diffusion along the phospholipid acyl chain will then lead to a $N(CH_3)_3$-ω-CH_3 NOESY crosspeak in case b only. The volume of the $N(CH_3)_3$-ω-CH_3 crosspeak in that mixture is predicted and found to be one-fourth of that observed in unlabelled DMPC multilayers, when 200-ms NOESY results are compared for the two phospholipid samples. It could have been very difficult to detect such a spectral feature a decade ago because of NMR spectrometer limitations. Finally, the NOESY buildup curves show a lag time for the $N(CH_3)_3$-ωCH_3 crosspeak **(Figure IV-18)**. This unusually sluggish cross relaxation is suggestive of spin diffusion, though it could also be attributed to more rapid motion, less orientational order, or simply smaller signals than for pairs of interacting $N(CH_3)_3$-CH_2O and $N(CH_3)_3$-CHO groups.

In summary, a large quantity of structural information is derived from the crosspeaks between the lipid headgroup segments and the glycerol backbone and the hydrocarbon chain. Of particular interest is that the issue of whether NOEs between the termini of the acyl chains and protons of the headgroup are indicative of spatial proximity. The series of 2D MAS assisted NOESY experiments we developed exclude the possibilities of intramolecular spin diffusion, chain-bending, and interdigitation in DMPC multilayers, and the mechanism we proposed reveal in detail how spin diffusion influences the cross peak intensities.

3. Phosphatidylcholine (PC)/Cholesterol (CH) and Sphingomyelin (SPM)/Cholesterol (CH) Multilayer Systems

Cholesterol, phospholipids, and sphingomyelin as well as their supramolecular assemblies are essential constituents of biological membranes. Cholesterol plays many important roles in the modulation of phospholipid packing density, separation of phospholipid headgroups and disruption of interactions between neighboring headgroups, alteration of membrane permeability behavior, and regulation of membrane-bound enzyme activity. Also, there is considerable evidence that the lateral packing density of cholesterol with sphingomyelin is higher than that with PCs (Bittman, 1993). Thus, understanding cholesterol's interaction with phospholipids and with sphingolipids is important from a biological as well as a physical perspective (Keough et al., 1996; Bittman, in press).

In the last few decades, functional and calorimetric assays of lipid behavior have been augmented increasingly by structural and organizational investigations, using such tools as X-ray scattering, IR and fluorescence spectroscopy, and magnetic resonance. From the point of view of NMR, ^{1}H and ^{13}C NMR spectroscopy has been widely used to study the structural and dynamic properties of model and biological

membranes. The studies presented below share with others the goal of obtaining the maximum amount of structural information from straightforward ^{1}H, ^{13}C, and ^{31}P measurements on lipid bilayers without the requirements of sonication, isotopic labeling or other spin probes (Oldfield et al., 1987; Le Guerneve & Auger, 1995). Because all of our systems are partially ordered liquid crystals, their NMR behavior has elements of both liquid-like and solid-like phases.

Our study makes complementary use of ^{1}H and ^{13}C semisolid NMR methods and evaluates their potential as a potent investigative strategy for the molecular structure and organization of lipid mixtures. We applied these techniques to aqueous lipid dispersions as follows: (a) 50:50 egg PC-CH mixtures and (b) 70:30 SPM-CH mixtures. This work was carried out on unsonicated aqueous dispersions with standard techniques of natural-abundance MAS NMR spectroscopy.

With lipid assemblies for which fast lateral diffusion and axial rotation make it possible to obtain narrow spectral lines using MAS only (Wennerstrom, 1973), it is of practical interest to determine what spinning speeds are required for complete line narrowing, whether the resulting centerband spectra are reliable, and what information is

readily available from spinning-sideband peak intensities. The ^{13}C NMR data presented herein are obtained primarily by observation of a simple Bloch decay (direct polarization), using both magic-angle spinning and ^{1}H-^{13}C dipolar decoupling (DD) to enhance spectral resolution. The impact of CH on order and mobility has been assessed for acyl chains, backbones, and headgroups of PC and SPM, representatives of two important classes of phospholipids.

^{1}H MAS NMR Spectra of PC/CH and SPM/CH

Typical MAS ^{1}H NMR data for PC/CH model membranes are shown in **Figure IV-19**. Key structural features of the phospholipid head group (NCH_3) and acyl chains are easily resolved, but no spin-spin couplings are observed by us at 200 MHz or by others operating at higher resonance frequencies. Although reliable high-resolution ^{1}H NMR spectra can be obtained for multilamellar lipid dispersions using 2-3 kHz MAS, the situation becomes more complicated upon incorporation of CH within the lipid bilayer. CH imparts order to the bilayer and also leads to a reduction in molecular motion. These changes give rise to a greatly increased line width via T_2 relaxation and residual dipolar interactions and as a result, the NMR signals of CH are not observed and the signals of PC are broadened. Compared with pure PC multilayers, the signals from acyl chain groups are severely attenuated.

The lines can be narrowed by changing the composition or increasing the spinning speed. When the mole fraction of PC is increased, the overlapped peaks are narrowed because the bilayer rigidity imparted by CH is reduced. Nevertheless, no resolved CH peaks are observed in the ^1H MAS spectra.

When these semisolid samples are examined using combined rotation and multiple-pulse spectroscopy (CRAMPS) (Ryan et al., 1980), the partially ordered chain segments become better represented in the centerband spectrum and the overall resolution is improved **(Figure IV-20)**. However, no preferential enhancement of CH signals is observed. Ultimately, the best resolution is achieved simply by rapid sample spinning at the magic angle. With MAS experiments run at 11 kHz, the sideband intensities become negligible and the centerband resonances are quantitatively reliable. Nevertheless, the spectral resolution is not sufficient to see CH signals in the presence of nearby PC protons.

Figure IV-21 compares the ^1H MAS NMR spectra for 50:50 PC-CH and 70:30 SPM-CH dispersions. In addition to the anticipated transfer of $(CH_2)_n$ signal intensity from the centerband region to the spinning sidebands, the SPM-CH mixture shows a similar behavior of the lipid acyl-chain order with a smaller proportion of cholesterol present.

(Comparisons of the NMR data at two magnetic-field strengths should be valid, since the spectral properties under MAS conditions are thought to be determined by (inhomogeneous) dipolar broadening (Forbes et al., 1988).

In samples with large CSA or DD (dipole-dipole interactions) such as solid or semisolid systems, the intense spinning sidebands make it difficult to interpret the centerband spectra. Nevertheless, the spinning sideband intensities at different rotation frequencies are useful because they reflect order parameters for the chain methylene segments. A complementary structural view of these lipid mixtures is revealed by their spinning-sideband intensities **(Figure IV-22)**.

All samples (PC/TO, PC, and PC/CH) show an increase in spinning sideband intensities at slower speeds, but no appreciable line broadening. The progressive decrease in sideband intensities (PC/CH, PC, PC/TO) reflects several trends: (a) PC-CH mixtures show larger sidebands for the $(CH_2)_n$ resonance, indicative of more chain order (Forbes et al., 1988); (b) the chains are less ordered in the PC/TO mixtures compared with pure PC; (c) PC-CH systems also exhibit discernible sidebands for the backbone and headgroup protons; (d) all mixtures exhibit high-resolution ^1H MAS NMR spectra, since rapid motions average many of the

intermolecular dipolar interactions between pairs of nuclear spins.

^{13}C MAS NMR Spectra of PC/CH and SPM/CH

The dominant line broadening mechanism in solids and semisolids is usually the DD interaction, with CSA also playing a substantial role for spin -1/2 nuclei other than ^{1}H. At natural abundance (1%), ^{13}C is a dilute spin. Homonuclear dipole-dipole interactions will occur only over long distances and be very weak, so heteronuclear (^{1}H-^{13}C) dipole-dipole interactions dominate the ^{13}C broadening. The combination of dipolar decoupling and MAS will remove both dipolar broadening and CSA. In our systems, MAS ^{13}C NMR conducted under various decoupling conditions can identify the mobile chemical groups in these multilayers. Information about mobility may then be correlated with ordering and structural trends deduced from ^{1}H spinning sidebands and NOEs.

Figure IV-23 shows the ^{13}C spectra of PC/CH (1:1, 50% by wt) and pure PC, both acquired with MAS and low-power decoupling to remove only the CSA broadening. Only pure PC multilayers give fairly narrow lines and signals from all expected functional groups. **Figure IV-24** shows the spectra of PC/CH acquired with MAS, direct polarization (DP) and either low-power decoupling (SD at 6 kHz; bottom) or high-

power decoupling (DD at 50 kHz; top). The combination of direct polarization (DP), MAS, and higher-power decoupling (DD at 50 kHz) produces well-resolved spectra of the PC/CH system **(Figure IV-25, bottom)**, but not for pure CH in the solid phase **(Figure IV-25, middle and top)**.

These spectra reflect motional restrictions present in the organized PC/CH structures. Inspection of the *N*-methyl and CH_2N resonances which remain narrow and almost unaffected under various NMR acquisition conditions (DP-MAS-SD and DP-MAS-DD) suggests that only carbons of the headgroup NCH_3 and CH_2N retain sufficient mobility in the mixed aggregates to fully average heteronuclear dipolar interactions and retain their basic liquid character. The intensities of the peaks between 0 and 30 ppm increase greatly under DP-MAS-DD conditions. Also, substantial broadening of resonances from carbonyls and unsaturated double bonds (120-180 ppm) is expected and observed with DP-MAS-SD acquisition, but these lines narrow with increasing decoupling strength. Thus the acyl chains and backbone of PC become more immobilized in the presence of cholesterol because of the increase in bilayer rigidity. These ^{13}C results complement the observed dependence of ^{1}H spinning sideband intensities vs rotation frequency, which showed the PC acyl chains to be more ordered in the presence of CH. ^{13}C

NMR has the advantage that many chemical moieties of the CH component can be seen directly.

When we compare the PC/CH system with pure PC and pure CH systems, the conclusion is that CH confers some rigidity upon the acyl chains and selectively broadens different chemical groups. At the same time, CH itself is fluidized by PC so that some peaks from CH (C9, C17, C19, C21, and C=C) become well resolved.

The change in the bilayer structure on adding CH is biologically interesting. It is not surprising that introduction of a relatively flat rigid molecule into the bilayer leads to a substantial increase in the molecular order for lipid chain segments in contact with the cholesterol rings. The groups nearer the bottom segment of the lipid chains may be in contact with the relatively flexible CH isooctyl side chain and experience much more disorder and more freedom. At the same time CH condensation of the PC hydrocarbon chains always coincides with a decrease in the density of PC molecules in the plane of the membrane. This latter effect causes the choline head groups to become less crowded, less restricted and much more mobile (Oldfield et al., 1978).

Efficient data acquisition is possible if high-power decoupling (DD) is added to our MAS procedures. **Figure IV-26** shows typical MAS ^{13}C NMR spectra obtained for SPM and its 70:30 mixture with cholesterol, using DP acquisition (Bloch decays) with suppression of the $^{13}C\{^{1}H\}$ nuclear Overhauser effects. The spectral resolution compares quite favorably with that reported at higher field strengths (Montez et al., 1993). Although the DP method underrepresents some of the carbons in the solid cholesterol, they are observed easily in NMR spectra of SPM-CH (and PC-CH) aqueous mixtures obtained with manageable recycle delays.

These studies demonstrate the feasibility of one dimensional ^{1}H and ^{13}C NMR spectroscopy for the study of lipid-lipid interactions on the molecular level. The results presented here lay the groundwork for systematic studies of packing and organization in model membranes with varying constituents and compositions.

Table IV-1

^1H NMR resonance assignments for MeDOPE

Proton type	Chemical shift (ppm)*	Chemical shift (ppm)#
ω-CH_3	0.90	0.90
$(CH_2)_n$	1.30	1.30
β-CH_2	1.61	1.61
$C\underline{H}_2CH{=}CHC\underline{H}_2$	2.05	2.04
α-CH_2	2.36	2.32
NCH_3	2.80	2.71
CH_2N	3.32	3.16
CH_2O, $POCH_2$	4.14	3.98, 4.18
CH_2O	4.44	4.40
HOD	4.75, 4.88	
CHO, CH=CH	5.24	5.24, 5.36

* 300-MHz data obtained on an aqueous dispersion of MeDOPE with 2.00-kHz magic-angle spinning at a temperature of 25 °C. Shifts are referenced to the ω-CH_3 peak at 0.90 ppm (Li, et al., 1993).

600-MHz data obtained for MeDOPE dissolved in $CDCl_3$ at a temperature of 25 °C. The assignments were confirmed with double-quantum-filtered correlated spectroscopy (data not shown).

Figure IV-1. The topography of membrane proteins, lipids, and carbohydrates in the fluid mosaic model of a typical eucaryotic plasma membrane (Cullis and Hope, 1991).

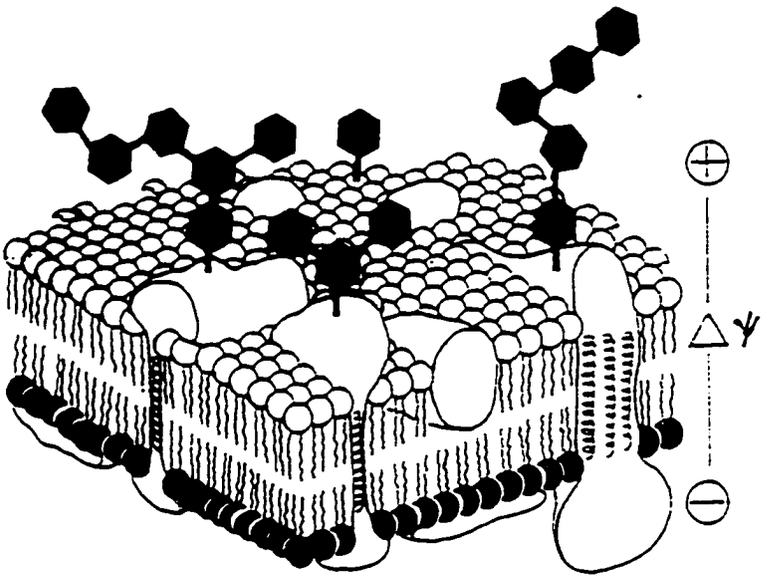

Figure IV-2. ^{31}P NMR spectrum at different temperatures for MeDOPE and DOPC. (a) DOPC at 25 °C; (b) MeDOPE at 25 °C; (c) MeDOPE equilibrated at 75 °C; (d) MeDOPE kept at 75 °C for about 2 h and then cooled to 25 °C.

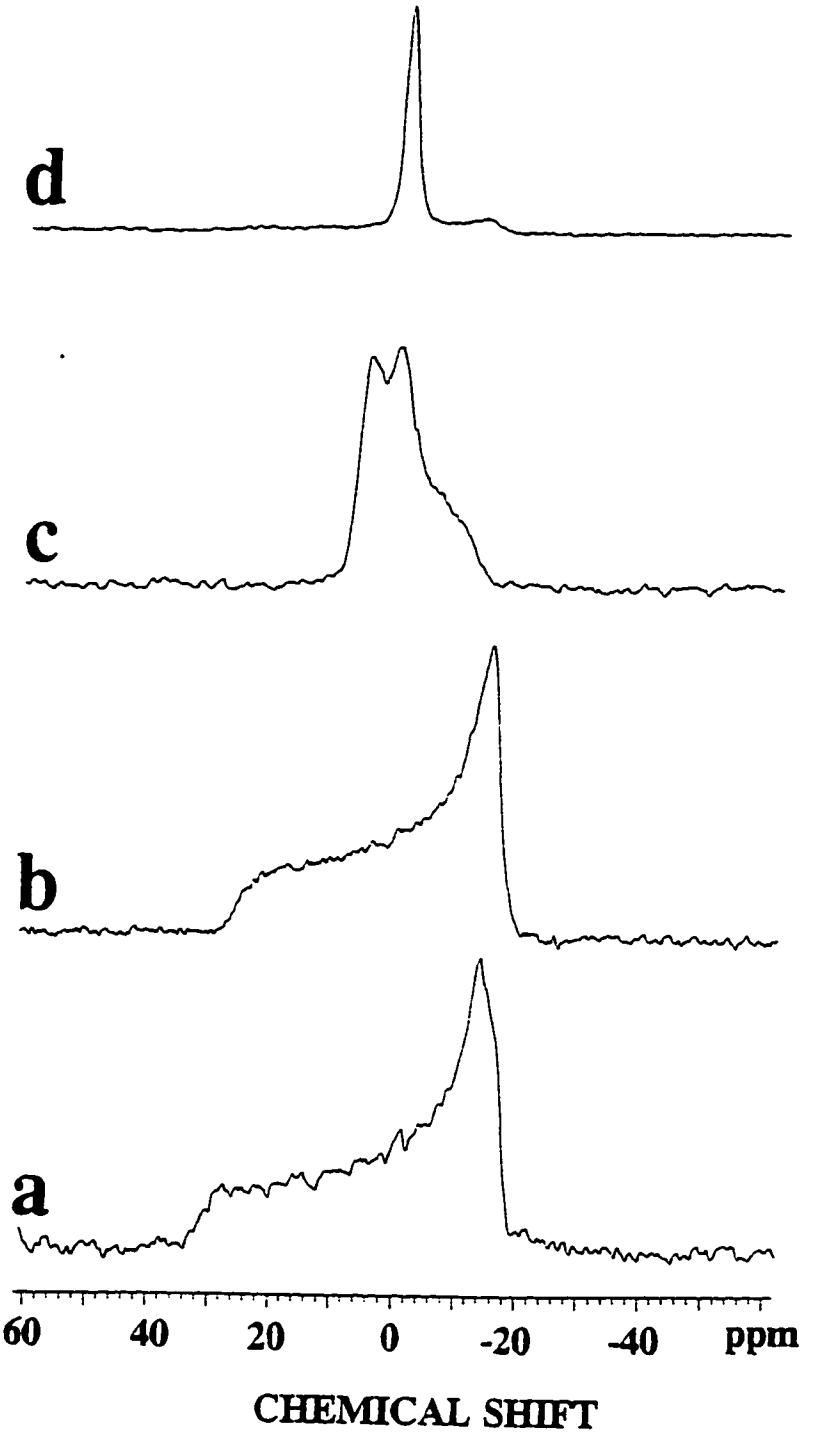

Figure IV-3. ^{1}H 300-MHz MAS NMR spectra at room temperature for MeDOPE and DOPC. (a) DOPC at 25 °C; (b) MeDOPE at 25 °C.

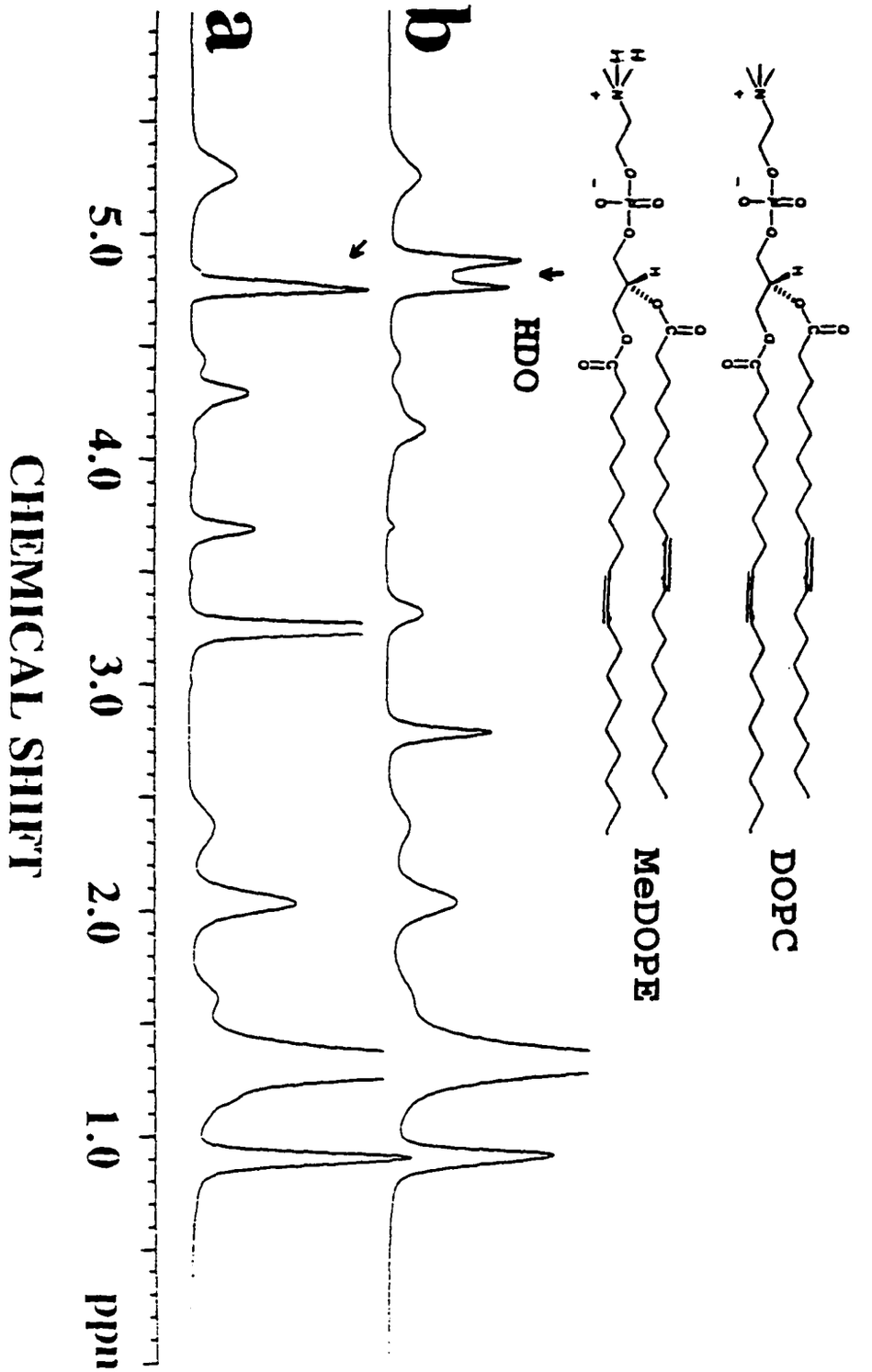

Figure IV-4. ^{1}H 300-MHz MAS NMR spectra at different temperatures for MeDOPE.

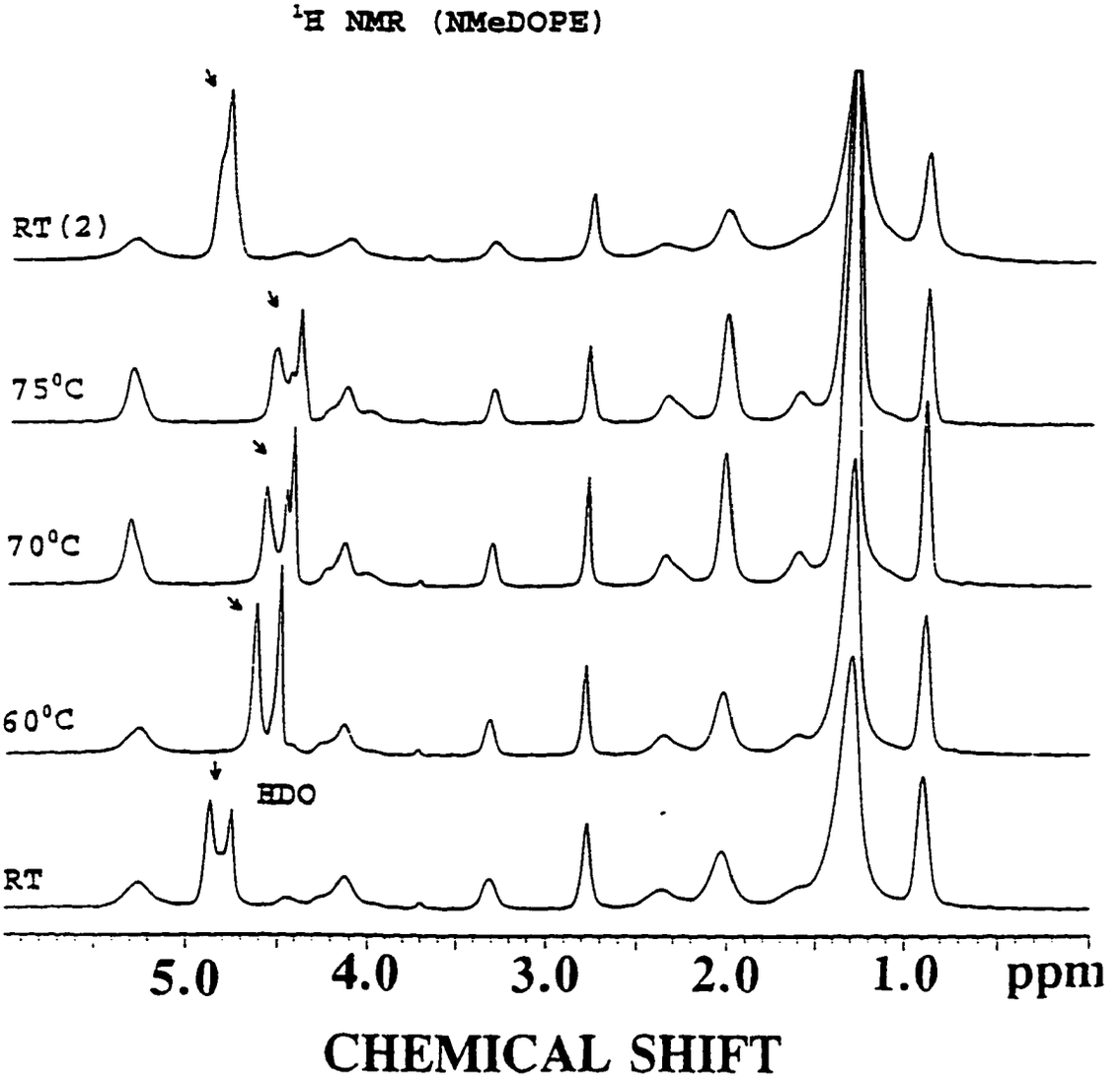

Figure IV-5. Proton T_1 vs temperature for two water peaks observed in MeDOPE dispersions. The arrow on the temperature axis indicates the value of the phase-transition temperature T_H.

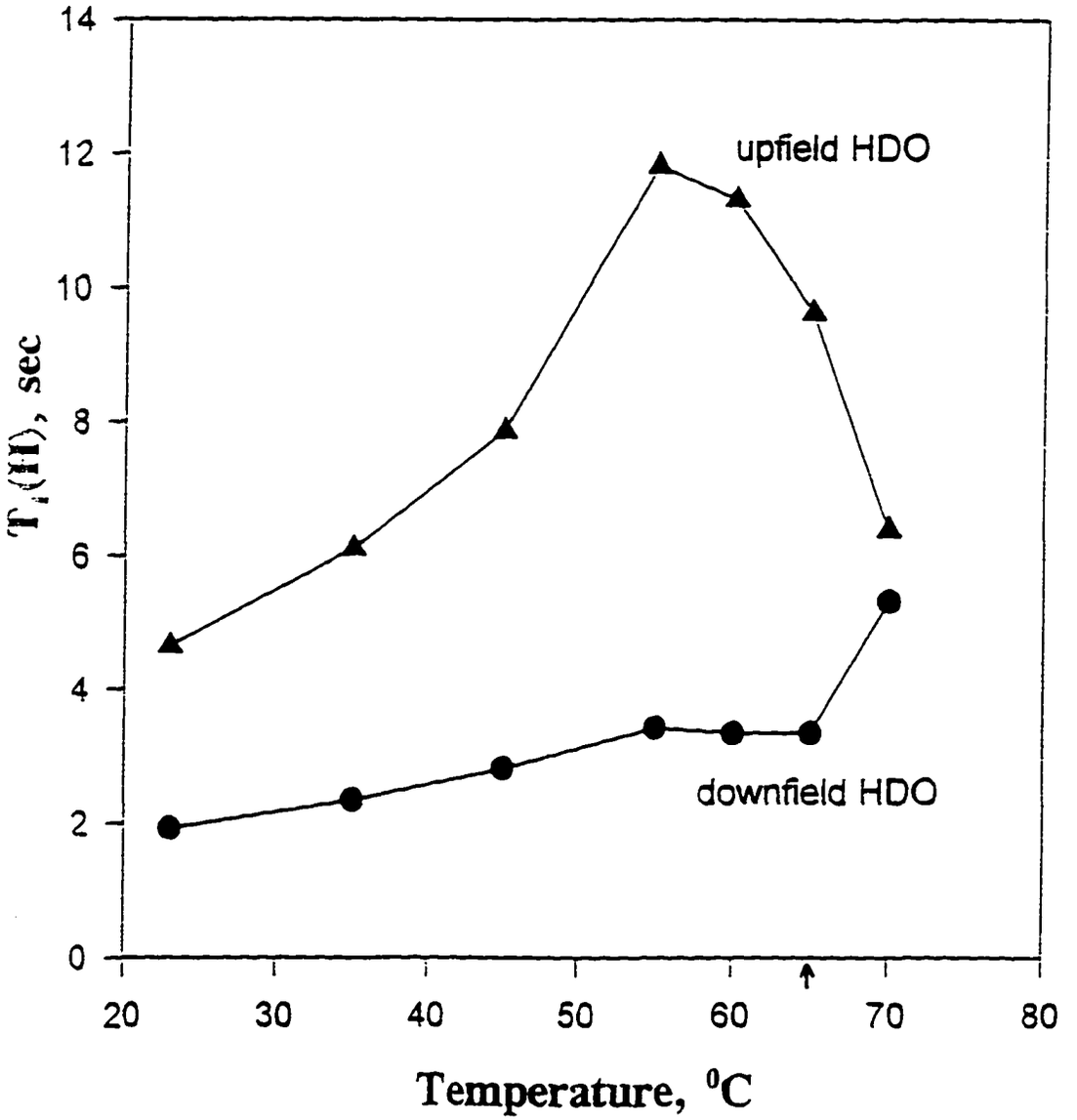

Figure IV-6. ^{1}H 300-MHz MAS 2D NOESY NMR spectrum at room temperature for DOPC.

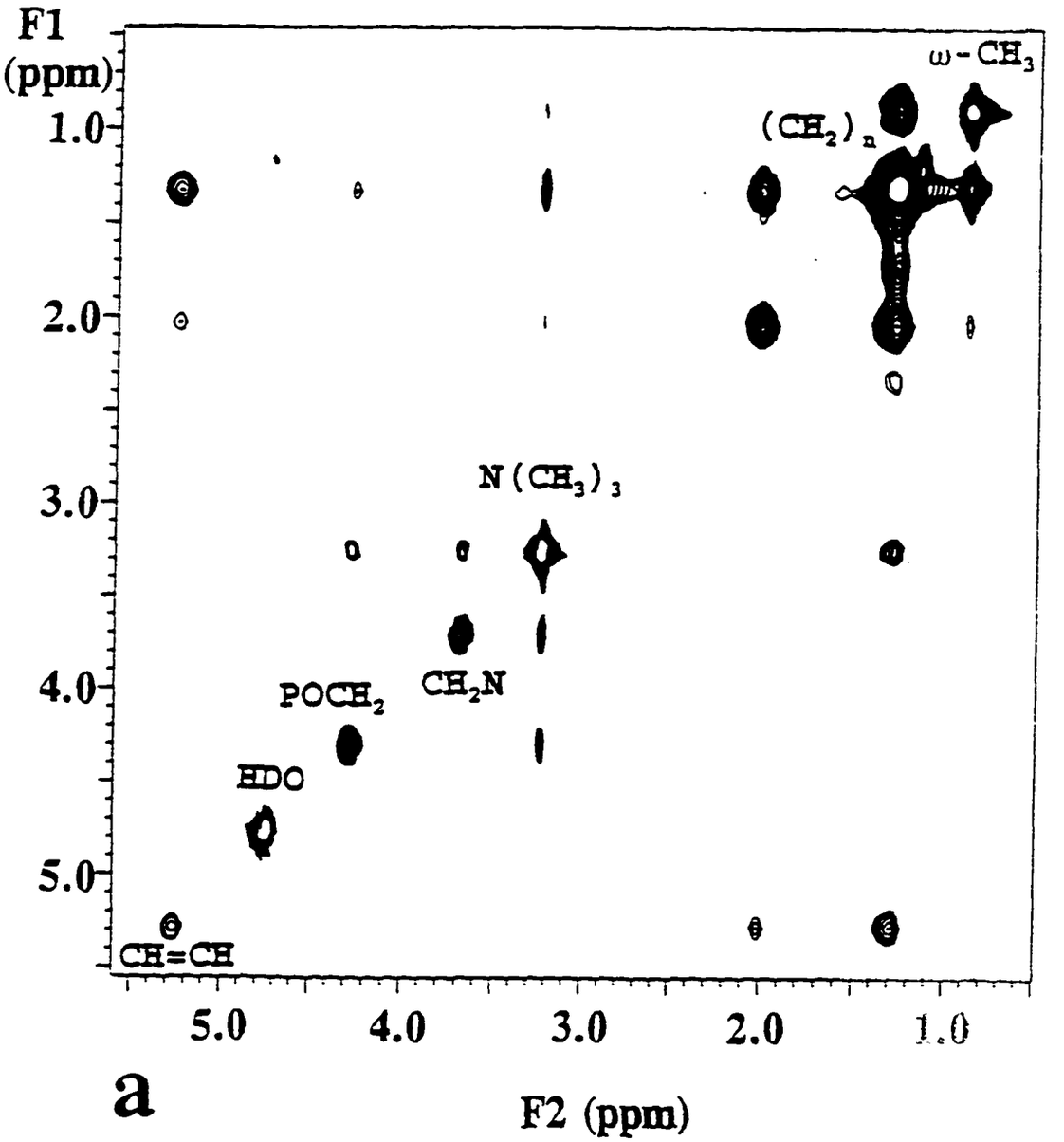

a

Figure IV-7. ^{1}H 300-MHz MAS 2D NOESY NMR spectrum at room temperature for MeDOPE. The dashed lines show NOESY connectivities between the downfield water resonance and protons of the phospholipid.

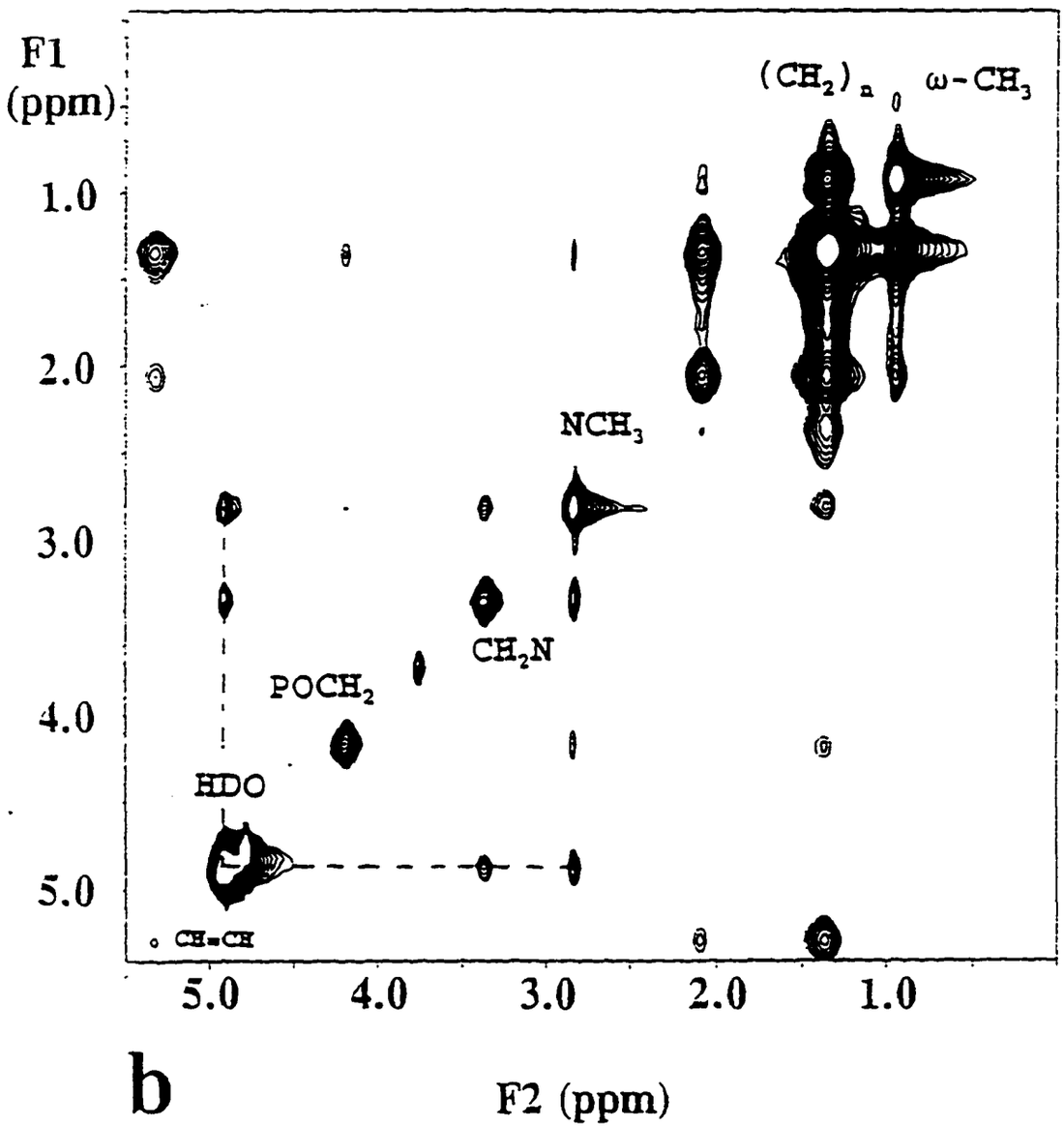

b

Figure IV-8. Variation of water-lipid MAS-NOESY crosspeak volumes with temperature for MeDOPE dispersions. The integrated intensities for crosspeaks between the downfield water and headgroup methyl peaks are plotted as a percentage of the diagonal peak intensity for NCH_3 protons.

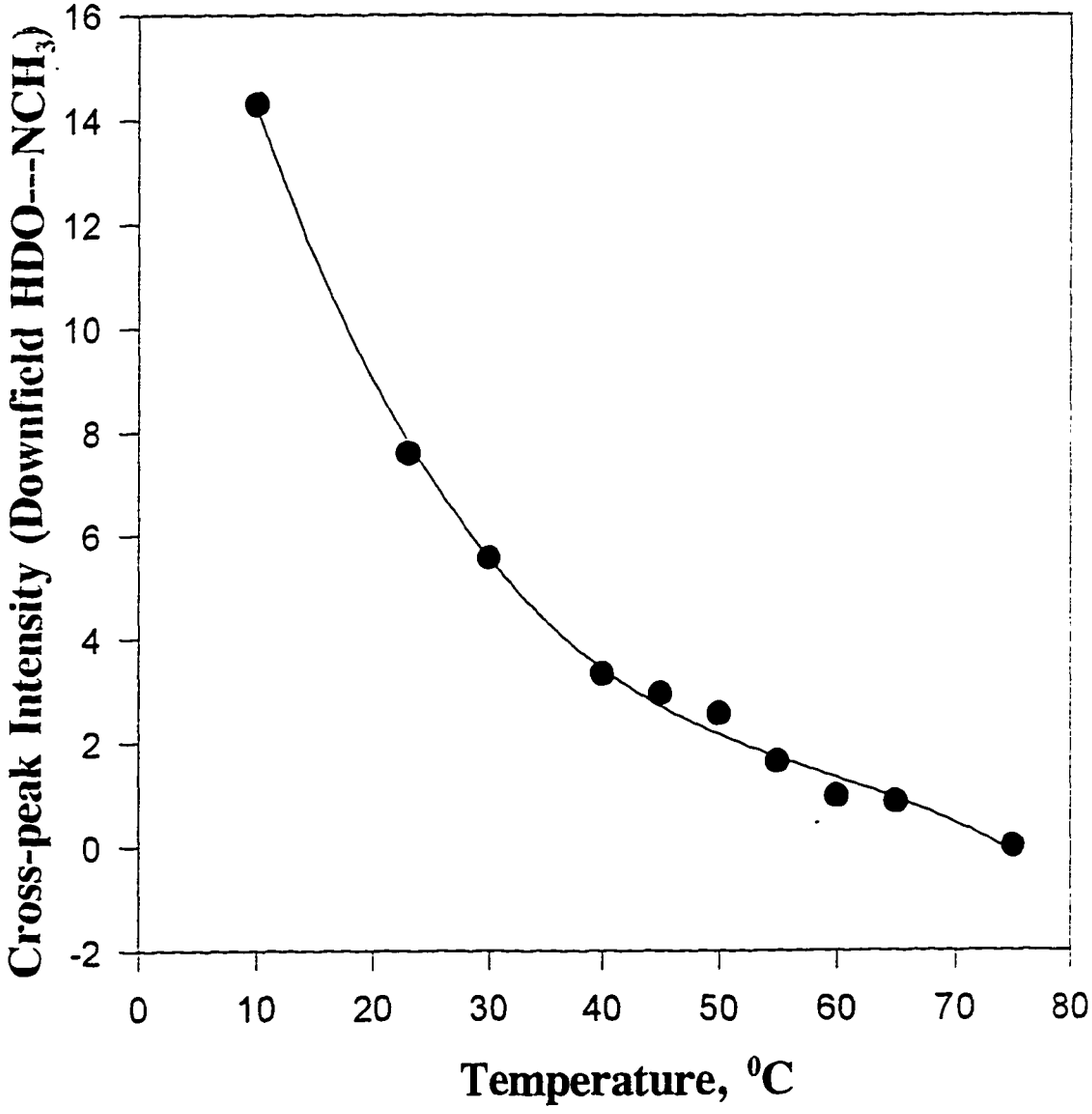

Figure IV-9. ^{1}H 300-MHz MAS 2D NOESY NMR spectrum at room temperature for MeDOPE (MeDOPE heated to 75 °C and then cooled to 25 °C).

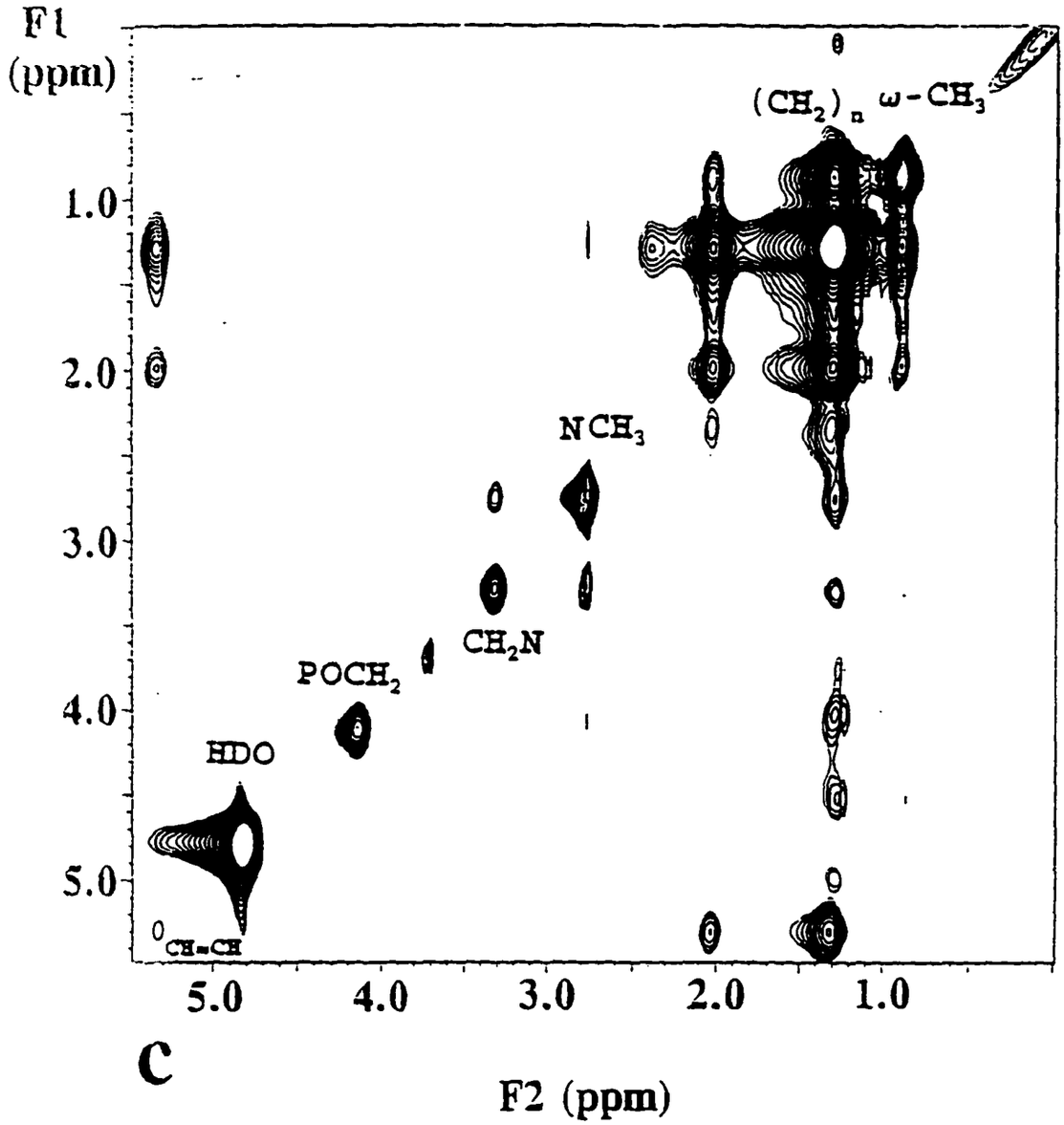

Figure IV-10. A schematic view of lipid bilayer arrangements and spin-communication mechanisms. (a) spin diffusion in a standard bilayer; (b) interdigitation of acyl chains; (c) and (d): bendback of either acyl chain toward the aqueous interface.

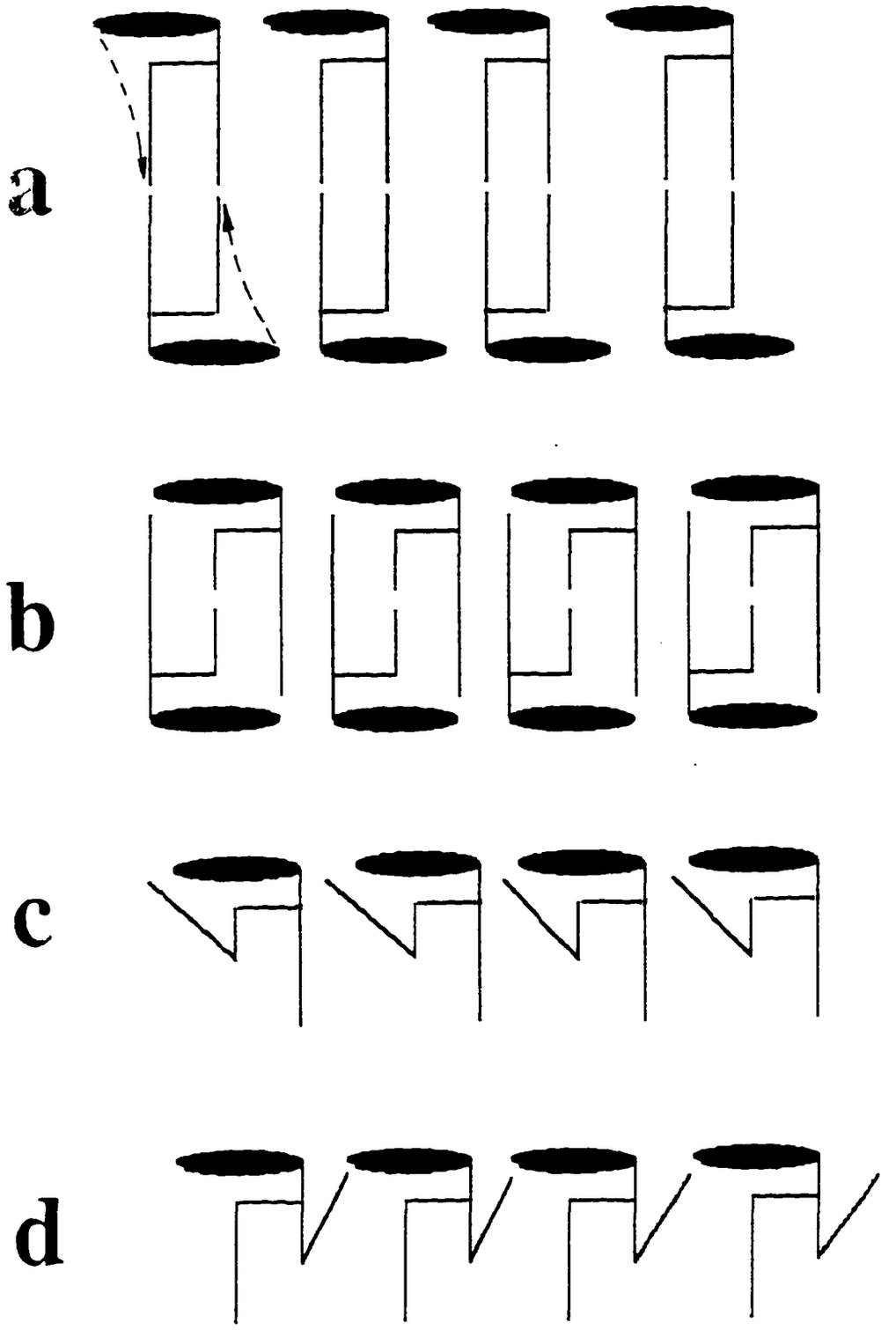

Figure IV-11. Chemical structures and deuteration sites for DMPC. (a): ball-and-stick model of the unlabeled DMPC; (b): DMPC-d_4; (c) and (d): DMPC-d_{27}, perdeuterated on the 1- and 2-acyl chains, respectively; (e): DMPC-d_9; (f): DMPC-d_{54}.

a

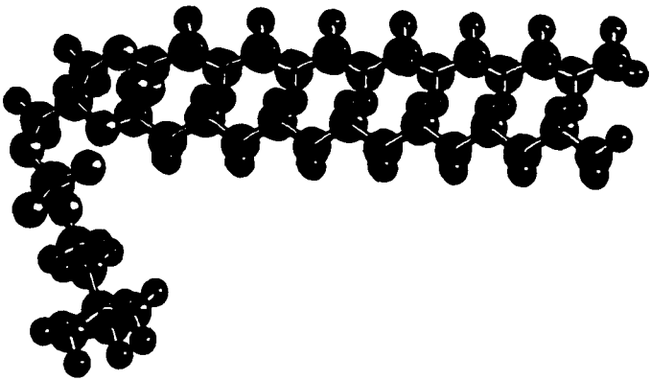

b

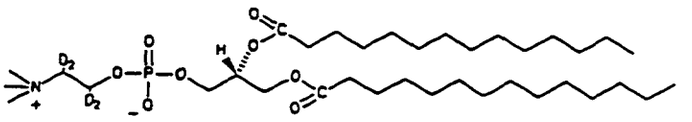

c

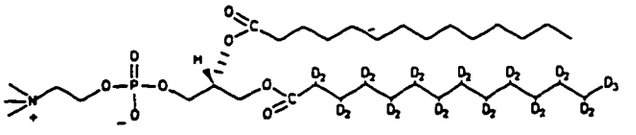

d

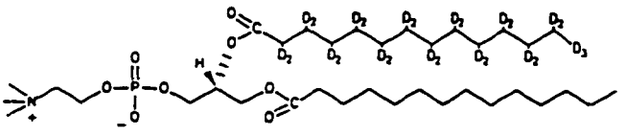

e

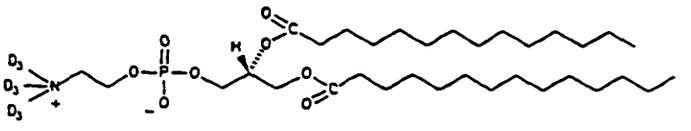

f

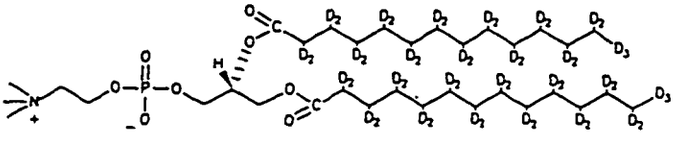

Figure IV-12. ^{1}H 300-MHz MAS NMR spectrum above its gel-to-liquid crystalline transition temperature for unlabeled DMPC.

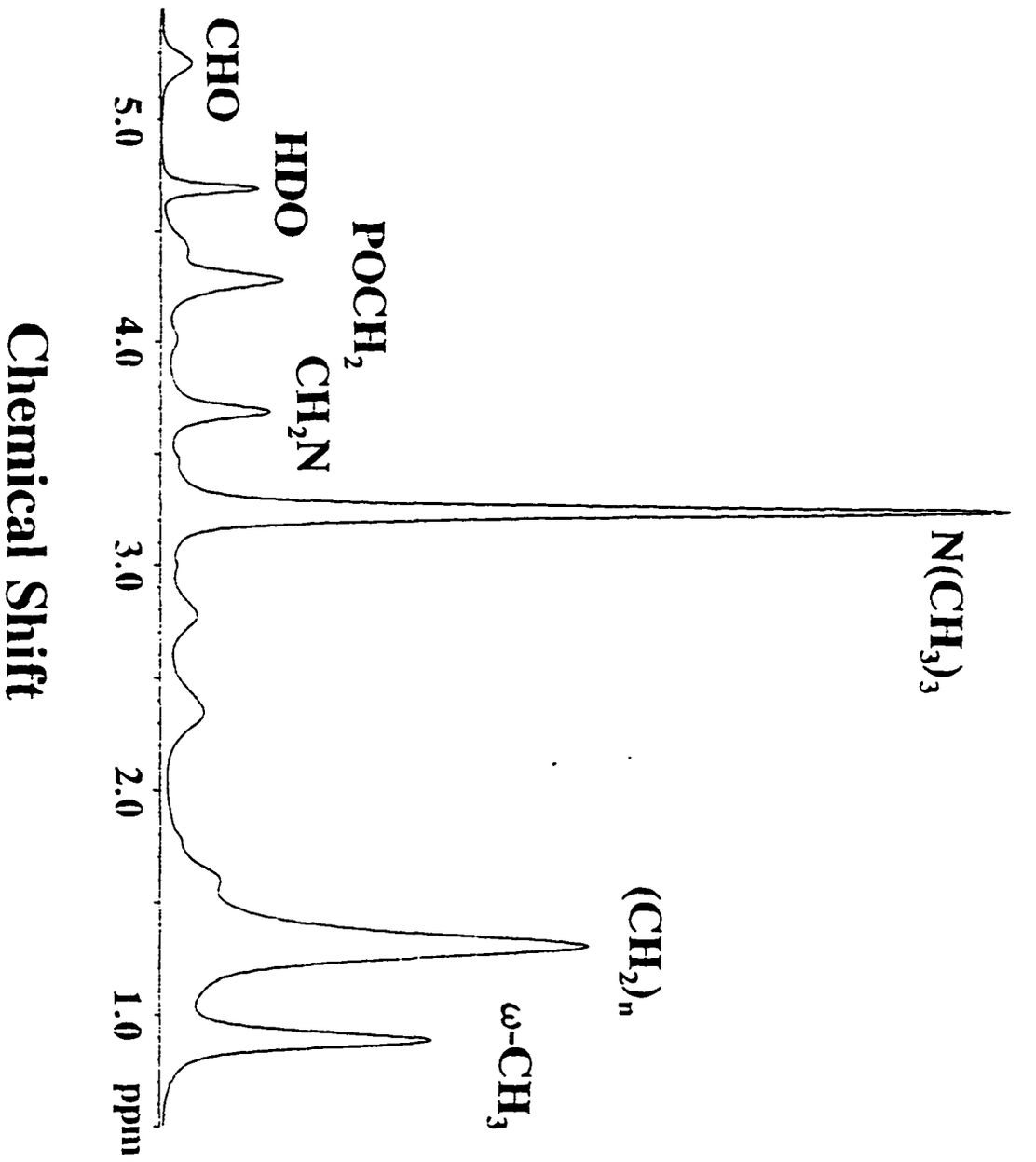

Figure IV-13. ^{1}H 300-MHz MAS NOESY NMR spectrum for unlabeled DMPC (T = 30 °C, τ_m = 150 ms).

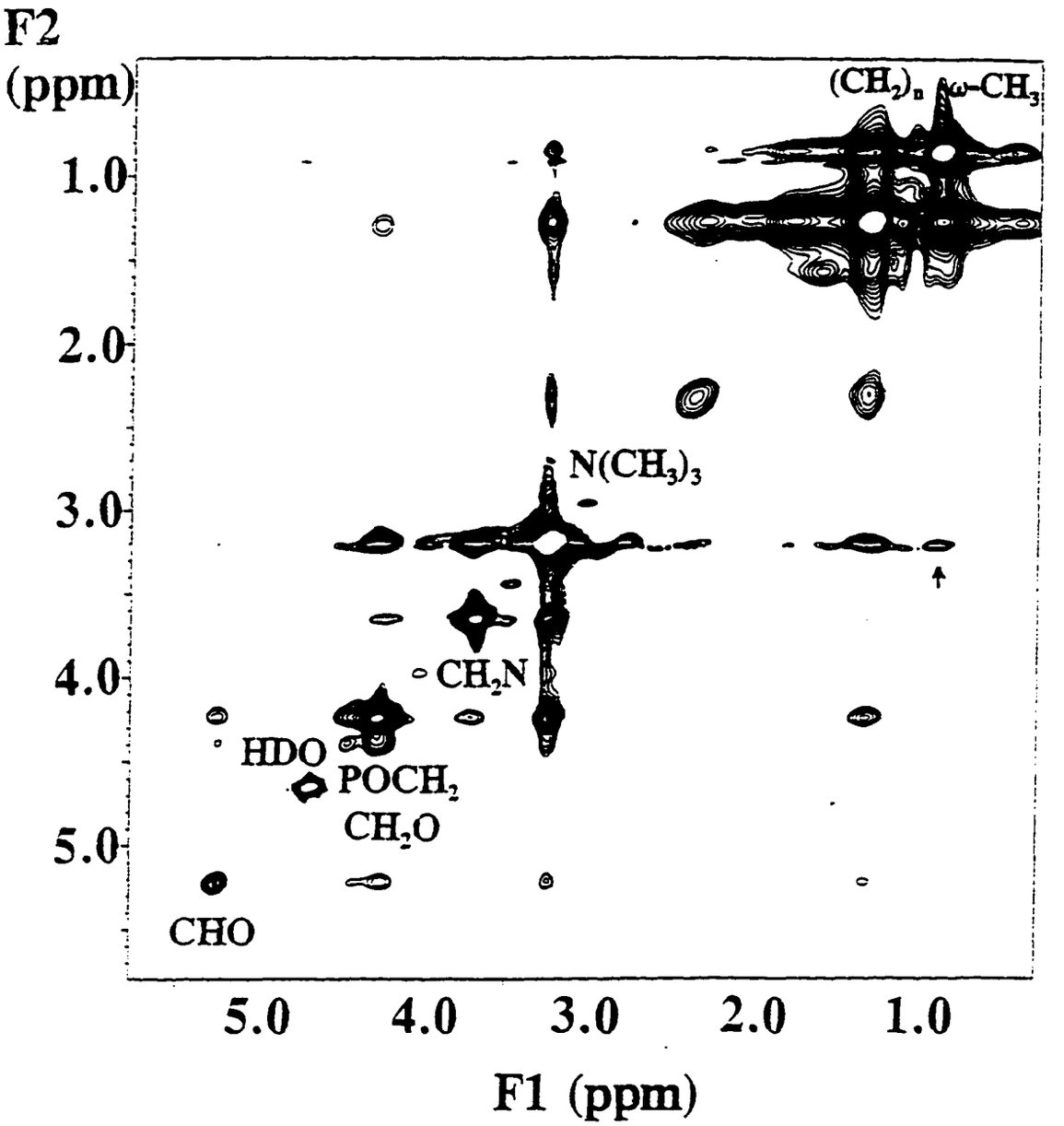

Figure IV-14. ^{1}H 300-MHz MAS NOESY NMR spectrum for labeled DMPC-d_4 (T = 35 °C, τ_m = 300 ms).

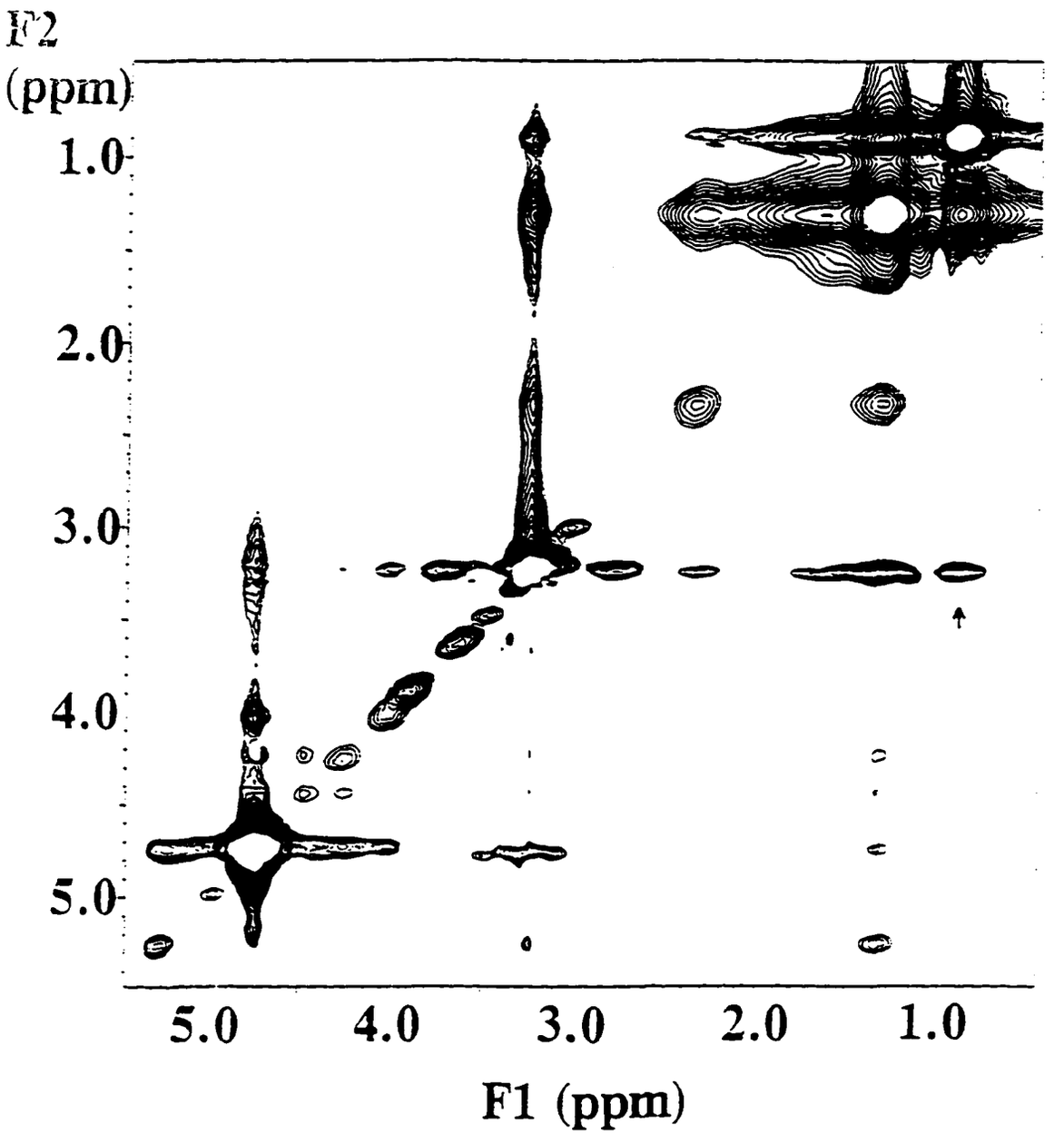

Figure IV-15. ^{1}H 300-MHz MAS NOESY NMR spectrum for labeled 1:1 mixed dispersion of DMPC-d_9 and DMPC-d_{54} (T = 30 °C, τ_m = 250 ms).

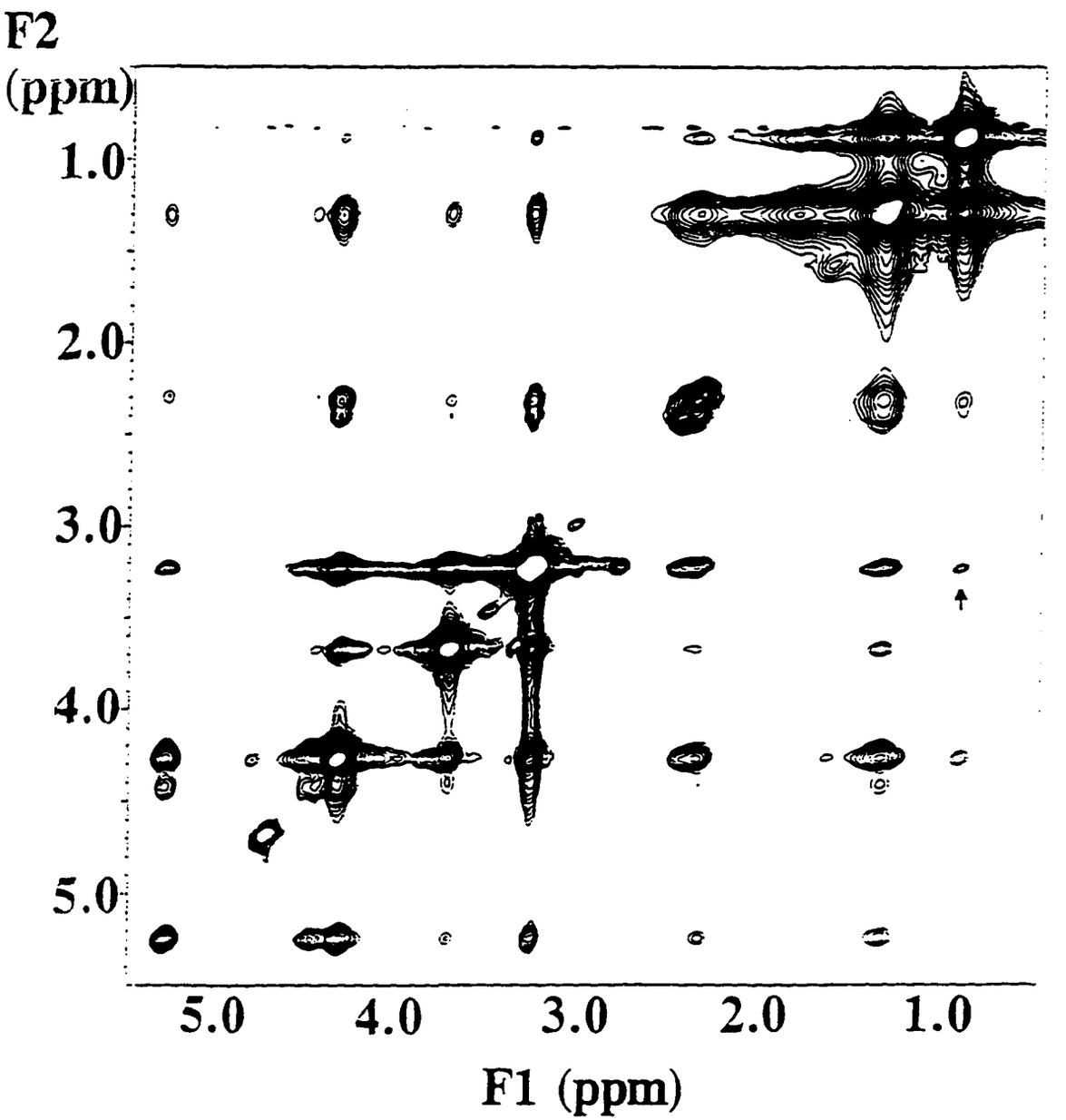

Figure IV-16. ^{1}H 300-MHz MAS NOESY NMR spectra for labeled DMPC-d_{27} (T = 35 °C, τ_m = 300 ms), with 1-chain perdeuteration (bottom) and 2-chain perdeuteration (top).

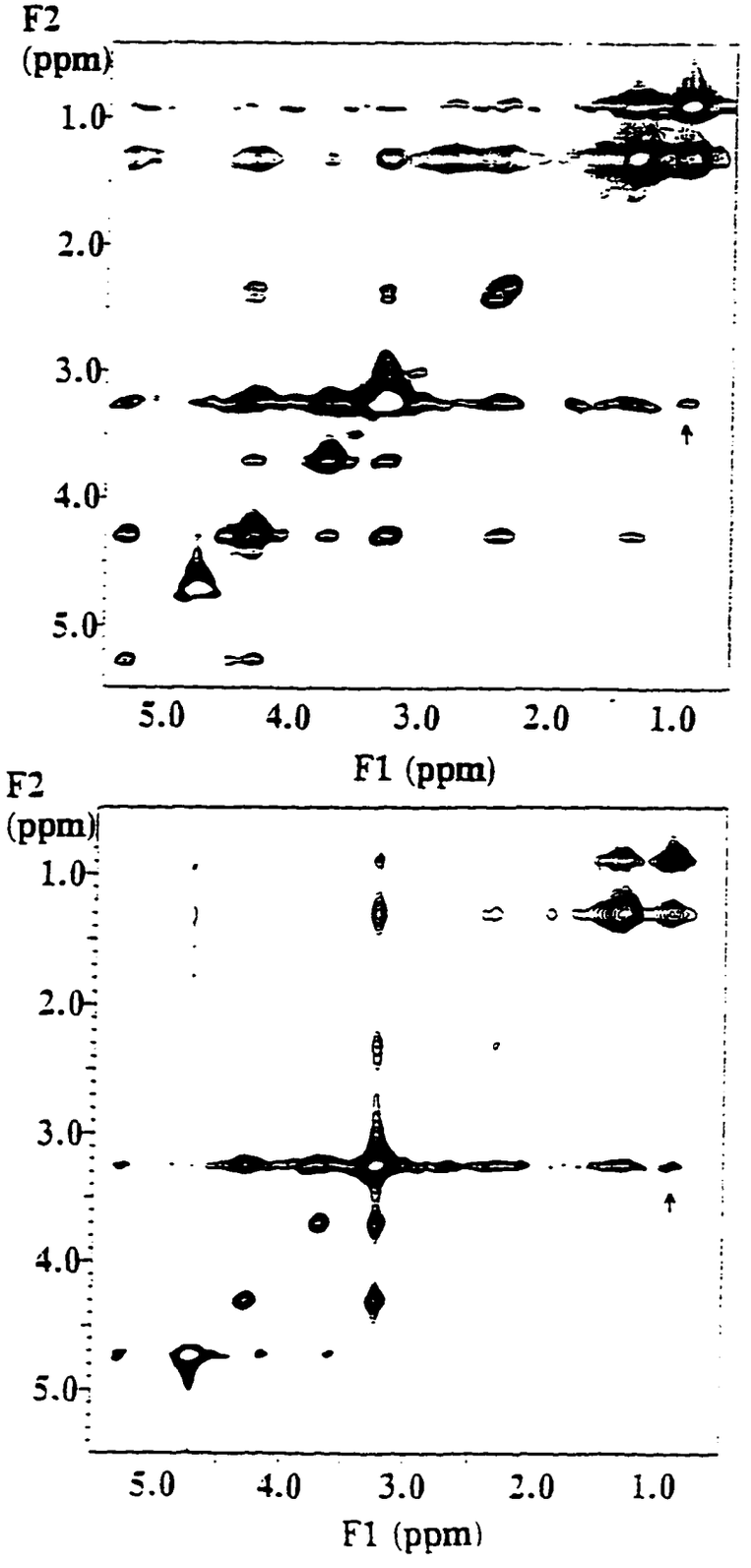

Figure IV-17. Four possible schemes for intermolecular interactions between labeled DMPC-d_9 and DMPC-d_{54}, where blackened headgroups and thickened acyl chains correspond to perdeuterated residues.

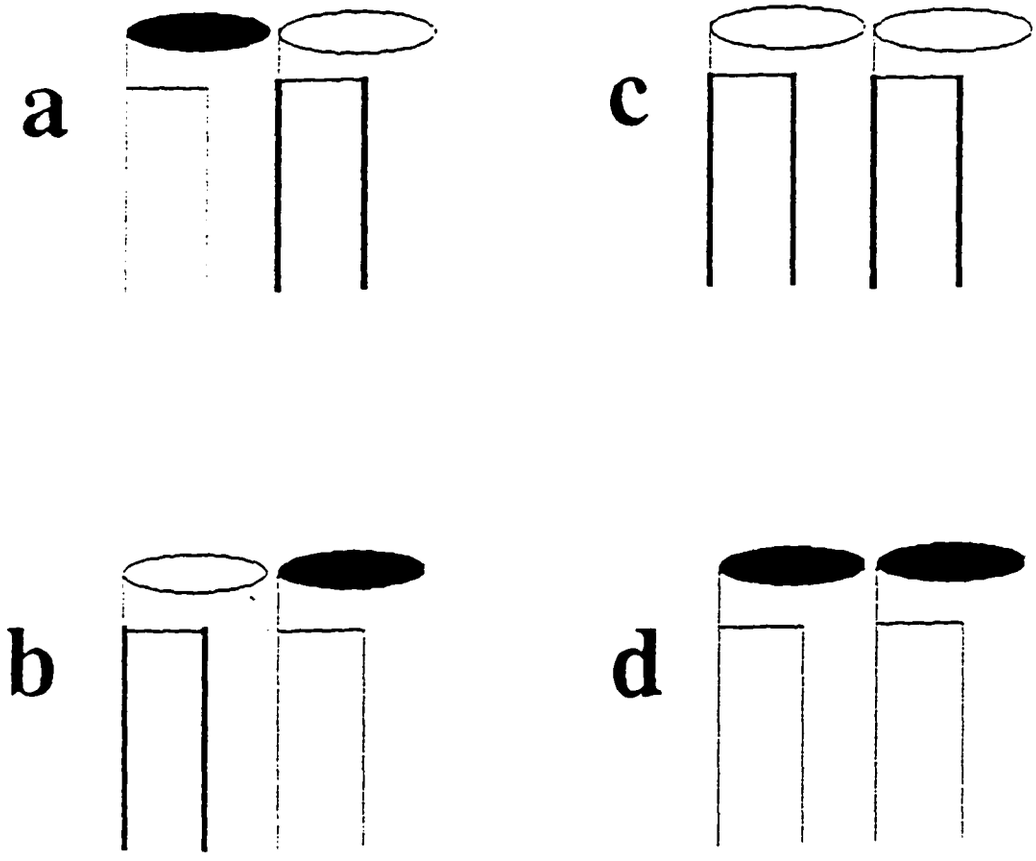

Figure IV-18. Variation of selected MAS-NOESY crosspeak volumes with mixing time for a 1:1 mixed dispersion of labeled DMPC-d_9 and DMPC-d_{54}. The volumes are normalized to the $N(CH_3)_3$ resonance.

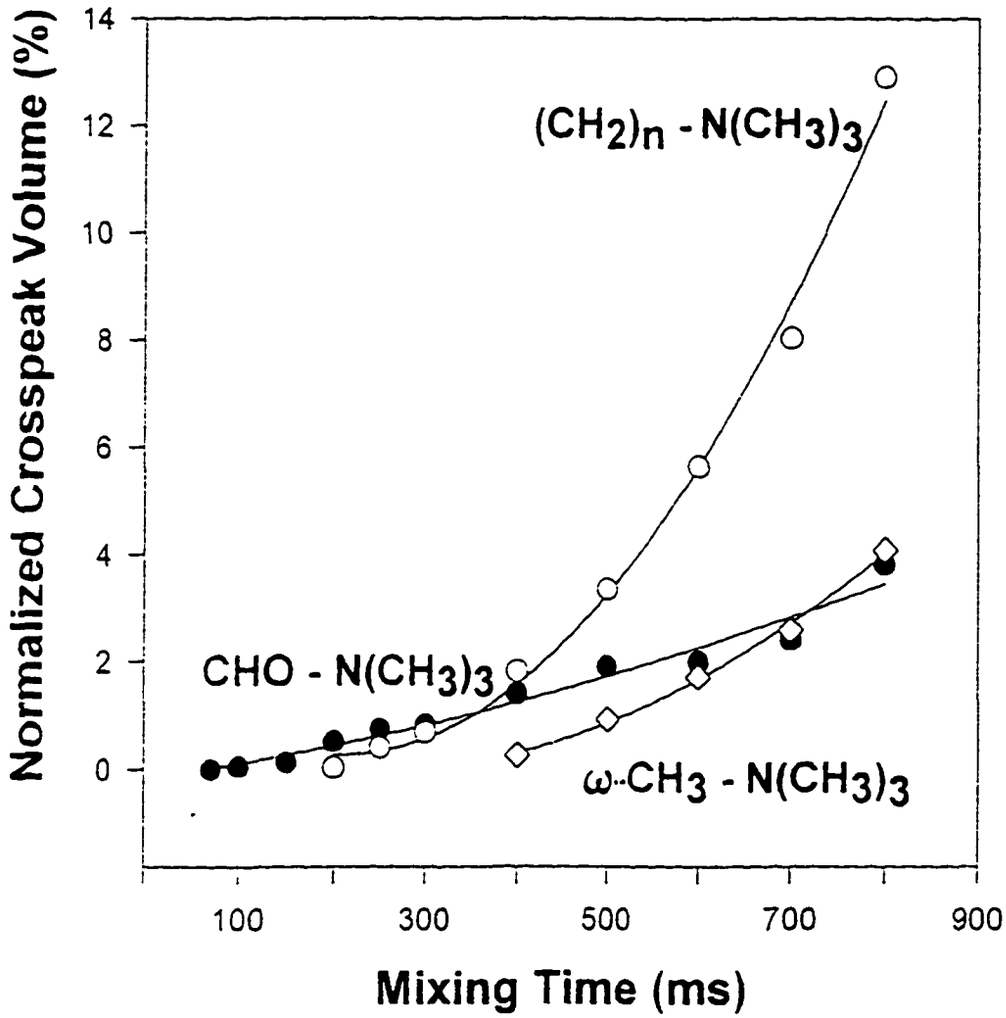

Figure IV-19. ^{1}H 200-MHz MAS NMR spectra for PC/CH systems with varying lipid composition. All spins rates are in the range 2-3 kHz.

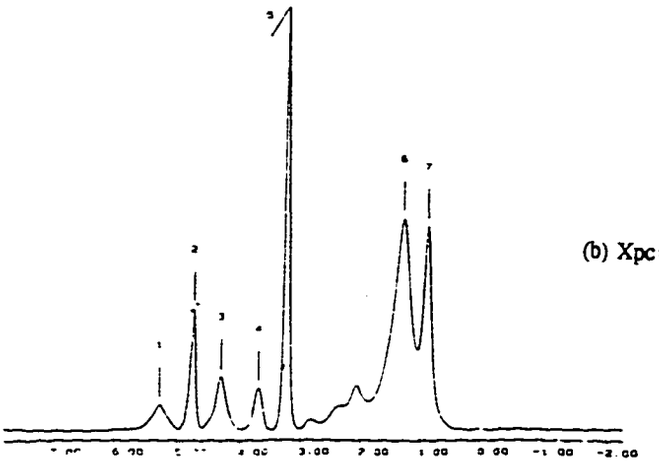

(b) Xpc=0.75

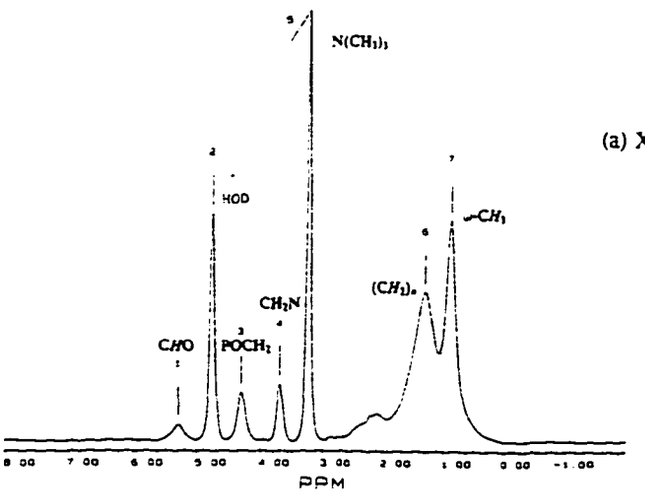

(a) Xpc=0.50

Figure IV-20. Centerband region of MAS ^{1}H NMR spectra of 1:1 PC/CH mixtures, obtained with contrasting acquisition strategies. (a) and (b): 300-MHz MAS and CRAMPS spectra acquired with spinning speeds of 1200 and 1225 Hz, respectively; (c) 300-MHz spectrum with 7-kHz MAS; (d) 400-MHz spectrum with 11-kHz MAS.

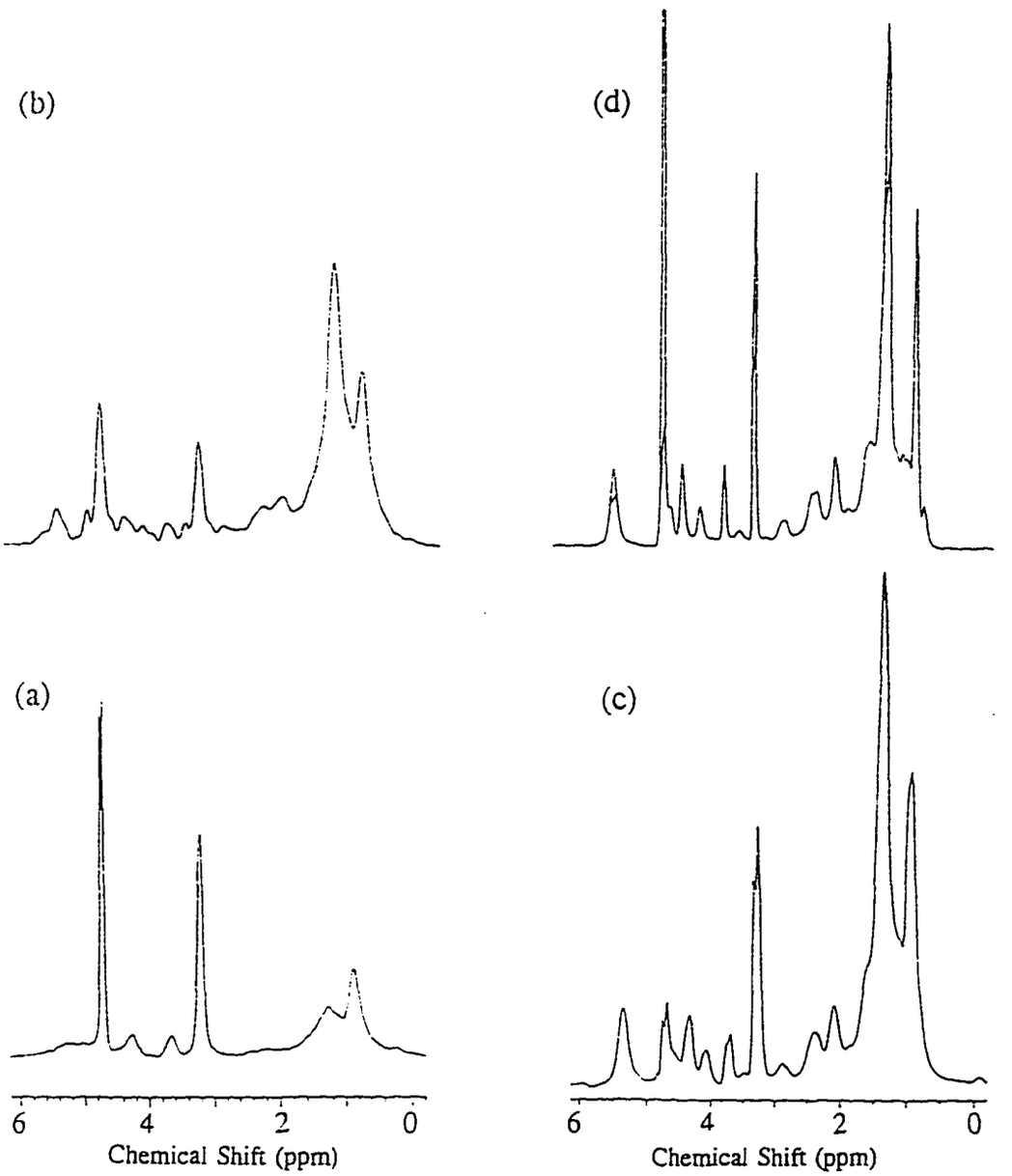

Figure IV-21. MAS ^{1}H NMR spectra (200.13 MHz, unless noted otherwise) of 50% (w/w) aqueous lipid dispersions, showing a full spectrum of one mixture at the bottom and several centerband regions as insets. (a) and (d): 1:1 PC-CH mixture, υ_{rot} = 2.2 kHz; (b): 3:1 PC-TO mixture, υ_{rot} = 2.0 kHz; (c): pure egg PC, υ_{rot} = 2.0 kHz; (e): 7:3 SPM CH mixture, υ_{rot} = 2.0 kHz (data obtained at 300 MHz).

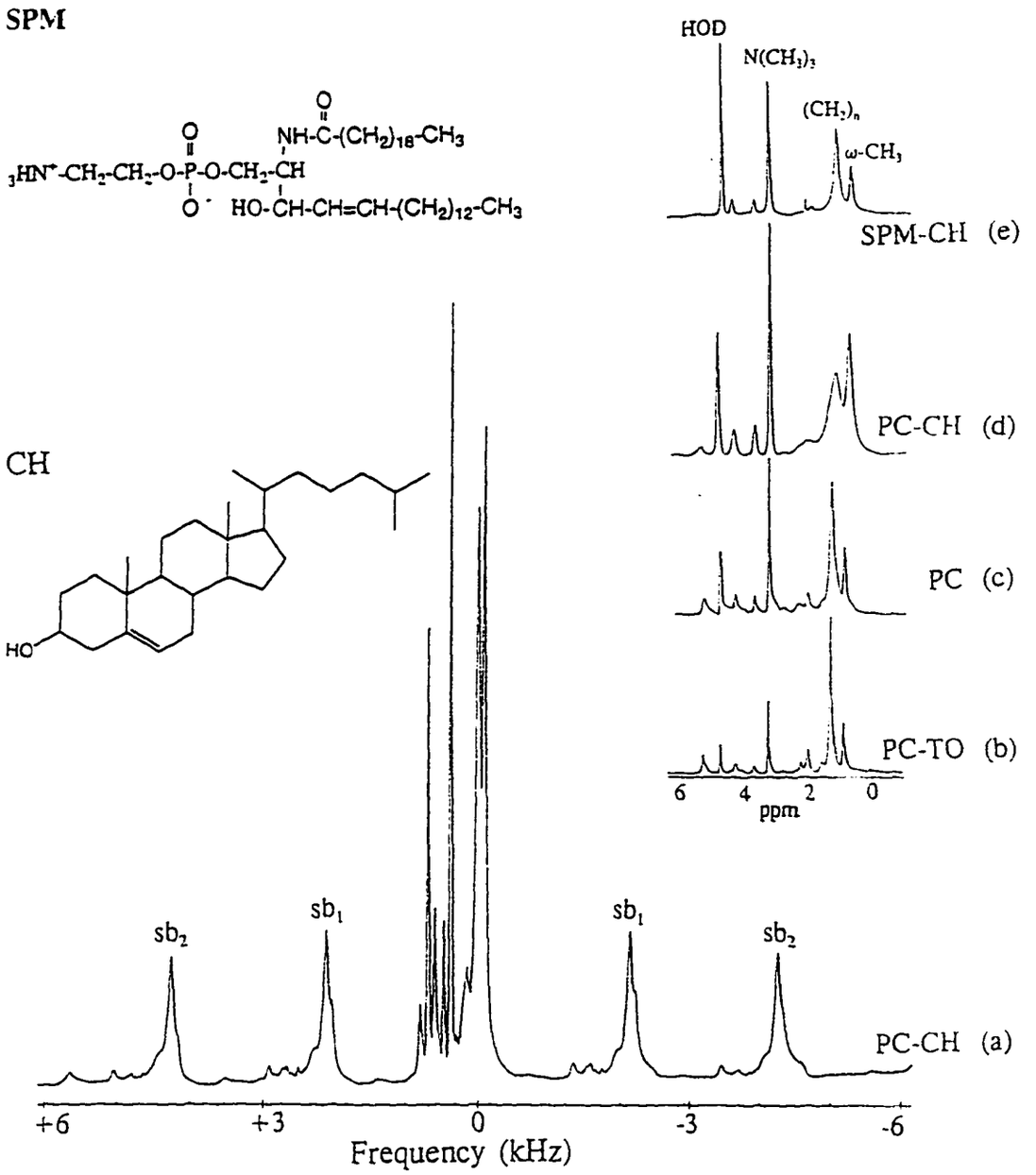

Figure IV-22. The variation of ^{1}H NMR spinning sideband intensities (I) with rotation speed (υ) for the bulk-methylene resonance of the PC=TO, PC-CH, and pure PC aqueous dispersions.

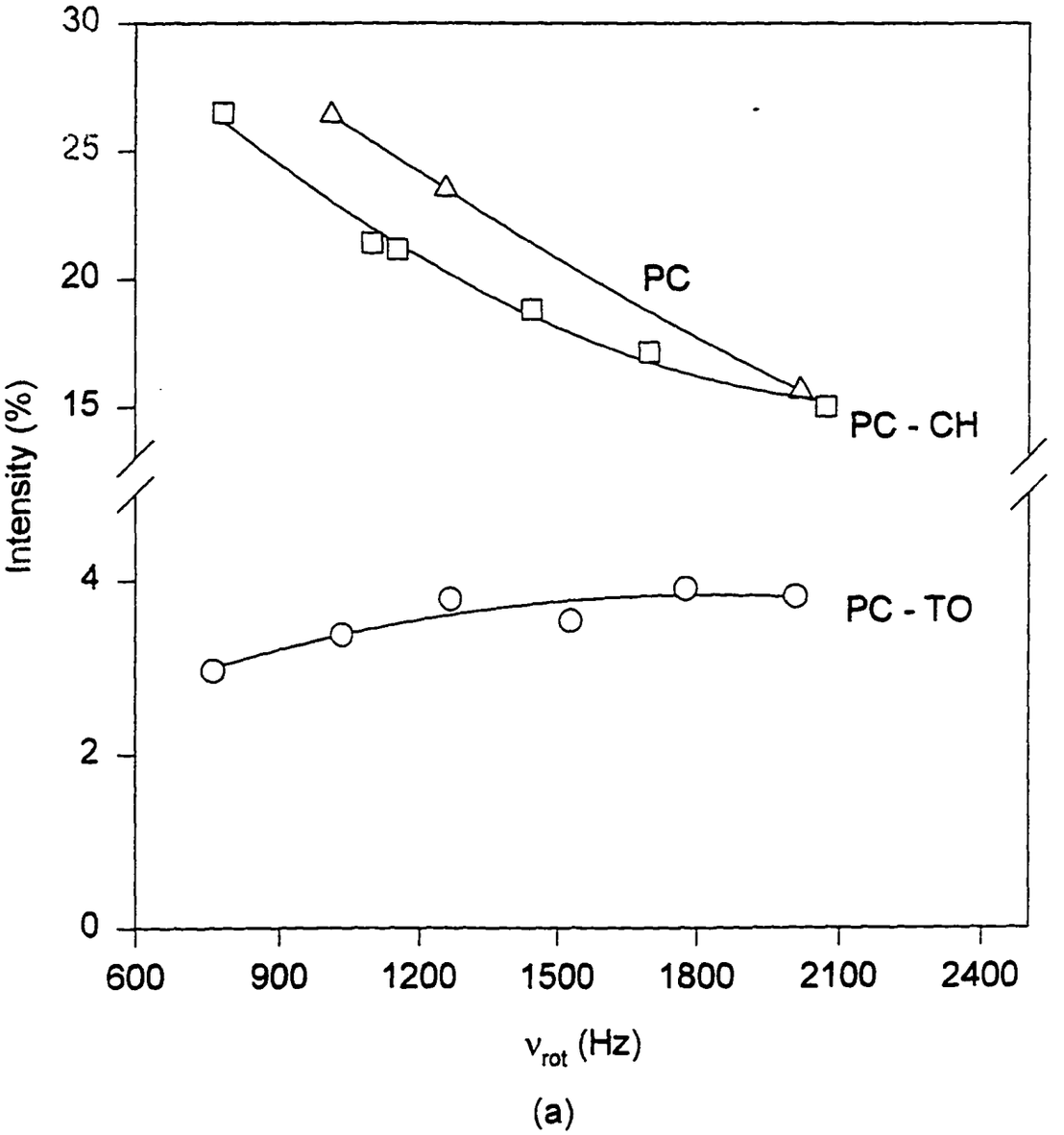

(a)

Figure IV-23. 50-MHz ^{13}C DP-MAS-SD NMR spectrum for PC-CH systems. MAS at 2.0 kHz was used to acquire both spectra.

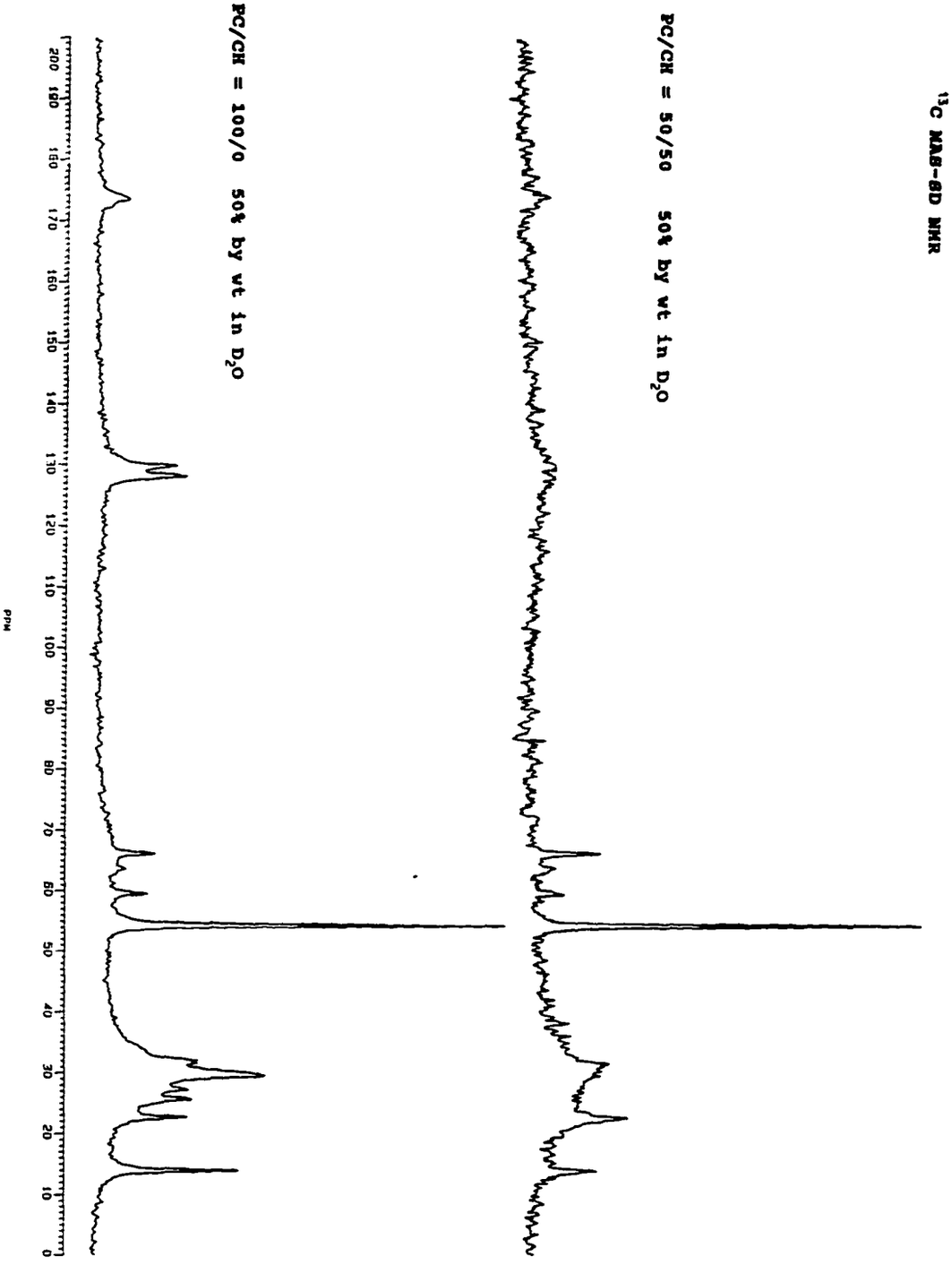

Figure IV-24. 50-MHz ^{13}C MAS NMR spectra for PC-CH systems, obtained using different decoupling schemes.

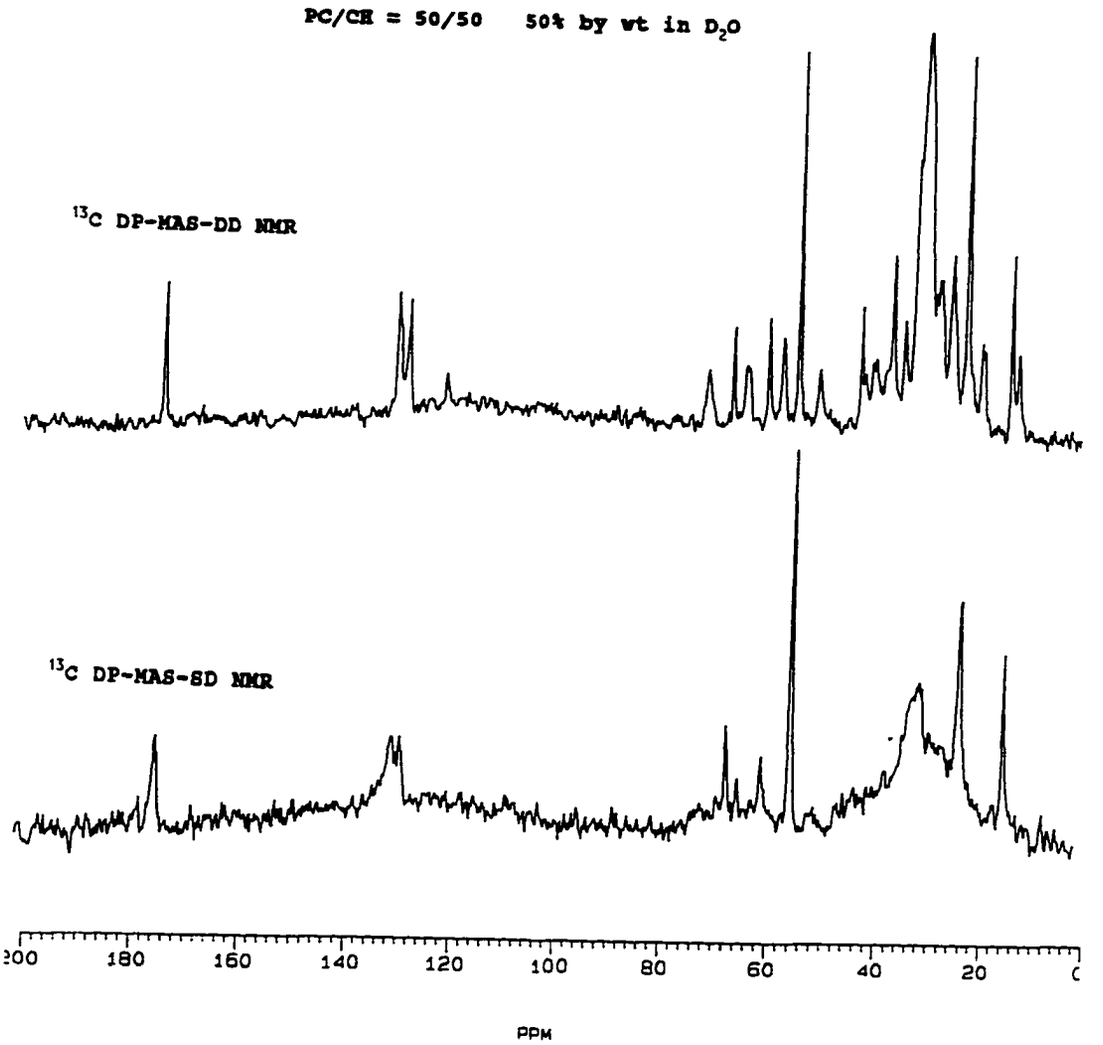

Figure IV-25. 50-MHz ^{13}C MAS NMR spectra for PC-CH systems, obtained using different polarization methods (CP and DP).

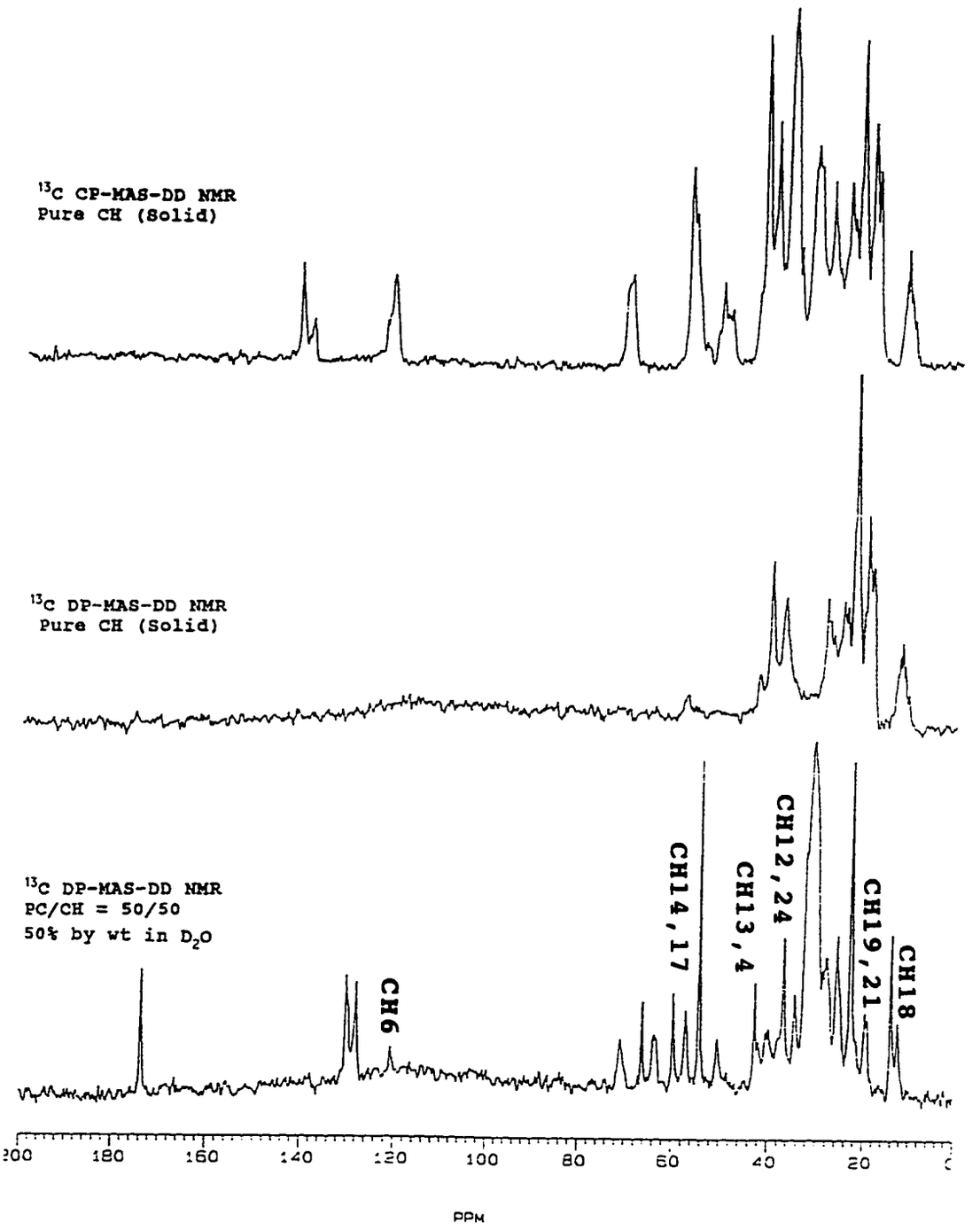

Figure IV-26. Upfield region of the DPMASDD 75-MHz ^{13}C NMR spectra of a 70:30 SPM-CH aqueous dispersion (middle), the SPM constituent (bottom), and the CH constituent (top).

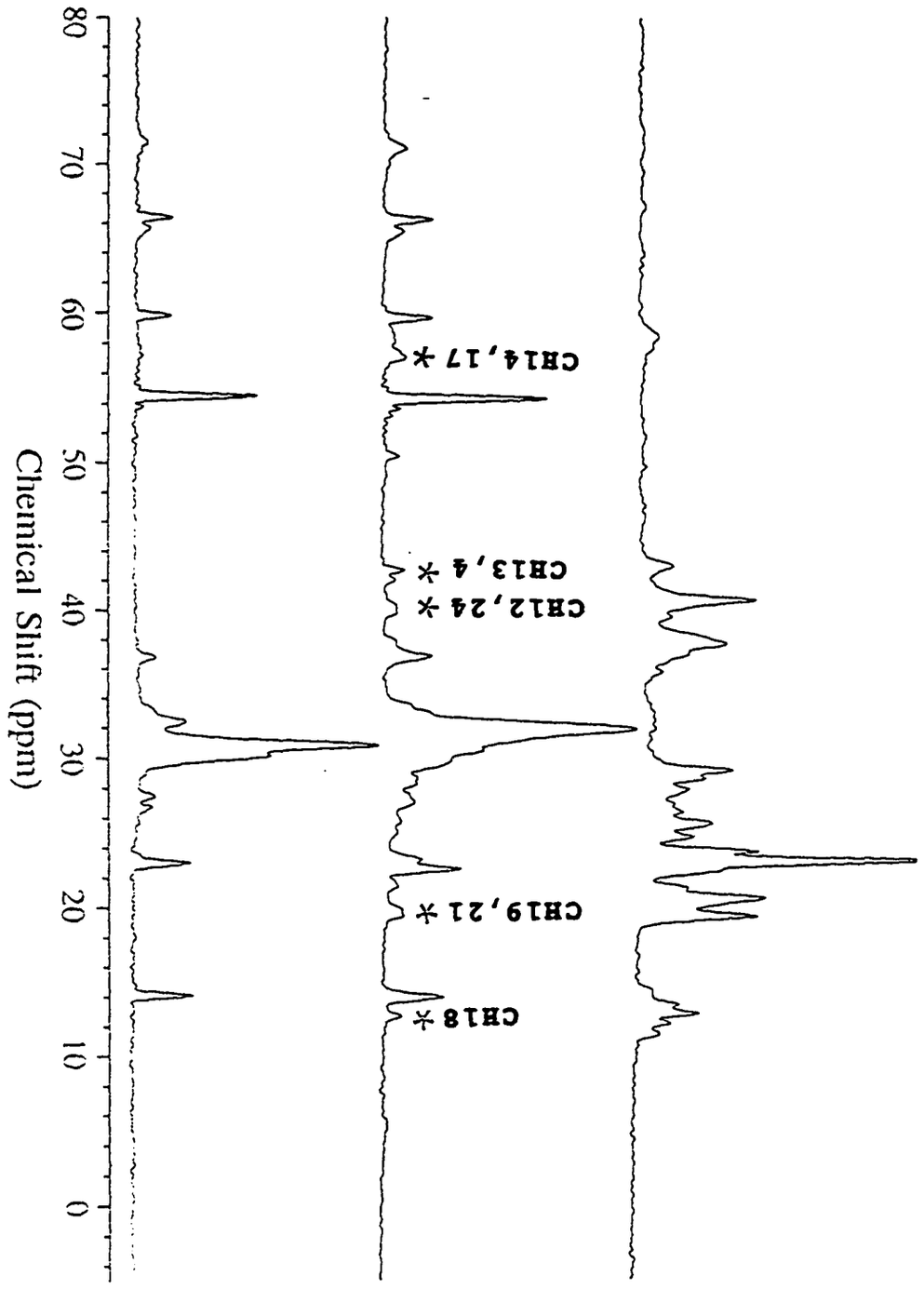

V. Insoluble Plant Polyesters

A. Introduction

The cuticle of higher plants serves primarily to protect the leaves and fruit from their environment and controls molecular diffusion among various organs. It forms a barrier against chemical, bacterial, and fungal attack and prevents water loss **(Figure V-1a)**. Its major chemical constituents are waxes that provide waterproofing and either of two insoluble structural polyesters which serve as the structural support: cutin, in the aerial parts, and suberin, in the underground parts and at wound surfaces **(Figure V-1b)**. Cuticular breakdown may occur though the action of bacterial or fungal pathogens, with potentially devastating agricultural and economic losses (Kolattukudy, 1984; Goodman et al., 1986).

In order to develop a molecular rationale for cuticular function, it is very important to have compositional and structural information for these polyester materials, as well as their assemblies with waxes and cell-wall carbohydrates. Their chemical composition and monomer units have been the subject of numerous investigations (Holloway, 1982; Kolattukudy, 1984; Stark et al., 1989; Walton, 1990), including the use of various chemical and enzymatic methods

such as hydrogenolysis with $LiAlH_4$, hydrolysis with alcoholic KOH or HCl, and cleavage with cutinases. As a more direct route to molecular structure determination in the cuticle, the cutin and suberin systems have been the subject of solid-state nuclear magnetic resonance investigations (Zlotnik-Mazori and Stark, 1988; Garbow et al., 1989; Stark et al., 1989; Stark et al., 1994).

CPMAS ^{13}C NMR, conducted with variation of the decoupling strength (low power, SD; high power, DD), has revealed surprising molecular flexibility of the cutin polyester; the relationship between dynamic behavior and polymer mechanical properties has been explored by combining ^{13}C and ^{2}H NMR techniques and sorting out the effects of magic angle spinning, cross polarization, and nuclear spin relaxation. Our experiments on plant polyesters are designed to understand how the monomer units of cutin are linked to each other, how the polymers are embedded within wax or cell-wall matrices, and how their supramolecular architecture might be related to cuticular function.

B. Results and Discussion

1. Solid ^{13}C NMR Studies of Lime Cutin After Selective Degradation

(Portions of this section were published: Ray et al., 1995)

A typical ^{13}C CPMAS spectrum is compared with DPMAS (direct polarization magic-angle spinning) and DPMANS (direct polarization magic-angle non-spinning) experiments for intact lime cutin in **Figure V-2**. **Table V-I** summarizes chemical-shift assignments for this material, including moieties observed by CPMAS and DPMAS methods (Stark et al., 1989).

Partial depolymerization of the cutin polyester has been accomplished using chemical methods, including hydrolysis with alcoholic KOH and breakdown with $(CH_3)_3SiI$. The soluble monomers from hydrolysis are listed in **Table V-2**, but these monomers do not reveal crosslinks or molecular architecture within the intact biopolymer and they represent only partial (60-80%) depolymerization.

A complementary view of lime cutin hydrolysis is obtained from examination of the solid residue recovered after the above treatment. **Figure V-3** compares high-resolution ^{13}C NMR data for intact cutin and the unreacted residues after 8 and 22 hours, respectively. In contrast to the broad cutin lines attributed previously to a dispersion of chemical environments within an irregular polymer, the narrower signals observed in spectra of the lime cutin residue are consistent with removal of the monomers to yield a more homogeneous material. In the bulk methylene region,

for instance, the carbons that resonate at 25 and 41 ppm are absent from ^{13}C NMR spectra of the residues. As the hydrolysis proceeds, the CPMAS ^{13}C NMR spectra reveal that particular carbon types are removed or retained. The carbonyl signals from secondary esters (173 ppm) are progressively and strikingly diminished in size, whereas the carbonyls of primary esters (168 ppm) are retained in the lime residue. Concomitantly, the CHO signal intensity (72 ppm) increases with respect to the $(CH_2)_n$ resonances (29 ppm). These two observations suggest that KOH preferentially hydrolyzes esters of secondary alcohols, thus converting CHOC=O to CHOH groups within the solid residue. As these CHOH groups are produced, the $(CH_2)_n$ signals are diminished by the removal of long-chain fragments, which ultimately appear as soluble monomers. The aromatic or unsaturated resonances in the ^{13}C NMR spectrum (115 and 129 ppm) are also reduced in intensity, though we identified only minor monomers that contain these functional groups.

Although intact cutin contains significant numbers of mobile methylene and carbonyl carbons that give NMR signals under low-power decoupling conditions, its residues yield very weak DPMASSD spectra and thus consist almost exclusively of rigid, solidlike functional groups **(Figure V-4)**. As expected, the mobility of $(CH_2)_n$ groups depends dramatically on reaction temperature and reaction time.

Bulk methylene carbons of intact cutin exhibit considerable segmental mobility as described above and shown in **Figure V-4a**. By comparison **(Figure V-4b-d)**, the methylene groups after reaction exhibit surprising motional restrictions and thus weak DPMASDD spectra. Particularly notable is, the peak at 29 ppm for $(CH_2)_n$, which appears as a weak, broad feature after KOH treatment at 78 °C for 8 hours. These results show that cross-linked regions are resistant to depolymerization, making the cutin residue more rigid.

In summary, solid-state ^{13}C NMR provides structural information regarding lime cutin. The spectral linewidths and spectra obtained under varying acquisition conditions suggest that a more homogeneous, more rigid polymetric residue is retained after transesterification or hydrolytic treatment. In addition, the surprising selectivity of the methanolic KOH reagent is evidenced by the CPMAS ^{13}C NMR spectra: resonances from esters of secondary alcohols are removed preferentially. Perhaps because of their abundance at the surface of the cutin particles, these crosslinks may be cleaved quite readily, thus relieving strain within the polymeric structure. Further studies of cutin molecular structure and dynamics are currently in progress.

2. ^{2}H NMR Studies of Tomato Cuticle After Physical and Chemical Exchange

It is essential to understand how the supramolecular architecture and interactions of plant cuticle polyesters are tied to their protective functions. In conjunction with our efforts to understand the protective functions of the fruit cuticle, we used chambers of controlled relative humidity to swell tomato skins with D_2O (Stanley, 1994). The impact of hydration on the cuticular polymers has been examined with ^2H and ^{13}C NMR experiments, conducted as a function of the degree of hydration and temperature. Since the quadrupole splitting in the ^2H NMR spectrum depends on the angular orientation of the deuterium and the extent to which its orientation is averaged by molecular motion, the water (D_2O) mobility can be studied in detail by ^2H NMR. These experiments establish whether the water exists in pools or films and whether it becomes incorporated at specific sites of the cutin polymer.

The two principal features that have emerged from ^2H NMR studies of hydration of cuticle are the presence of two inequivalent water environments. A damp cuticle sample containing 1% by weight water yields the quadrupole echo data shown in **Figure V-5**. A narrow central resonance is observed in each spectrum, albeit 200-1000 times broader than bulk D_2O. In addition a broader feature is present; its lineshape indicates some motional averaging even at -10 °C. As the temperature is lowered through the range of

plausible growth and frost conditions for tomatoes, we observed an increasing spectral contribution from the semirigid population of deuterons. A wet cuticle sample containing 8%-by-weight water provides the data shown in **Figure V-6**. As before, a narrow central resonance is observed in each spectrum, but it broadens somewhat and shows very modest contributions from rigid deuterons even at -25 °C.

The narrow peak is attributable to mobile but anisotropically tumbling water absorbed within the tomato cuticle, but what is the broader pattern? It could be a more immobilized population of hydrogen-bonded water in the cuticle polymer, or it could also arise from OD groups exchanged with hydroxyl groups of the cutin polymer. If water exchanges with hydroxyl groups on the cutin polymer itself, then a broad ^2H NMR signal should remain after drying of the sample. In fact, we observe no signals after removing the water (data not shown); thus the broader pattern may be attributed to hydrogen-bonded water in association with the cutin polymer.

Nevertheless, we wished to establish whether the tomato cuticle has OH groups that are accessible to water D_2O. **Figure V-7** shows the spectra of tomato cuticle exchanged with D_2O by chemical methods (see Experimental Methods) and

dried for 48 h in a SpeedVac. If the broad pattern came from bound water it would disappear, as it did in the series of hydrated wet or damp samples **(Figures V-5 and V-6)**. The retention of this pattern demonstrates that deuterium can be made to exchange with cuticle OH groups. Taken together, these results may be interpreted in terms of "free" water, bound water and exchanged water. First, we define "free" water as mobile and behaving like pure water. The observation of a narrow central peak provides evidence for very mobile water. If hydration produced pools of water (free water) rather than films (bound water), only narrow ^{2}H power patterns characteristic of ice would have been observed.

Second, bound water which is distributed homogeneously throughout the sample should have some kind of binding sites on the surface of the cuticle. This population of water shows a significant degree of order and motional restriction, as evidenced by spectral patterns 140-180 kHz in breadth. It is likely that this water is hydrogenbonded to hydroxyl groups on the surface of the tomato cuticle.

Finally, after extensive reflux of the cutin with D_2O, the water exchanges with polymer hydroxyl groups that have now become -OD groups. Our ^{2}H NMR results not only demonstrate the presence of free water and bound water, but

they also improve the fundamental understanding of molecular details concerning the interaction of bound water on the surface of the cuticular polymer.

Table V-1. ^{13}C Chemical Shifts for Intact Lime Cutin

Carbon Type	Chemical Shift (ppm)
$(\underline{C}H_2)_n$	29
$\underline{C}H_2CH_2OCOR$	42
$\underline{C}H_2OCOR$	64
$\underline{C}HOCOR$, $\underline{C}HOH$	72
ROCOCH=CH<u>Ph</u>	105-156
$CH_2O\underline{C}=O(R)$	168
$CHO-\underline{C}=O(R)$	173
$\underline{C}=O$	209

Table V-2. Soluble Monomers from Alkaline Hydrolysis

	Monomer Type	Composition of Soluble (mol %)
Cutin	$HOCH_2(CH_2)_5$- $CHOH(CH_2)_8COOH$	28
Cutin	$HOCH_2(CH_2)_5$- $CO(CH_2)_8COOH$	51
Waxes	$CH_3(CH_2)_nCH_3$, $CH_3(CH_2)_nCH_2OH$ $n \approx 30$	

Figure V-1. (a). Schematic drawings of cuticle in epidermal and peridermal locations of higher plants (Kolattukudy, 1984; Watton, 1990). (b). Proposed molecular structures for cutin (Kolattukudy, 1980; Zlotnik-Mazori & Stark, 1988).

a

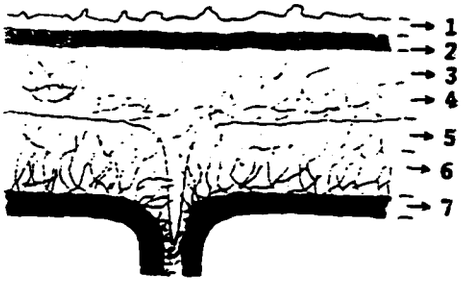

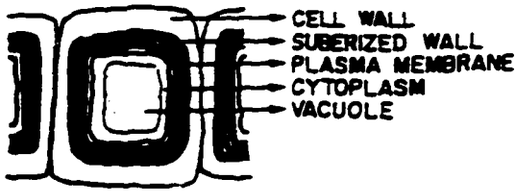

1. epicuticular wax. 2. cuticle proper. 3. exterior cuticular laver. 4. interior cuticular laver. 5. exterior cellin wall. 6. interior cellin wall. 7. epidermal cell wall.

b

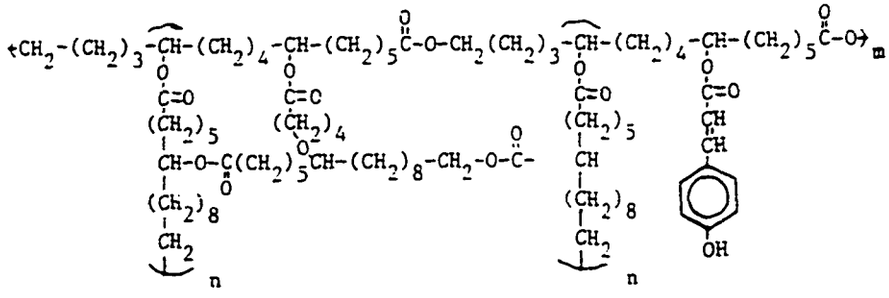

Figure V-2. 50-MHz CPMASDD ^{13}C NMR spectrum, compared with DPMASSD and DPMASSD (non spin) ^{13}C NMR spectra for intact lime cutin.

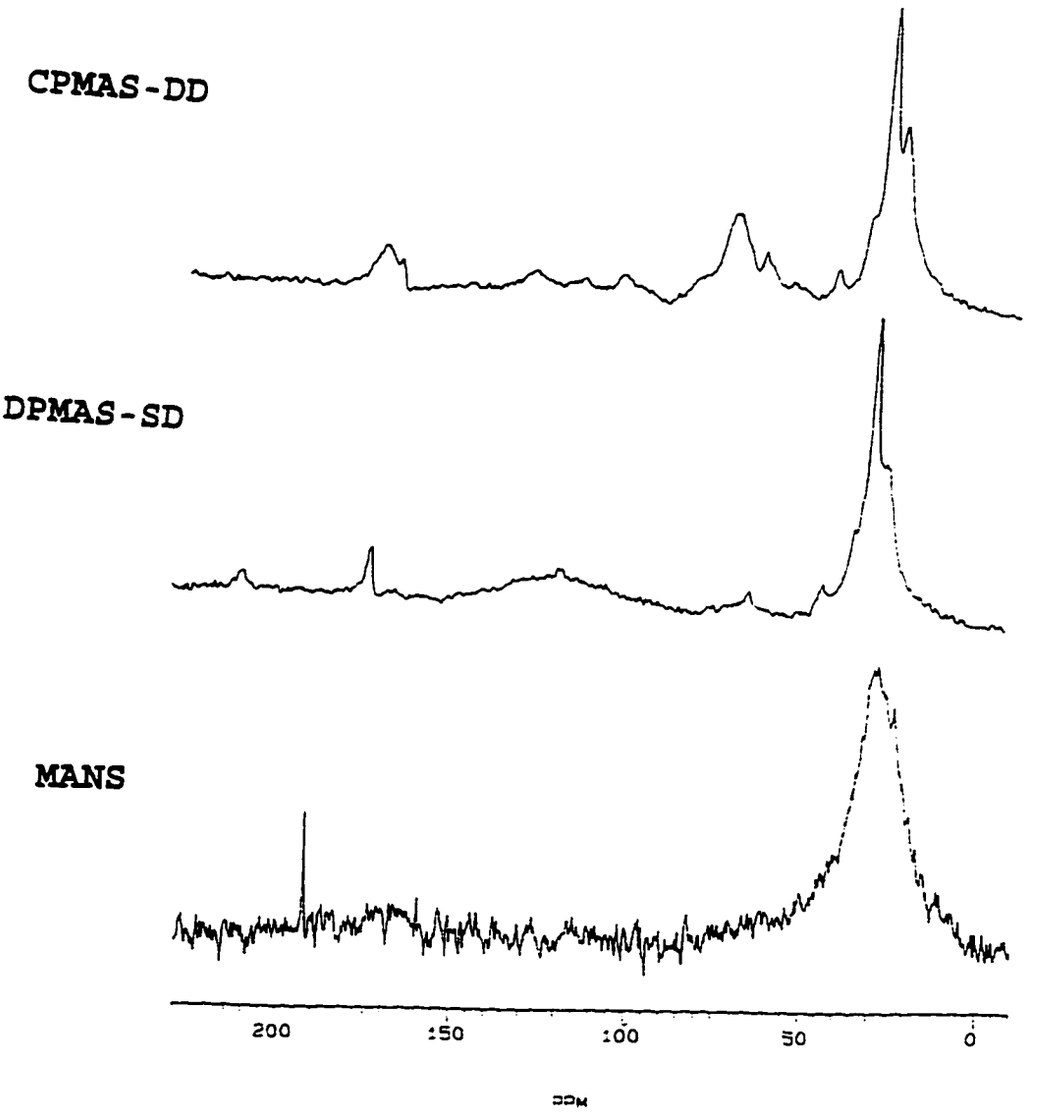

Figure V-3. 50-MHz CPMAS ^{13}C NMR spectra of lime cutin a: before degradative treatment; b: after 8-h treatment; and c: after 22-h treatment with methanolic KOH.

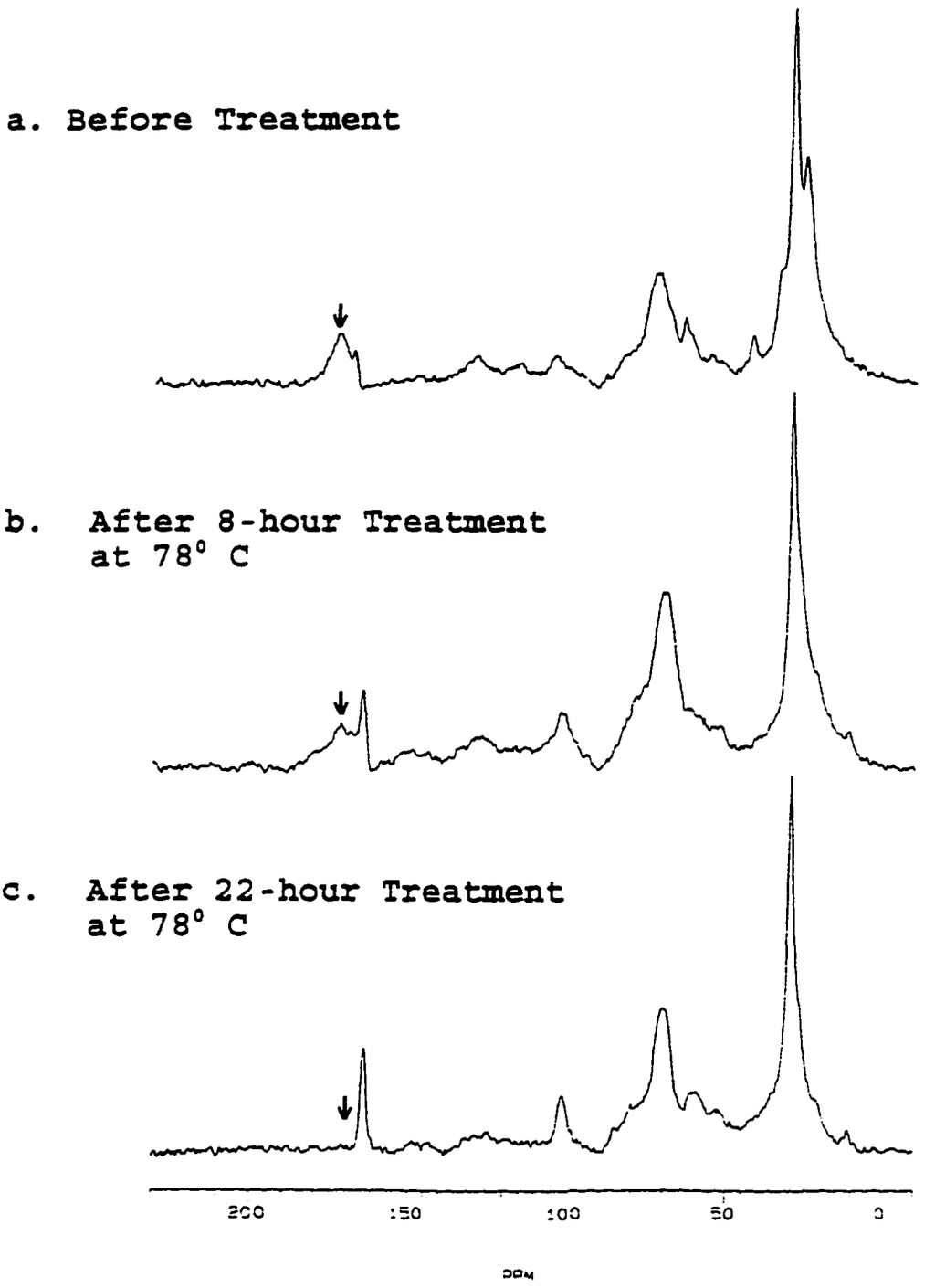

Figure V-4. 50-MHz DPMASSD ^{13}C NMR spectrum of lime cutin: a: before treatment; b: after 1-h at 0 °C treatment; c: after 1-h at 78 °C treatment; and after 8-h at 78 °C treatment with methanolic KOH.

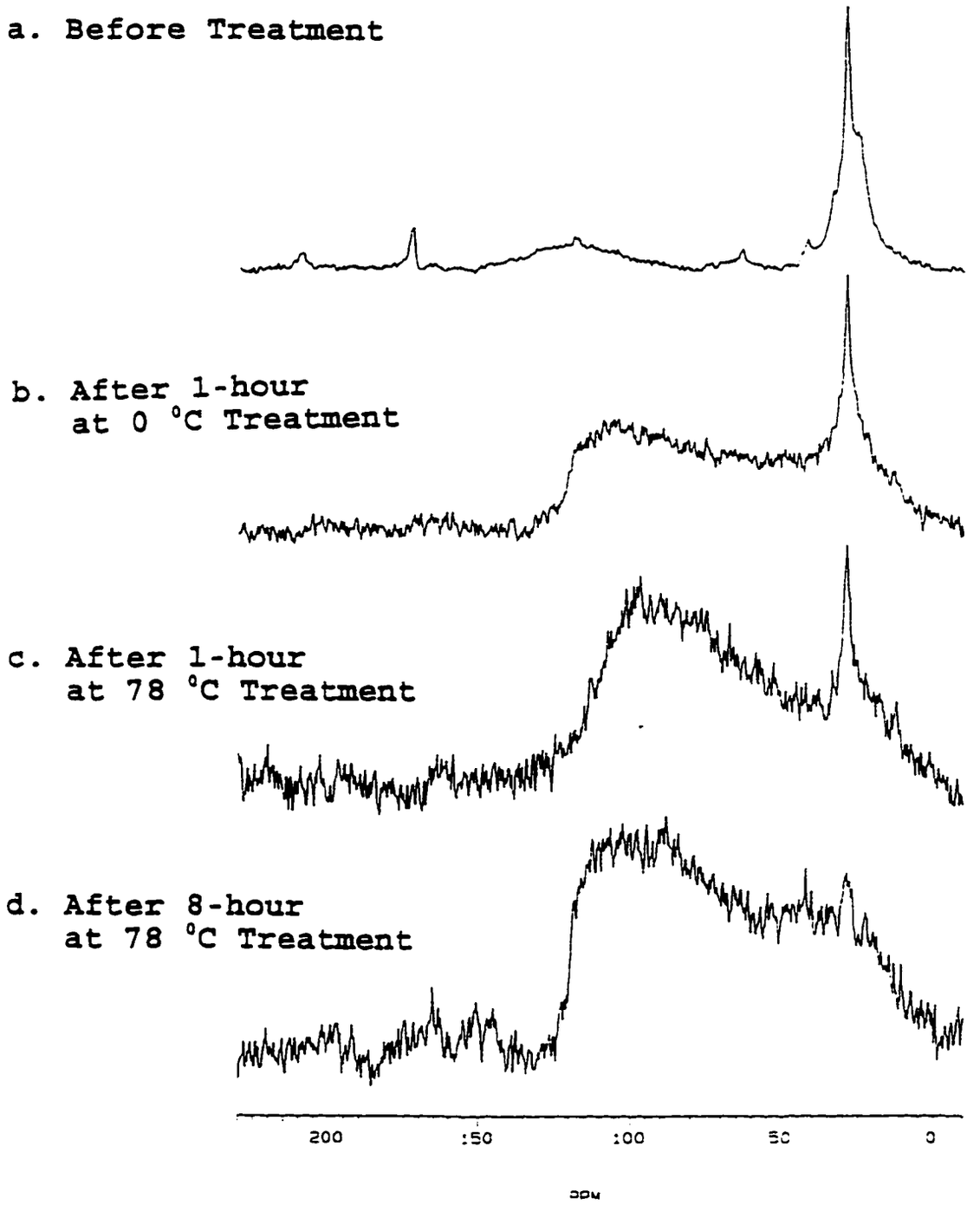

Figure V-5. 46-MHz ^2H quadrupole echo spectra of tomato cuticle containing 1% D_2O at different temperatures. The data were obtained using a 5-mm Varian wideline probe, P(π/2) = 2.4 ms, SW = 2 MHz, RD = 1 s, plots normalized to the tallest peak.

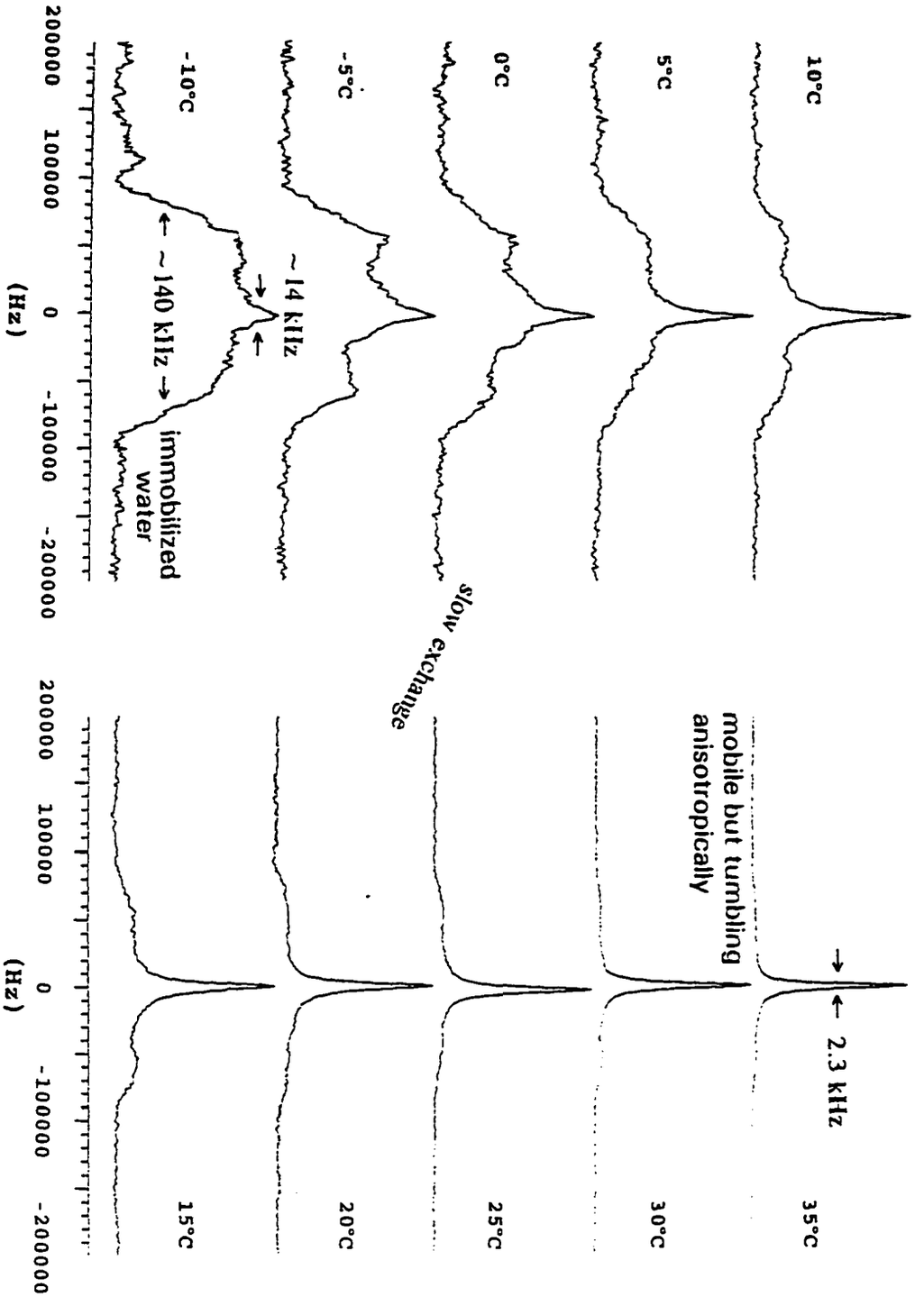

Figure V-6. 46-MHz ^2H quadrupole echo spectra of tomato cuticle containing 8% D_2O, obtained as described in Figure V-5.

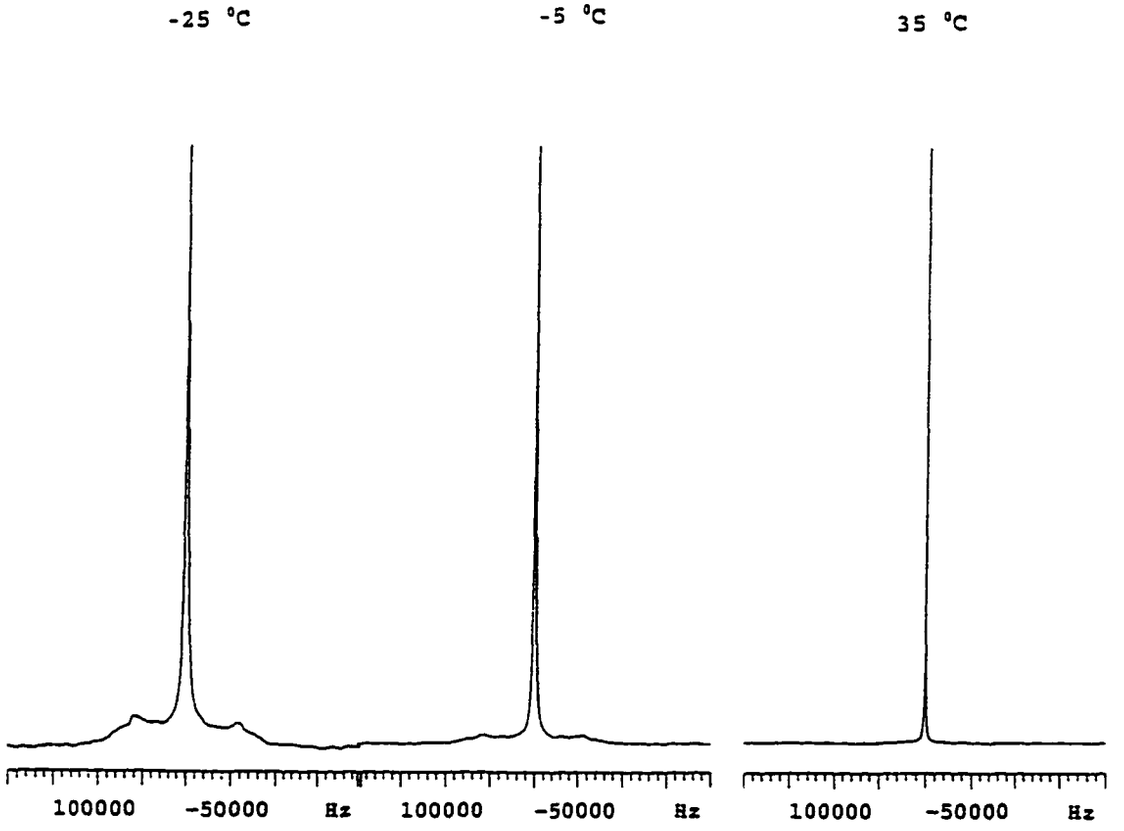

Figure V-7. 46-MHz ^2H quadrupole echo spectra of tomato cuticle exchanged with D_2O using chemical methods and subsequently dried (see Experimental Methods), obtained as described in Figure V-5.

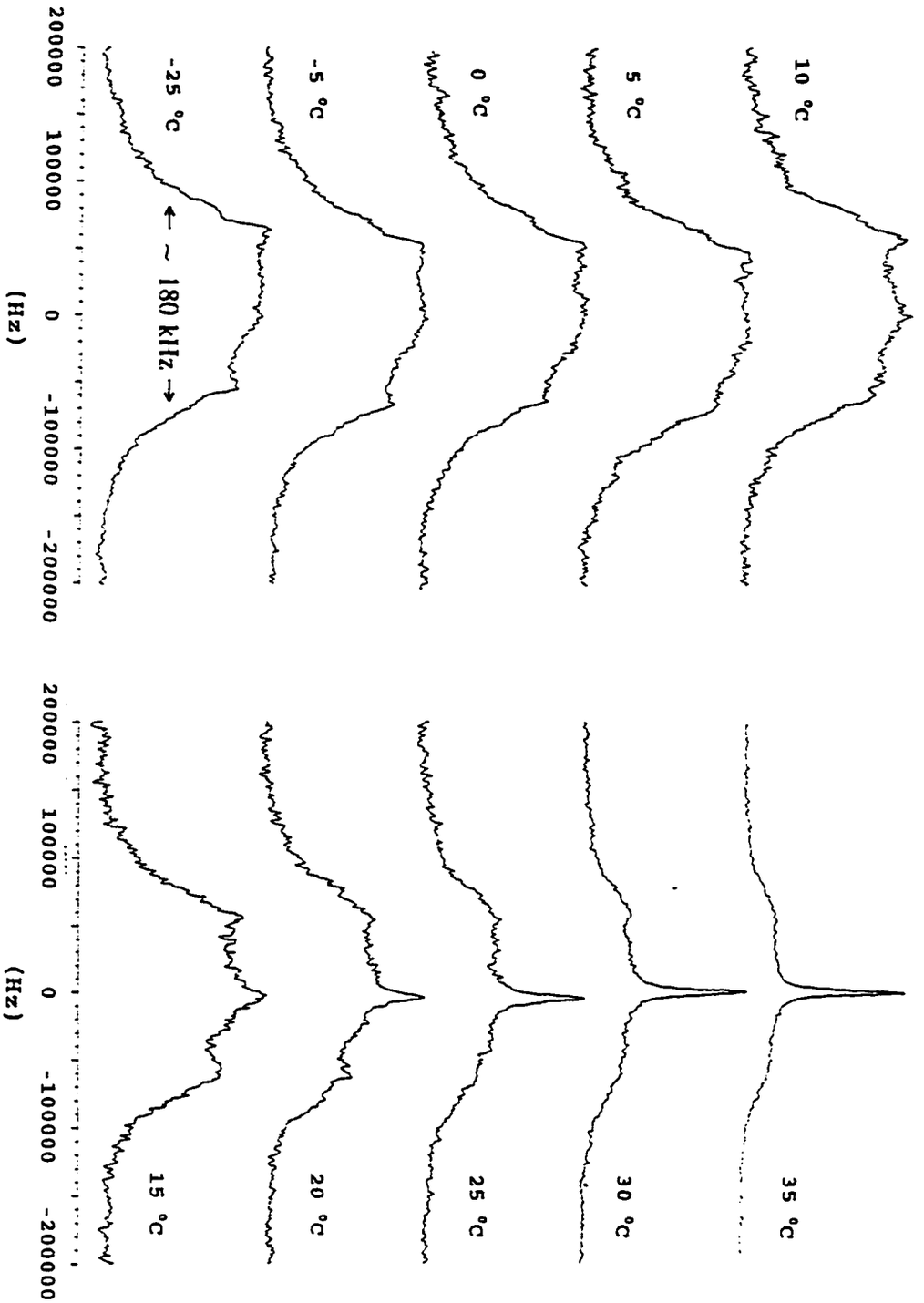

VI. Conclusions

The drive behind NMR spectroscopic studies on lipid model membranes is to discover links between biophysical properties of these lipid structures and their ultimate function. In the work presented herein, solution, semisolid, and solid NMR have been used to study the molecular structure and organization of different kinds of intestinal lipids, phospholipids and plant lipids of interest in human physiology, cell biology, and agriculture.

In an attempt to understand digestive processes from substrates' point of view, C_8 model mixtures of late-stage triglyceride digestive products were prepared from a monoglyceride, fatty acid, and bile salt, which are representative of butter-fat breakdown products or therapeutic nutrient cocktails undergoing digestion in the small intestine. An NMR study of this mixture containing C_8 components was carried out by means of high-resolution, solution state ^1H, ^{13}C, and 2D NMR experiments. Using a combination of 1D and 2D solution NMR, it was possible to assign all of the ^1H resonances for two complex C_8-based model digestive mixtures. The NOESY connectivities between BS protons provide strong evidence for back-to-back bile-salt dimers within the mixed micelle. A number of intercomponent crosspeaks between BS and FA are observed,

confirming the involvement of FA (and MG) molecules in large molecular aggregates. Our new structural model based on two dimensional NOESY and ROESY describes the molecular organization of FA, MG, and BS constituents. This model accounts for a large body of new NMR data, including Mn^{2+} titrations and NOE connectivities.

Aggregation phenomena are often of central importance to the function of macromolecules, from industrial applications such as surfactant-assisted oil recovery to biomedical phenomena such as the intestinal digestion of acylglycerols. Based on our NMR line broadening and NOESY/ROESY results we proposed an aggregate structure that sequesters hydrophobic and hydrophilic functionalities and maximizes favorable intermolecular interactions. It was also possible to test the proposal against size measurements from quasielastic light scattering. Our finding of different size aggregate arrangement for C_8 suggest a structural basis for the different ways in which digestive products are processed physiologically. These micellar aggregates may be thought to play a role in these latter processes as vehicles for transport of digestive products to the absorptive mucosa of the small intestine. Thus our work provides a molecular picture of how the hydrophobic products of glyceride digestion are packaged by bile salts for association with fatty acid-binding proteins and transport

to the absorptive mucosa of the small intestine. For these complex systems, solution state NMR techniques provide direct structural information on molecular organization at physiologically relevant concentrations.

For lipid mixtures that form multilamellar dispersions rather than mixed micelles, our studies define several approaches using one- and two-dimensional MAS NMR spectroscopy for the study of water-lipid, lipid-lipid and cholesterol-lipid interaction on a molecular level. First, semisolid ^{1}H NMR has been used to examine surface hydration in suspensions of MeDOPE. The known thermotropic phase behavior of this lipid was verified using static ^{31}P powder patterns. The MAS ^{1}H spectra for aqueous suspensions of MeDOPE in the Lα phase exhibited two resonances of roughly equal integrated intensity, where the downfield shifted peak with the shorter T_1 relaxation time was ascribed to hydrogen-bonded interlamellar water in slow exchange with other water molecules. The upfield peak with a long T_1 relaxation time arises from an exchange averaging between the bulk water and lipid solvation water. For lamellar suspensions of MeDOPE, positive NOESY crosspeaks were observed between the downfield-shifted water resonance (only) and both CH_2N and $NH_2CH_3^+$ protons of the lipid headgroup. Such a population of water molecules exists in association with MeDOPE in the lamellar phase but not for its inverted phases or for

lamellar dispersions of DOPC. Thus, semisolid state NMR provides a unique tool for studying the population of water molecules associated with lipid and allows determination of the conditions under which such water molecules exist. The ability to measure this population of water molecules will allow for further assessment of the role such lipids play in the membrane function. The results presented here show how ^{1}H spectral characteristics may provide detailed information on packing and organization of these physiologically important states.

In a second initiative, we used several deuterated DMPCs to critically evaluate the structural information content of a NOESY crosspeak between methyls of the lipid headgroup and the acyl chains. Although the spin-relaxation and line-narrowing behavior in these multilamellar systems argue against efficient spin diffusion, interdigitated or chain-bendback structural models that bring these ^{1}H nuclei into close proximity are not implicated by the MAS-NOESY results for this phospholipid system. We have proposed a new mechanism for formation of these types of crosspeaks: through-space interactions link the headgroup and backbone protons on adjacent molecules and then spin diffusion occurs along the acyl chains.

Thirdly, we have developed MAS ^{1}H and ^{13}C NMR protocols for the investigation of lipid order in unlabeled dispersions of cholesterol-containing model membranes. Although ^{2}H NMR methods have been applied widely and successfully to structural studies of gel and liquid-crystalline lipids, selective deuteration is often a difficult, expensive, and time-consuming process. A series of MAS ^{1}H and ^{13}C NMR experiments were carried out for multilamellar dispersions formed by PC/CH and SPM/CH: high-speed MAS ^{1}H NMR yields narrow, multiline spectra for both PC/CH and SPM/CH in liquid-crystalline lipid systems; the average degree of chain order was judged from spinning-sideband intensities measured in the ^{1}H MAS NMR spectra. Because molecular motion reduces the efficiency of CP in liquid-crystalline multilayer systems, the combination of direct polarization (DP), MAS, and high-power dipolar decoupling (DD) produced well-resolved ^{13}C NMR spectra, allowing us to observe signals from both phospholipid and cholesterol components of the mixture. DPMAS experiments conducted under low-power decoupling (SD) conditions complemented these results by identifying the most mobile functional groups of the phospholipid headgroups and revealing the impact of CH on bilayer flexibility. These methodological studies set the stage for more systematic investigations of cholesterol interactions in model biological membranes.

Finally, we have employed solid-state NMR to study the molecular structure and dynamic properties of lime and tomato cuticles. Controlled hydrolysis of the lime cutin polyester has been carried out in order to elucidate its molecular architecture and allow identification of its major monomeric constituents; the insoluble residues have been analyzed with CPMAS ^{13}C NMR, which supports a surprising preferential cleavage of the ester of secondary alcohols. This work has aided our understanding of chain and crosslink structures in plant cuticle, which in turn may impact its resiliency and ability to support the waxy protective waterproofing.

Because the plant cuticle must control the influx and efflux of water, our ^{13}C and ^{2}H NMR investigations have also included a molecular assessment of how hydration affects both tomato cuticle and absorbed D_2O. Cuticular swelling with water renders the polymeric membrane more flexible, particularly at oxygenated carbon sites that might participate in hydrogen bonding. Water (D_2O) absorbed by tomato cuticle is less mobile than in the bulk: one population of deuterons tumbles rapidly but is not frozen. Under vigorous hydration conditions, exchange of water with cutin hydroxyl groups is demonstrated by ^{2}H NMR. This work illustrates that solid-state NMR is a powerful tool for the

study of molecular architecture and resiliency in the protective cuticle of higher plants.

The future prospects for the NMR methods as applied to the study of lipid model membranes are very promising. Encouraged by the results of solution, semisolid, solid state NMR studies on the above lipid model membrane systems, the following systematic structural studies should be feasible:

(1) on late-stage triglyceride digestive products, we can evaluate the structural impacts of (a) change of each component, simulating the progress of glyceride digestion or conditions of bile-salt deficiency; (b) change in the identity of digestive products, using diglycerides or longer-chain analogs in the mixed aggregates. In addition to 2D NMR methods, QLS measurements of shape and size distribution should be integrated into the investigative methodology for these mixtures.

(2) on lipid membrane systems, we can improve our ability to obtain sensitive and quantitatively reliable ^{13}C NMR spectra by using a new CP method, the so-called ramped-amplitude (RAMP)-CP, to overcome the disadvantages of both CP and DP. Moreover, it should be possible to compare

phospholipid order and mobility in multibilayer dispersions composed of PC/CH and SPM/CH in the identical molar ratios.

(3) on the plant lipid system, we can conduct MAS ^{13}C NMR to provide detailed structural and dynamic information about the resiliency of the cutin biopolymer: (a) DPMAS with contrasting decoupling strengths will permit determination of the numbers of relatively mobile and immobile carbons; (b) $T_1(C)$, $T_{1\rho}(C)$, and $T_{1\rho}(H)$ relaxation experiments will indicate the motional restrictions of those carbons that cross polarize and provide evidence for hydrophobic association of the long aliphatic chains of cutin and wax, respectively. It will be useful to examine these properties of the plant cuticle under dry, damp, and wet conditions such as might be encountered in agricultural production.

VII. References

Andrew, E. R., Bradbury, A., and Eades, R. G. (1959) Nature *183*, 1802.

Aue, W. P., Bartholdi, E., and Ernst, R. R. (1976) J. Chem.Phys. *64* 2229.

Barnes, S., and Geckle, J. M. (1982) J. Lipid Res. *23*, 161.

Bax, A., and Davis, J. (1985) J. Magn. Reson. *58*, 2077.

Bittman, R., (1993) in Cholesterol in Membrane Models, (L. Finegold, ed.), p45, CRC Press, Boca Raton, FL

Bittman, R., (1997) in Cholesterol: Its Functions and Metabolism in Biology and Medicine, (R. Bittman, ed.), Chapter 6, Plenum Press, New Tork.

Bligh, E. G., and Dyer, W. J. (1959) Can. J. Biochem. Physiol. 37, 911.

Bloch, F., Hansen, W. W., and Packard, M. E. (1946) Phys. Rev. *69*, 127.

Bovey, F. A., (1988) Nuclear Magnetic Resonance Spectrscopy, Academic Press, New York.

Braunschweiler, L., and Ernst, R. R. (1983) J. Magn. Reson. *53*, 521.

Brindley, D. N. (1991) Biochemistry of Lipids, lipoproteins and Membranes (D. Vance and J. Vance, Eds.), Elsevier Science Publishers, New York, Chapter 6.

Burns, R. A., Jr., and Roberts, M. F. (1981) J. Biol. Chem. *256*, 2716.
Campredon, M., Quiroa, A., Allouche, A., and Pouzard, G. (1986) Magn. Reson. Chem. *24*, 624.

Carey, M. C., Small, D. M., and Bliss, C. M. (1983) Anna. Rev. Physiol. *45*, 651.

Chen, Z., and Stark, R. E. (1996) Solid NMR in press.

Chen, Z., Van Gorkom, L. C. M., Epand, R. M., and Stark, R. E. (1996) Biophys. J. *70*, 1412.

Croasmun, W. R., and Carlson, R. M. K. (1987) in Two-Dimensional NMR Spectroscopy: Application for Chemists and Biochemists (W. R. Croasmun and R. M. K. Carlson, Eds.), VCH Publishers, New York, Chapter 7.

Cullis, P. R., Hope, M. J., DeKruijff, B., Verkleij, A. J., and Tillock, C. P. S. (1985) Phospholipids and Cellular Regulation, *I*, 1.

Davis, D. G., and Thompson, M. B. (1993) J. Lipid Res. *34*, 651.

Davis, J. H., Jeffrey, K. R., Bloom, M., Valic, M. I., and Higgs, T. P. (1976) Chem. Phys. Lett., *42*, 390.

Deas, A. H. B., Baker, E. A., and Holloway, P. J. (1974) Phytochemistry *13*, 1901.

Dixon, W. T., Schaefer, J., Sefcik, M. D., Stejskal, E. O., and McKay, R. A. (1982) J. Magn. Reson. *49*, 431.

Epand, R. M. (1996) in Structural and Biological Roles of Lipids Forming Non-Lamellar Structures. JAI Press, Greenwich, CT. in press.

Epand, R. M., and Epand, R. F. (1994) Biophys, J. *66*, 1450.

Ernst, R. R., Bodenhausen, G., and Wokaun, A. (1987) Principles of Nuclear Magnetic Resonance in One and Two Dimensions, Clarendon, Oxford.

Fejzo, J., Krezel, A. M., Westler, W. W., Macura, S., and Markley, J. L. (1991) J. Magn. Reson. *92*, 651.

Forbes, J., Bowers, J., Shan, X., Moran, L., and Oldfield, E. (1988) J. Chem. Soc., Faraday Trans. 1 *84*, 3821.

Forbes, J., Husted C., and Oldfield, E. (1988) J. Am. Chem. Soc. *110*, 1059.

Gabriel, N. E., and Roberts, M. F. (1987) Biochemistry *26*, 2432.

Garbow, J. R., Ferrantello, L. M., and Stark, R. E. (1989) Plant Physiol. *90*, 783.
Gawrich, K., Ruston, D., Zimmerberg, J., Parsegian, V. A., Rand, R. P., and Fuller, N. (1992) Biophys. J. *61*, 1213.

Goodman, R. N., Kiraly, Z., and Wood, K. R. (1986) The Biochemitry and Physiology of Plant Disease, University of Missouri Press, Columbia, MO.

Griffin, R. G. (1981) Methods Enzymol. *72*, 108.

Gross, J. D., Costa, P. R., Dubacq, J.-p., Warschawski, D. E., Lirsac, P.-N., Devau, P. F., and Griffin, R. G. (1995) J. Magn. Res. B. *106*, 187.

Gruner, S. M. (1992) in The Structure of Biological Membranes (P. L. Yeagle, Ed.), CRC Press, Boca Raton, FL, 211.

Gruner, S. M., Tate, M. W., Kirk, G. L., So, P. T. C., Turner, D. C., Keane, D. T., Tilcock, C. P. S., and Cullis, P. R. (1988) Biochemistry *27*, 2853.

Halladay, H. N., Stark, R. E., Ali, S., and Bittman, R. (1990) Biophys. J. *58*, 1449.

Hartmann, S. R., and Hahn, E. L. (1962) Phys. Rev. *128*, 2042.

Halvorsen, R. A., Jr., Ribeiro, A., Blinder, R., Water, C., and Thompson, W. M. (1989) Invest. Radiology *24*, 903.

Holloway, P. J. (1982) in The Plant Cuticle (D. F. Curler, K. L. Alvin, and C. E. Price, Eds.), Academic Press, New York, 45.

Jeener, J. (1971) Ampere Summer School, Basko Polje, Yugoslavia.

Jeener, J., Meier, B. H., Bachmann, P., and Ernst, R. R. (1979) J. Chem. Phys. *71*, 4546.

Kalk, A., and Berendsen, H. J. C. (1976) J. Magn. Res. *24*, 343.

Keepers, J. W., and James, T. L. (1984) J. Magn. Reson. *57*, 404.

Keough, K. M. W., Morrow, M. R., and Bittman, R. (1996) in Encyclopedia of Nuclear Magnetic Resonance (D. M. Grant and R. K. Harris, eds.), p3601, Wiley, Chichester, U. K.

Kessler, H., Gehrke, M., and Griesinger, C. (1988) Angew. Chem. Int. Ed. Eng. *27*, 490.

King, M. D., and Marsh, D. (1989) Biochemistry *28*, 5643.

Knowles, P. F., and Marsh, D. (1991) Biochem. J. *274*, 625.

Kolattukudy, P. E. (1984) Can. J. Botany *62*, 2918.
Lee, C. W. B., and Griffin, R. G. (1989) Biophys. J. *55*, 355.

Le Guerneve, C., and Auger, M. (1995) Biophys. J. *69*, 1952.

Li, K-L., Tihal, C., Guo, M., and Stark, R. E. (1993) Biochemistry *32*, 9926.

Lowe, I. J. (1959) Phys. Rev. Lett. *2*, 285.

Mascioli, E. A., Lopes, S., Randall, S., Porter, K. A., Kater, G., Hirschberg, Y., Babayan, V. K., Bistrian, B. R., and Blackburn, G. L. (1989) Lipids *24*, 793.
McIntosh, T. J., and Simon, S. A. (1994) Annu. Rev. Biophys. Biomol. Struct. *23*, 27.

Montez, B., Oldfield, E., Urbina, J. A., Pekerar, S., Husted, C., and Patterson, J. (1993) Biochim. Biophys. Acta *1152*, 314.

Nemethy, G., and Scheraga, H. A. (1962) J. Phys. Chem. *66*, 1773.

Oldfield, E., Bowers, J. L., and Forbes, J. (1987) Biochemistry *26*, 6919.

Oakenfull, D. G. and Fisher, L. R. (1977) J. Phys. Chem. *81*, 1838; ibid., (1978) *82*, 2433.

Pacchiano, R. A., Jr., Sohn, W., Chanda, V. L., Garbow, J. R., and Stark, R. E. (1993) J. Agric. Food Chem. *41*, 78.

Peersen, O. B., and Smith, S. O. (1993) Concepts in Magnetic Resonance, *5*, 303.

Pearson, R. H., and Pascher, I. (1979) Nature *281*, 499.

Piantini, U., Sørensen, O. W., and Ernst, R. R. (1982) J. Am. Chem. Soc. *104*, 6800.

Pines, A., Gibby, M. G., and Waugh, J. S. (1972) J. Chem. Phys. *56*, 1776.

Purcell, E. H., Torrey, H. C., and Pound, R. V. (1946) Phys. Rev. *69*, 37.

Rand, R. P., and Parsegian, V. A. (1989) Biochim. Biophys. Acta *988*, 351.

Ray, A. K., Lin, Y. Y., Gerard, H. C., Chen, Z., Osman, S. F., Fett, W., Moreau, R. A., and Stark, R. E. (1995) Phytochemistry *38*, 1361.

Ryan, L. M., Taylor, R. E., Paff, A. J., and Gerstein, B. C. (1980) J. Chem. Phys. *72*, 508.

Schaefer, J., and Stejskal, E. O. (1976) J. Am. Chem. Soc. *98*, 1031.
Siegel, D. P. and Banschbach, J. L. (1990) Biochemistry *29*, 5975.

Slater, S. J., Ho, C., Taddeo, F. J., Kelly, M. B., and Stubbs, C. D. (1993) Biochemistry *32*, 3714.

Small, D. M. (1968) Advances in Chemistry Series, No. 84, Molecular Association in Biological and Related Systems, ACS, p31.

Staggers, J. E., Hernell, O., Stafford, R. J., and Carey, M. C. (1990) Biochemistry *29*, 2028.

Staney, S. (1994) B.S. Honors Thesis, College of State Island, CUNY.

Stark, R. E., Gosselin, G. J., Donovan, J. M., Carey, M. C., and Roberts, M. F. (1985) Biochemistry *24*, 5599.

Stark, R. E., Storrs, R. W., Levine, S. E., Yee, S., and Broido, M. S. (1986) Biochim. Biophys. Acta *860*, 399.

Stark, R. E., Sohn, W., Pacchiano, R. A., Al-Bashir, M., and Garbow, J. R. (1994) Plant Physiol. *104*, 527.

Stark, R. E., Zlotnik-Mazori, T., Forfantcllo, L. M. and Garbow, J. R. (1989) ACS Symp. Ser. *399*, 214.

States, D. J., Haberkorn, R. A., and Ruben, D. J. (1982) J. Magn. Reson. *43*, 286.

Sternin, E., Bloom, M., and MacKay, A. L. (1983) J. Magn. Reson. *55*, 274.

Vance, D. E., and Vance, J. E. (1991) in New Comprehensive Biochemistry: Biochemistry of Lipids, Lipoproteins and Membranes, (A. Neuberger, and L. L. M. van Deenen, Eds), Elsevier Press, New York, p1.

van Tilbeurgh, H., Sarda, L., Verger, R., and Cambillau, C. (1992) Nature *359*, 159.

van Gorkom, L. C. M., Nie, S-Q., and Epand, R. M. (1992) Biochemistry *31*, 671.

Volke, F., Eisenblatter, S., and Klose, G. (1994) Biophys. J. *67*, 1882.

Volke, F., and Pampel, A. (1995) Biophys. J. *68*, 1960.

Walton, T. J. (1990) Meth. Plant Biochem. *4*, 105.
Walton, T. J., and Kolattukudy, P. E. (1972) Biochemistry *11*, 1885.

Wang, D., Hadipour, N. L., Jerlin, E. A., and Stark, R. E. (1992) J. Lipid Res. *32*, 431.

Wang, D., Xu, X., Deng, N., Wang, G., Mao, S., and Stark, R. E. (1992) J. Phys. Chem. *96*, 8187.

Wennerstrom, H. (1973) Chem. Phys. Lett. *18*, 41.

Westerman, P. W. (1995) J. Lipid Res. *36*, 2437.

Winkler, F. K., D'Arcy, A., and Hunziker, W. (1990) Nature *343*, 771.

Xu, Z-C. and Cafiso, D. (1986) Biophys. J. *49*, 779.

Zakrzewska, J. Okon, M., and Vucelic, D. (1994) Magn. Reson. Chem. *32*, 93.

Zlotnik-Mazori, T., and Stark, R. E. (1988) Macromolecules *21*, 2412.